AN ABSTRACT OF THE DISSERTATION OF

Eric Andrew Patterson for the degree of Doctor of Philosophy in Materials Science presented on September 17, 2012.

Title: Development, Characterization, and Piezoelectric Fatigue Behavior of Lead-Free Perovskite Piezoelectric Ceramics

Abstract approved:

David P. Cann

Much recent research has focused on the development lead-free perovskite piezoelectrics as environmentally compatible alternatives to lead zirconate titanate (PZT). Two main categories of lead free perovskite piezoelectric ceramic systems were investigated as potential replacements to lead zirconate titanate (PZT) for actuator devices. First, solid solutions based on Li, Ta, and Sb modified $(K_{0.5}Na_{0.5})NbO_3$ (KNN) lead-free perovskite systems were created using standard solid state methods. Secondly, Bi-based materials a variety of compositions were explored for $(1-x)(Bi_{0.5}Na_{0.5})TiO_3$-$xBi(Zn_{0.5}Ti_{0.5})O_3$ (BNT-BZT) and $Bi(Zn_{0.5}Ti_{0.5})O_3$–$(Bi_{0.5}K_{0.5})TiO_3$–$(Bi_{0.5}Na_{0.5})TiO_3$ (BZT-BKT-BNT).

It was shown that when BNT-BKT is combined with increasing concentrations of $Bi(Zn_{1/2}Ti_{1/2})O_3$ (BZT), a transition from normal ferroelectric

behavior to a material with large electric field induced strains was observed. The higher BZT containing compositions are characterized by large hysteretic strains (> 0.3%) with no negative strains that might indicate domain switching. This work summarizes and analyzes the fatigue behavior of the new generation of Pb-free piezoelectric materials. In piezoelectric materials, fatigue is observed as a degradation in the electromechanical properties under the application of a bipolar or unipolar cyclic electrical load. In Pb-based materials such as lead zirconate titanate (PZT), fatigue has been studied in great depth for both bulk and thin film applications. In PZT, fatigue can result from microcracking or electrode effects (especially in thin films). Ultimately, however, it is electronic and ionic point defects that are the most influential mechanism.

Therefore, this work also analyzes the fatigue characteristics of bulk polycrystalline ceramics of the modified-KNN and BNT-BKT-BZT compositions developed. The defect chemistry that underpins the fatigue behavior will be examined and the results will be compared to the existing body of work on PZT. It will be demonstrated that while some Pb-free materials show severe property degradation under cyclic loading, other materials such as BNT-BKT-BZT essentially exhibit fatigue-free piezoelectric properties with chemical doping or other modifications. Based on these results, these new Pb-free materials have great potential for use in piezoelectric applications requiring a large number of drive cycles such as MEMS devices or high frequency actuators.

Development, Characterization and Piezoelectric Fatigue Behavior of Lead-Free Perovskite Piezoelectric Ceramics

by
Eric Andrew Patterson

A DISSERTATION

submitted to

Oregon State University

in partial fulfillment of
the requirements for the
degree of

Doctor of Philosophy

Presented September 17, 2012
Commencement June 2013

Doctor of Philosophy dissertation of Eric Andrew Patterson presented on September 17, 2012.

APPROVED:

Major Professor, representing Materials Science

Director of the Materials Science Graduate Program

Dean of the Graduate School

I understand that my thesis will become part of the permanent collection of Oregon State University libraries. My signature below authorizes release of my dissertation to any reader upon request.

Eric Andrew Patterson, Author

ACKNOWLEDGEMENTS

I want to start with a deep and sincere thanks to my advisor, Dr. David Cann, for all of the years of support and encouragement, starting all the way back at Iowa State University. Can you believe when I first met you, I told you I was going to study metals and polymers? It seems impossible now. Thanks for all of the great opportunities you have given me; from moving to Oregon, to working in Japan, and now studying in Germany. Also, thanks for all of the beer and good memories.

Thank you, Dr. Brady Gibbons for your continuous support, critiques and valuable input on my experiments. Working on the XRD with you, learning how to fix it when it broke, and training student users was a great experience. Your sense of humor and quick wit has been fun.

Next, I want to thank Atsushi Hitomi. Hitomi-san, I can't imagine a better experience than the one I had working at TDK in your group. I learned a great deal about many different topics, about ceramics processing, and bringing a new product out of development. More importantly I got to experience Japan in a

Peter Mardilovich, thank you for all of the coordinating you have done for us with HP. Thanks for the opportunity to work with you and learn so much about thin film PZT and characterization methods. It was great to expand and my knowledge into another area. You challenged me and I always enjoy are discussions and the way you get me to think deeper into a subject.

Thanks to Yu Hong Jeon. This is it buddy. Thanks for all of your help and discussions during really late nights in the office doing homework, to having me see your home in Korea, for being a fun roommate, and for everything in between.

I am grateful to all of the past members of our Electroceramics group that I have had the pleasure to know and work with. Thanks to Meagen Gillespie for being a good mentor at Iowa State and a good friend once you moved out to Oregon too. Thanks to Seunghwa

Kwon and Chien-Chih Huang for being great colleagues, for all of your work setting up the new lab, and for being dear friends.

Thank you dear roommates, old and new, at the Mat Sci Power House. You have been a great "family" and have been wonderful in making Corvallis feel like home. Sarah Gallops, thanks for the Southern Cookin' lessons and great memories. To Jon Mueller, thanks for all of the Minnesota Nice and for getting me to ride bikes again. To my friends back home in Iowa or around the world in Japan, I miss you and hope to see you again soon.

Last, but never least, a most heartfelt thanks to my family. To my Mom, thanks for all of the care packages and kind words of support. Thanks to my sisters, Lizzie and Cathy, who are funny, witty, kind and caring. I'm glad we've only become better friends as we've gotten older. To my Dad, thanks for always being there when I need to talk (or vent) and for driving out to see me so much. I couldn't have made it here with you all having my back. I love you guys.

CONTRIBUTION OF AUTHORS

Dr. Jan Pokorny assisted with the Raman spectroscopy measurements at the University of Sheffield (Sheffield, UK). Dr. Ian M. Reaney, also of the University of Sheffield assisted in the analysis and interpretation of data for the BZT-BKT-BNT system described in chapter 6.

TABLE OF CONTENTS

Page

TABLE OF CONTENTS (Continued)

Page

TABLE OF CONTENTS (Continued)

Page

TABLE OF CONTENTS (Continued)

Page

TABLE OF CONTENTS (Continued)

Page

LIST OF FIGURES

Figure Page

LIST OF FIGURES (Continued)

Figure Page

LIST OF FIGURES (Continued)

Figure Page

LIST OF FIGURES (Continued)

Figure Page

LIST OF FIGURES (Continued)

Figure Page

LIST OF FIGURES (Continued)

Figure Page

LIST OF TABLES

Table Page

1 Introduction and Motivation

Piezoelectric ceramics, particularly $PbZr_{1-x}Ti_xO_3$ (PZT), are the most widely used for key components in a wide variety of device applications, such as in U.S. Military underwater sonar systems, medical ultrasounds, actuators for fuel injection, printers or positioning systems, pneumatic valves, gas igniters, transformers or high voltage sources [1, 2]. While lead-based piezoelectrics currently hold exemptions from certain European Union environmental standards, including the Restriction of Hazardous Substances directive (RoHS), the Waste Elecrical and Electronic Equipment directive (WEEE), and End of Life Vehicles Directive (ELV), they are not expected to be extended indefinitely. These same regulations are also responsible for driving the development of the Pb-free solders that are currently in use throughout the electronics industry. Therefore, the search for lead-free alternatives to lead-zirconate-titanate (PZT) has been of increasing interest and gaining more attention as companies endeavor to reduce the environmental impact of their products. In addition to the environmental reasons, PZT is also known to exhibit quite poor piezoelectric fatigue properties with relatively severe degradation in strain behavior over only a few millions of cycles of applied field.

Recent research in Pb-free piezoelectrics has been focused on a few commonly studied ferroelectric systems. The most common systems involve a binary system, which typically includes $(Bi_{0.5}K_{0.5})TiO_3$ (BKT), $(Bi_{0.5}Na_{0.5})TiO_3$ (BNT), or $(K_{0.5}Na_{0.5})NbO_3$ (KNN) with another ABO_3 perovskite, such as $BaTiO_3$ or one of the other starting components[3, 4]. In this work, new binary and ternary systems will be explored in order to further enhance these piezoelectric properties. Fatigue of these lead-free systems will also be

evaluated in detail to determine if their behavior is as detrimental and if the mechanisms are the same as those found for PZT based systems.

1.1 Composition Studies

1. Characterize piezoelectric properties of KNN-based LF4
2. Explore and optimize piezoelectric properties of the new Bi-based system: $Bi(Zn_{0.5}Ti_{0.5})O_3$ - $(Bi_{0.5}K_{0.5})TiO_3$ - $(Bi_{0.5}Na_{0.5})TiO_3$ or BZT-BKT-BNT.
3. Characterize and investigate MPB compositions using X-ray diffraction, dielectric and Raman spectroscopy, and polarization measurement techniques using temperature-controlled environments to further understand changes in structure.

1.2 Fatigue Studies

1. Characterize unipolar fatigue of undoped and CuO doped LF4 at multiples of coercive field level.
2. Investigate the bipolar fatigue of the key compositions developed from the Bi-based ternary systems in the previous section
3. Examine the nature of the transition between ferroelectric and new high strain compositions to check if the level of degradation and mechanism are the same.

2 Literature Review

2.1 Piezoelectricity

Piezoelectric materials act to transmute mechanical energy into electrical energy, or the exact opposite process, by means of changes to the crystal structure of the material in question. The direct piezoelectric effect is the proportional electrical polarization that is formed in response to a strain caused by an applied stress to a material. The corresponding 'converse' or indirect effect is the development of a strain in a material in response to an applied electric field. Pierre and Jacques Curie first discovered the piezoelectric effect in 1880 while investigating the ability of pressure to generate charge in quartz[5].

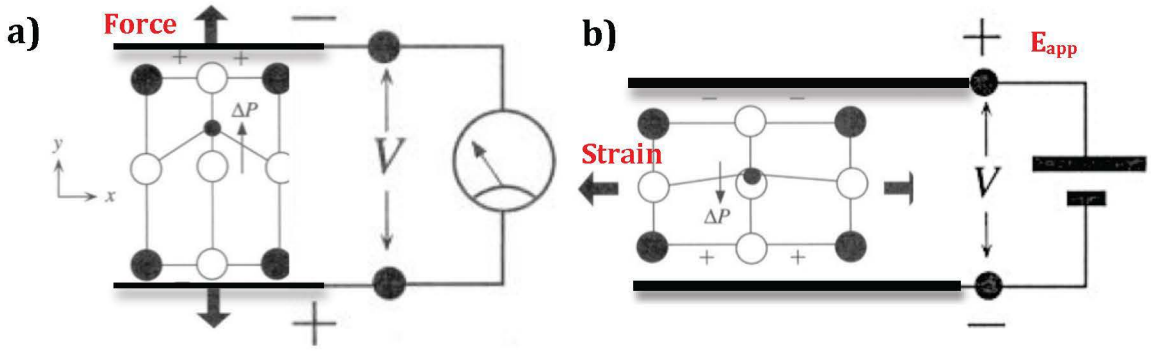

Fig. 2.1 *a) direct and b) indirect piezoelectric effect, adapted from[6].*

The direct piezoelectric effect shown in Figure 2.1 a), shows an exaggerated example of ceramic with a specific crystal structure generating a voltage that drives a current through a circuit when a stress is applied. For the indirect effect, Figure 2.1 b) shows an electric field applied that is causing a material to strain by contracting vertically while

expanding horizontally. It is due to these effects that piezoelectric ceramics have so many applications (sensors, actuators, ultrasonic devices, generators, etc) mentioned previously.

The direction and degree of the induced polarization depends on the direction of the applied stress on the crystal and the symmetry of crystal structure in question. This is demonstrated in the generic 2D hexagonal structure shown in Figure 2.2 [6]. When a compressive stress in the y-direction is applied to the stress-free unit cell in Figure 2.2 a), the resulting motion of positive "A" and negative "B" atoms will result in a separation of the centers of positive and negative charge and a dipole is generated along the y axis, as shown in Figure 2.2 b). If instead, a stress is applied along the x axis, there is no induced polarization along the direction of the applied stress because there is no net displacement between the center of positive and negative charge along the x-axis, but there can be a net change along another direction (the y-axis in this simple case), as shown in Figure 2.2 c) below.

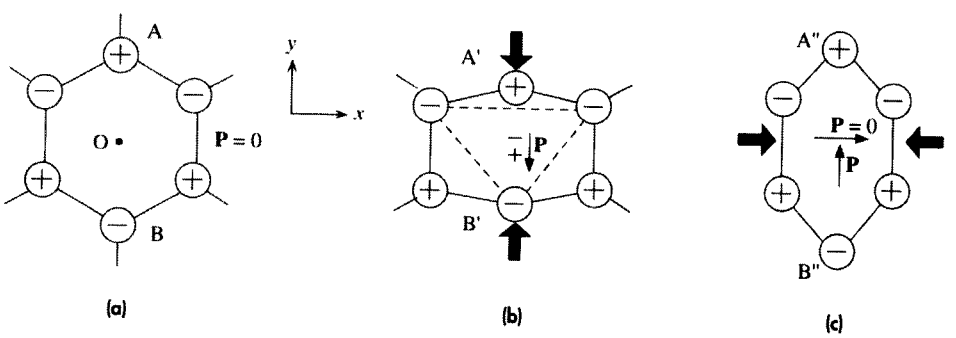

Fig. 2.2 *Importance of direction of applied stress on simple hexagonal structure a) with no applied force, b) dipole generated in the y-direction c) no dipole generated along x-axis, taken from [6]*

In bulk solid systems, applied stress in one direction can likewise induce polarization in other directions in a highly anisotropic manner. In piezoelectrics, polarization is linearly proportional to stress by means of the piezoelectric coefficient, *d*. Through thermodynamic calculations, strains are similarly shown to be directly proportional to applied electric field [7]. Because stress (or strain) is a second rank tensor and polarization (or field) is a vector, the piezoelectric coefficient is therefore described by a third rank tensor, d_{jkl}, having 27 tensor components after transforming the stress to the new coordinate system. The direct and indirect piezoelectric effect should be written as tensors, but due to the symmetry of the stress, *i.e.* $X_{ij} = X_{ji}$, only 18 components are independent, which can be described by a 6x3 matrix conveniently given the form shown in equations (2.1) and (2.2):

Direct Effect:

$$P_i = d_{ij} X_j \qquad (2.1)$$

Indirect Effect:

$$x_i = d_{ij} E_j \qquad (2.2)$$

Where X is stress (N/m^2), P is polarization, x is strain, and E is electric field. In both cases, d_{ij} is the piezoelectric coefficient (pC/N or pm/V), the magnitude of which is related to crystal structure. In either equation the letters i = 1 to 3 and j = 1 to 6, which

are used form the matrix for the 18 independent components of the piezoelectric coefficient. In converting between tensor and matrix form, a factor of two arises for piezoelectric involving shear stresses or shear strains. If j = 1,2,3 matrix coefficient $d_{ij} = d_{ijj}$. If j = 4, 5, 6, then $d_{ij} = 2d_{ikl}$.

The piezoelectric matrix can be derived for all of the crystallographic point groups, as well as the limiting (Curie) groups. Poled ferroelectrics, to be discussed in the following section, have the symmetry point group ∞m and are a key example. The poling process consists of a strong DC field applied to a sample at elevated temperatures so that the domain walls can move more easily giving a highly domain aligned sample. The ∞m point group has an ∞-fold axis parallel to Z_3 and an infinite number of mirror planes (m) parallel to Z_3. Three of the mirror planes are perpendicular to Z_1, to Z_2 and at 45° angle to Z_1 and Z_2. For the mirror planes perpendicular to Z_1, $d_{ijk} = 0$ whenever there is an odd number of 1s in the subscript, which reduces the matrix by 8 coefficients. For m perpendicular to Z_2, all of the remaining tensor coefficients with an odd number of 2s likewise go to zero, leaving only 5 non-zero coefficients in the matrix (d_{31}, d_{32}, d_{33}, d_{24}, and d_{15}). The third symmetry element was the mirror plane 45° to X_1 and X_2. This transformation would take 1→2, 2→1, and 3→3. This results in $d_{15} = d_{24}$ and $d_{31} = d_{32}$, leaving only 3 independent coefficients (d_{31}, d_{33}, and d_{15}) for poled ferroelectric ceramics and other ∞m point group materials.

The effectiveness of the piezoelectric effect can also be represented by the electromechanical coupling factor, k. This term gives the relative fraction of electrical

energy that is converted to mechanical energy or vice versa. The coupling factor can be written as shown in equation (2.3) below:

$$k_{eff}^{\ 2} = \frac{\text{output mechanical energy converted from input electrical energy}}{\text{total input electrical energy}}$$

Or (2.3)

$$k_{eff}^{\ 2} = \frac{\text{output electrical energy converted from input mechanical energy}}{\text{total input mechanical energy}}$$

There is always energy loss during this conversion, so k^2 will necessarily be less than 1 for any system under consideration. The k value for quartz is 0.1, for $BaTiO_3$ ceramics ~0.4, $Pb(Zr,Ti)O_3$ ceramics range between 0.5 to 0.7 depending on composition, and Rochelle salt is approximately 0.9 (T_c = 24°C). The k value for single crystals of $Pb(Zr, Ti)O_3$ or $BaTiO_3$ have been found to be larger than 0.9 [8].

2.2 Ferroelectricity

Rochelle salt ($KNaC_4H_4O_6 \cdot 4H_2O$) was the first known ferroelectric discovered by Valasekin 1921[9]. After his research, a large number of crystals possessing ferroelectric behavior were discovered. Ferroelectrics are an important subset of piezoelectric

materials because the piezoelectric effect is enhanced from contributions associated with domain wall motion, which will be described in more detail in this section. Ferroelectric solid solutions are therefore among the most common materials systems used in applications and as a system in general make for an obvious starting point for developing new, competitive lead-free piezoelectrics. Specific symmetry requirements exist for a material to qualify as a ferroelectric. They must be non-centrosymmetric (i.e. lack inversion symmetry) like piezoelectrics but must also have a polar axis. Ferroelectricity arises from these crystal distortions, so it is convenient to define these systems by the relevant crystallographic point groups. There are a total of 32 possible point-groups for different crystals, however 11 can be immediately eliminated from consideration due to the presence of a center of symmetry. Out of the 21 remaining systems, another 11 fail to qualify as ferroelectric due to the lack of a polar axis.

Table 2.1 *Classification of crystallographic point group in terms of piezoelectric and ferroelectric properties (taken from [10])*

Polar	COS	Cubic		Hexagonal		Tetragonal		Trigonal		Ortho	Mono	Tri
Non-Polar	$\bar{1}$	m3m	m3	6/mmm	6/m	4/mmm	4/m	$\bar{3}$m	$\bar{3}$	mmm	2/m	$\bar{1}$
	1	432	23	622	$\bar{6}$	422	$\bar{4}$	32		222		
		$\bar{4}$3m		$\bar{6}$m2		$\bar{4}$2m		Piezoelectric point groups				
Polar				6mm	6	4mm	4	3m	3	mm2	2	1
				Ferroelectric point groups							m	

Table 2.1 demonstrates the classification of crystallographic point groups in terms of the center of symmetry (COS) and polar axis [10]. From this, an important distinction should be noted that while all ferroelectrics can be classified as piezoelectrics, not all piezoelectrics are ferroelectric (e.g. quartz, AlN, etc).

Ferroelectricity is present in materials where a spontaneous electrical polarization exists that can be reoriented by the application of an external electric field. Most terms used in describing these effects were adapted from ferromagnetic materials due to their analogous behavior. The polarization comes from the separation of the center of positive and negative charges in the crystals with symmetries as shown in Table 2.1. Generally, distortions from a crystallographic phase transition from a high symmetry paraelectric state to a lower symmetry state result in the necessary separation in charge. The prototype for this behavior can be seen for the case of $BaTiO_3$ in Figure 2.3, where the crystal distortions of a $BaTiO_3$ crystal are shown at different temperatures. As the temperature is cooled below ~123°C, the separations of the centers of mass for the positive charges, Ba^{2+} and Ti^{4+}, and those of the negative, O^{2-}, produces ferroelectric behavior in the now tetragonal crystal. The temperature which ferroelectric property is lost upon heating through this phase transition is known as the Curie point (T_c).

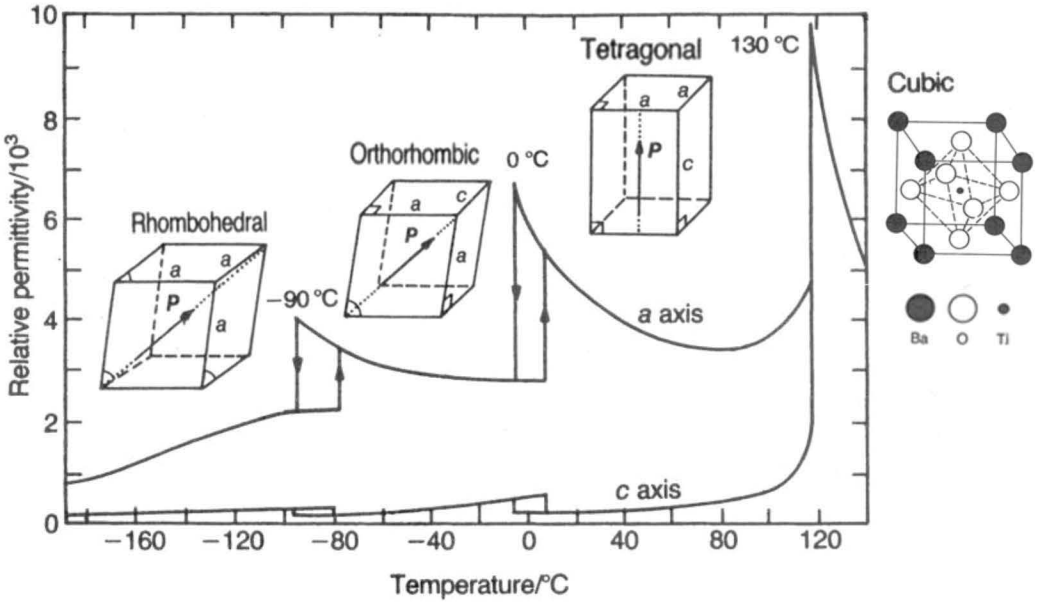

Fig. 2.3 *Permittivity vs. Temperature for transition from cubic, paraelectric $BaTiO_3$ to ferroelectric structures (Tetragonal, orthorhombic, rhombohedral) adapted from[11].*

For ferroelectrics the dielectric behavior when the temperature is above T_c, is given by the linear relation called the Curie-Weiss law, which is shown in equation (2.4).

$$\frac{1}{\varepsilon} = \frac{T - T_C}{C} \tag{2.4}$$

Where ε_r is the relative permittivity, C is a constant called the Curie constant, and θ_C is the Curie Temperature (an extrapolated constant, slightly different from the Curie point) [11].

The strength of the ferroelectricity exhibited by a material is determined from its degree of polarization. As a ferroelectric state forms in a material, regions with matching polarization vectors will tend to align to form sub-grain boundary regions known as

domains. Domain walls are defined as the regions where domains of different orientation meet within a grain. The energy required to split into domains and thus form a domain wall must reduce the overall energy of the system that arises from the depolarization field and/or mechanical stresses that form as the material transitions and distorts as it is lowered past the Curie point.

In the barium titanate example, these domains are generally oriented 180° from each other to minimize the inherent depolarization field. Also, 90° domain boundaries form to reduce mechanical stress introduced to the structure due to the transition to the ferroelectric phase upon cooling. These domains will initially nucleate randomly, much like the grains in polycrystalline materials, in order to most efficiently reduce the energy of the overall system. The polarizations vectors occur along one of the "allowed" symmetry directions, which are determined by crystal structure. Before any field is applied, there is neutral overall polarization due to this randomization of domains. With the introduction of an electric field, the domains oriented most closely to that applied electric field will grow at the expense of those domains oriented opposed to the field. Switching occurs when the direction of the electric field is changed and the polarization vectors within the domain are reoriented. The hysteretic behavior of the polarization and strain as a function of applied electric field (P-E loop and S-E loop respectively) is shown is Figure 2.4 a) and b) below.

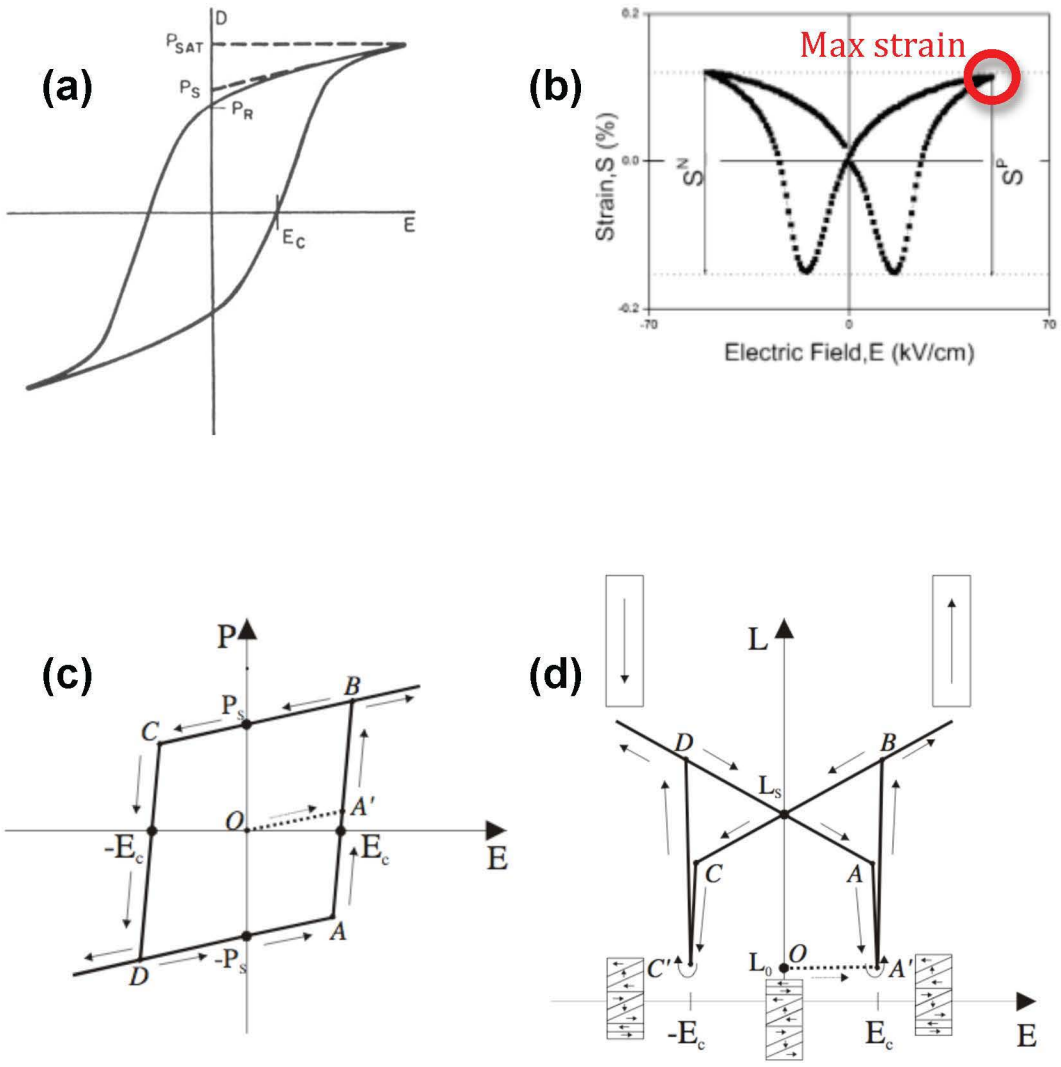

Fig. 2.4 *Typical ferroelectric hysteretic behavior of a) (generic) polarization loop and b) strain (0.955 $Pb(Zn_{1/3}Nb_{2/3})O_3$–0.045$PbTiO_3$) taken from [8, 12] and theoretical schematic of c) polarization and d) strain taken from [13]*

In Figure 2.4 a), the value of the remanent polarization, P_r, is used to measure ferroelectric strength and is the polarization observed once the applied electric field has been removed. The energy required to reorient the polarization vectors in domains is called the coercive field, E_C. The spontaneous polarization, P_s, is the linearly extrapolated

value from the maximum or "saturation" polarization at high electric field (P_{MAX} or P_{SAT}) back to zero field. In polycrystalline ceramics, P_s is larger than P_r due to the presence of domain switching being impeded by defects and internal strains arising from the random alignment of grains. In comparison, for single crystal piezoelectric materials the values of P_r are almost the same as P_s and both are closer to P_{sat}, so a more square shaped loop is observed.

A strain-electric field hysteresis loop with the characteristic, highly symmetric, "butterfly" shape is shown in Figure 2.4 b) [12]. The majority of the strain a ferroelectric experiences depends on the type switching of domains in the bulk. An idealized boxy polarization and butterfly-shaped strain loop are shown in Figure 2.4 c) and d), respectively. At fields above the coercive field, domains are switching from a mixture of 180° and 90° to only 180° domains resulting in the steep increase in strain until saturation is reached at point "B". At higher fields some further electrostrictive increases in strain occur. These consist of displacements of atoms relative to the lattice site and are generally much more minor in comparison to those resulting from piezoelectricity. Decreases of strain down to point "C" are from the switching of 180° domains from "up" to "down" orientation. As further negative field is applied and the coercive field is again reached, 90° domains are again formed as C→ C' and eliminated as C'→ D in favor of all "down" oriented 180° domains.

Using the maximum strain divided by the maximum field, a high-field or effective d_{33}^* can be calculated with units of pm/V. This unit is used for clarification of the measurement method but is an equivalent unit to the d_{33} values from direct

measurements reported in units of pC/N. The d_{33}^* values are often higher than d_{33} values found for poled samples through direct, low-field measurements. This is especially true for lead-free materials where the d_{33}^* values are at a more fully "poled"condition at the high field applied (used for calculation) than can be achieved at 0 field even after optimized high temperature DC bias poling conditions. This is directly tied to their generally lower remanent polarization values.

2.3 Perovskite Materials

Discovered in 1839 by Gustav Rose and named after renowned Russian mineralogist Count Les Alexseevich Perovski, the Perovskite structure has a wide variety of uses in technological applications. The perovskite structure is represented by the generic formula $A^{XII}B^{VI}X_3$, or ABO_3 for convenience [8, 11]. The A cation site is in 12-fold coordination and has larger cations, whereas the B cation site is in 6-fold coordination with generally smaller radius cations. The X sites represent 6-fold coordinated anions, which will always be oxygen in these studies. Through manipulation of the composition of each structural site, this versatile structure can serve as a catalyst, capacitor, magnetic material, magnetoresistive material, non-linear optical material or even superconductors [14]. Most importantly for this study, all of the most useful ferroelectric and piezoelectric materials in industrial use are derived from the perovskite structure. The generic crystal structure is shown in the right hand portion of Figure 2.3 for cubic $BaTiO_3$(BT).

To investigate the origin of ferroelectricity in perovskites, modeling done from first principal calculations has been studied for a wide variety of compositions, in

particular for the seemingly similar $BaTiO_3$ and $PbTiO_3$ (PT). When calculations are made that assume perfectly spherical electron clouds for ions (with no covalency), no ferroelectric state arises for either $BaTiO_3$ or $PbTiO_3$. This is despite the fact that long range coulombic forces (Madelung) favors the ferroelectric distortion, without the strong covalent type bonding between Ti-O (as well as in the A-O bond), the short range repulsions are strong enough to stabilize the paraelectric cubic phase in the model [15]. In a further modification to the model where covalency was used and the ferroelectric state was achieved, by raising the energy parameter to reduce variational freedom (essentially eliminating the Ti d-state interactions) the ferroelectric state was lost. In most perovskites, the B site is dominated by cations (Ti^{4+}, Ta^{5+}, Zr^{4+}, etc.) where the lowest unoccupied state is the d shell. So without the B cation hybridization with oxygen, the short-range repulsions again dominate and do not allow the ferroelectric state in the perovskite systems in general [15]. Essentially, the transition between the two states is sensitive to defects that modify short-range interactions, as well as to carriers that screen the long-range field effect. Both would tend to act against stabilization of ferroelectricity (e.g. more photoelectrons increases such screening).

The A-cation has a relatively minor, but still important effect on the ground state of the perovskite and the type of the transition. It acts to increase the ferroelastic strain and acts to couple additively with the ferroelectric distortions. It can also hybridize with the valence states leading directly to changes in the B-O interactions, such as in the case of Pb. This lead to an introduction of the concept of rhombohedral “ground state” (RGS) perovskites (BT, KNN) vs. tetragonal “ground state (TGS) perovskites (like PT). In the RGS case, the B-site atom’s average location is over low-energy [111] distortion

directions that lead to a more elaborate series of transitions. In TGS, the strain is large enough that the tetragonal phase is stabilized. However, even at high temperatures, PT cubic phase has multiple well potential surfaces that are anharmonic (also empirically observed by atoms that seldom sit on their equilibrium positions). This is also typical of rotation instabilities that are quite common in many perovskites or alternatively tilt instabilities in cuprate superconductors.

The perovskite structure can tolerate a wide range of compositional variation due to the large number of ions that have high substitutional solubility in both the A and B cation sites. In many cases the oxygen octahedral will exhibit tilting to some degree to lower the energy of the system when A and B cations vary greatly in size. A general rule for stable perovskites gives an average valence of 3 between the A and B site in combinations divided into three groups:$A^{2+}B^{4+}O_3$, $A^{1+}B^{5+}O_3$, $A^{3+}B^{3+}O_3$. All of these structure types can be made stable in compositions that are off-stoichiometry, with oxygen (anion) or cation deficiencies that will greatly affect their electrical properties. Titanates are among most common and useful compounds of the $A^{2+}B^{4+}O_3$ compounds (e.g. $BaTiO_3$, $PbTiO_3$-$PbZrO_3$) due to their high dielectric, ferroelectric and piezoelectric properties. Some examples for $A^{1+}B^{5+}O_3$perovskite include $KNbO_3$, $NaNbO_3$, and $LiTaO_3$. This group is of particular interest due to its piezoelectric properties. The third simple perovskite group, $A^{3+}B^{3+}O_3$, includes $BiFeO_3$ and $LaAlO_3$ and either possess a lower symmetry structure like rhombohedral or orthorhombic or are not stable outside of use as dopants or in solid solutions with other perovskites (e.g. $BiInO_3$) [16, 17].

Binary or ternary solid solutions of more than one of these simple perovskite allows for the creation of more complex perovskites. Essentially, multiple elements split the occupancy of the A or B site and must average out to the appropriate charge for that site according to the same principles used in the case of the three simple perovskite types listed above. The high stability of the perovskite structure allows for highly complex charge compensated compositions to form. The general formula for complex perovskites can be written as $(A'A'')^{XII}(B'B'')^{VI}X_3$.While many of the complex perovskite families are known to be relaxor ferroelectric, there has been significant success in modifying ferroelectric compositions such as $(Bi_{0.5}^{3+}K_{0.5}^{1+})TiO_3$, $(Bi_{0.5}^{3+}Na_{0.5}^{1+})TiO_3$, and many combinations of these two. Another highly investigated system to be covered is $(K_{0.5}^{1+}Na_{0.5}^{1+})(Nb_x^{5+}Ta_{1-x}^{5+})O_3$, with even further elements being introduced to enhance the piezoelectric properties.

2.4 Morphotropic Phase Boundary (MPB)

An MPB can be located at the compositional boundary between two perovskite materials with different symmetries by controlling the ratio of each perovskite component. The most common example of this phenomenon is the solid solution of lead zirconate-titanate, or $Pb(Zr_xTi_{1-x})O_3$ (PZT). In fact, PZT is the most analyzed system with an MPB due to its exceptionally large and constant piezoelectric properties. This is due to the fact that PZT shows a nearly vertical, temperature independent, phase boundary between the $PbTiO_3$ (tetragonal) and $PbZrO_3$ (rhombohedral) phases at a composition of $x\sim0.52$, as shown in Figure 2.5 [8]. The origin for this maximization of the piezoelectric

response in this MPB region is generally explained by the high degree of freedom for the electric dipoles.

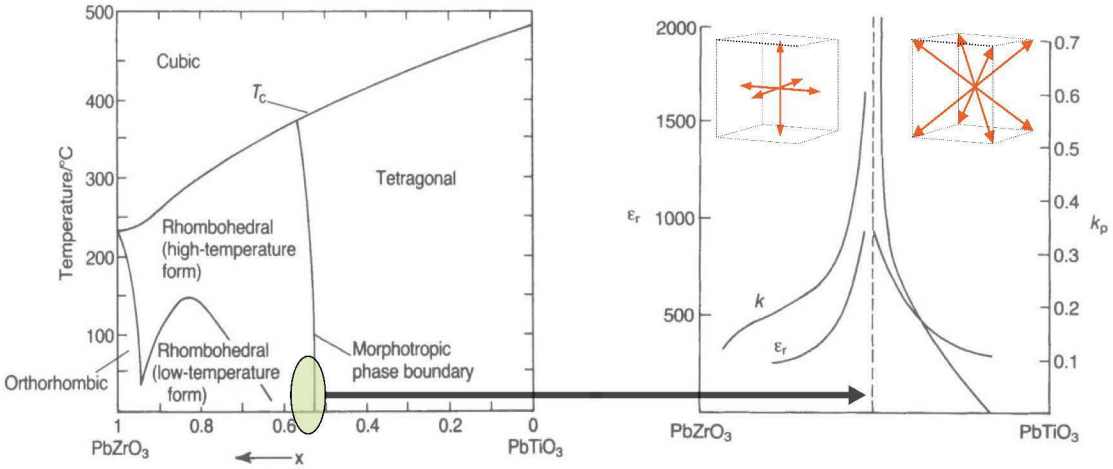

Fig. 2.5 *Phase diagram and piezoelectric properties for* $Pb(Zr_xTi_{1-x})O_3$ *taken from [8]*

This allows them to be easily oriented via an electric field in a large number of directions, essentially combining the possible orientations of tetragonal (6 along [001]) with those of rhombohedral systems (8 along [111]). Domain systems arising can orient along all of these directions and form a more highly oriented polycrystalline sample under optimal poling. More recent structural studies also indicate another possibility, that an intermediate phase of monoclinic symmetry may instead exist at the MPB composition and results in the enhancement of piezoelectric and dielectric properties [18]. Although many lead free systems are described as having an MPB, usually the phase transition observed is not highly independent of temperature, with fairly wide ranges of

compositions and the resulting enhancement of properties is not as compelling. These transitions are more aptly described by the term polymorphic phase transition.

Since various compositions of PZT are among the most utilized piezoelectric materials in industry, a significant amount of work has been completed studying the ability of dopants to change the switchability of domains. The resulting effects on dielectric and piezoelectric properties can be quite significant and are relatively easy to understand and control for Pb-based systems. In Table 2.2 the common aliovalent dopants and the nature of their effects are listed. When such doping results in increased coercive field and decreased dielectric properties, the PZT is termed hard PZT. Hard PZT is achieved by adding in lower valency acceptors like K^{+} and Fe^{3+} on the A and B site, respectively. Similarly, higher valency cation substitutions, or donors, like La^{3+} or Sb^{5+} are used to lower the coercive field and obtain soft PZT.

Table 2.2 *Common aliovalent dopants for PZT [11]*

A site donors	Soft PZT	La^{3+}, Bi^{3+}, Nd^{3+}
B site donors	Soft PZT	Nb^{5+}, Ta^{5+}, Sb^{5+}
A site acceptors	Hard PZT	K^{+}, Rb^{+}
B site acceptors	Hard PZT	Co^{3+}, Fe^{3+}, Sc^{3+}, Ga^{3+}, Cr^{3+}, Mn^{3+}, Mn^{2+}, Mg^{2+}, Cu^{2+}

Hard PZT results because the acceptor dopants form relatively unstable dipoles with oxygen vacancies and when aligned can set up fields that act to stabilize the domain structure, including pinning 90° wall motion. Thus the observed increase in coercive field and reductions in dielectric properties occur due to this domain wall pinning. Donor dopants form dipole pairs with A site vacancies and generally reduce the number of oxygen vacancies, thus increasing domain mobility and having the opposite effect on its properties.

2.5 Stability of Perovskites

One strategy for developing new piezoelectric compositions involves forming solid solutions between two or more perovskite phases of different symmetries. The proportions of each phase added are modified in an attempt to discern a morphotropic phase boundary (MPB) similar to that found for PZT. The higher dielectric and piezoelectric properties of materials at the MPB composition are then tested by common dielectric and polarization techniques. The overall stability of these solid solutions can be roughly calculated by means of a simple geometric relationship known as tolerance factor, t, developed by Goldschmidt in 1926 and given as:

$$t = \frac{r_A + r_O}{\sqrt{2}(r_B + r_O)} \tag{2.4}$$

fwhere r_A, r_B, and r_O are the ionic radii of the A, B and O ions, respectively[19].

For a tolerance factor equal to 1, an ideally cubic structure is formed, such as for the case of $SrTiO_3$. For values of t < 1, a lower symmetry phase is expected (rhombohedral or orthorhombic). The opposite is observed for t > 1, resulting in either hexagonal or more importantly ferroelectric tetragonal phases. If t is found to be between 0.88-1.09 for a given composition there is a high probability that it will form a stable perovskite structure. Combining two or more perovskite end members to reach a tolerance factor value between 0.99 and 1.01 often results in a single-phase perovskite near a much desired MPB [20]. Figure 2.6 illustrates a selection of perovskite phases and the location of the MPB for a number of previously developed solid solutions, especially focusing on those with $PbTiO_3$ as an end member. Note that the MPB is indeed commonly located within a tolerance factor range of 0.99 to 1.01 for most binary solid solutions.

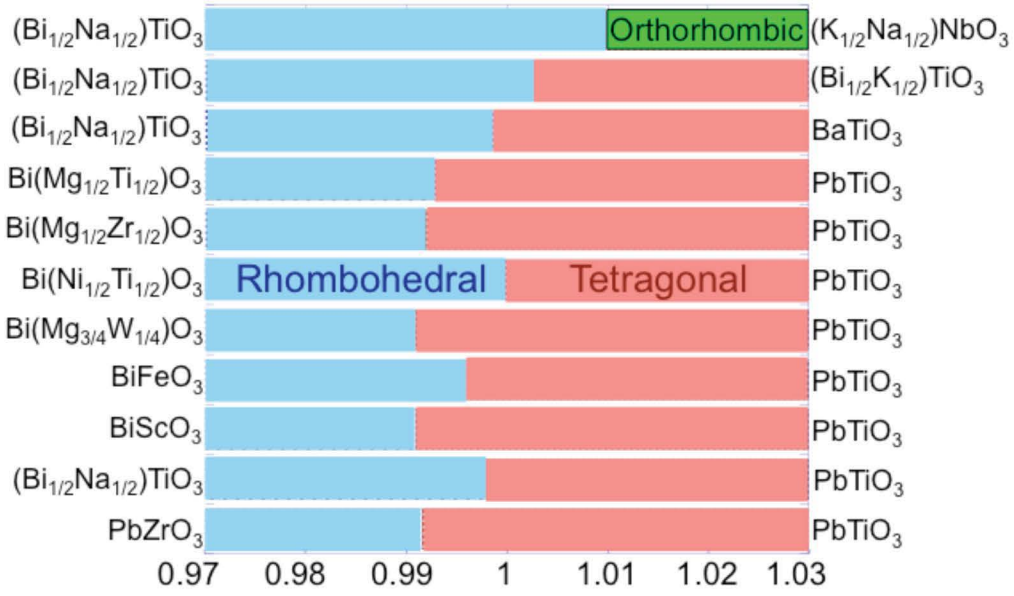

Fig. 2.6 *Schematic of the perovskite phases present in a number of binary solid solutions with t of the 'MPB' composition indicated.*

Tolerance factor alone is not sufficient to describe the stability of a compound in the perovskite phase. For example, even though $BiGaO_3$ has a tolerance factor equal to one, the structure does not form as a stable perovskite. Another factor used in conjunction with tolerance factor as a guide to phase stability is the electronegativity difference between the various cations and anions present in the structure and is given as:

$$\Delta EN = \frac{(\chi_{A-O} + \chi_{B-O})}{2} \qquad (2.10)$$

Where $\chi_{A\text{-}O}$ is the electronegativity difference between the A site and oxygen and $\chi_{B\text{-}O}$ is the electronegativity difference between the B site and oxygen[21, 22].

This difference in electronegativity specifies the degree of ionic character of bonding in the compound. In the more complex perovskite solid solutions, an appropriate weighted average of the different A or B site cations must be used for the component electronegativity differences. Larger electronegativity differences with higher degree of ionic bonding tend to result in more stable perovskite structures. Together these models provide a useful starting point for synthesizing new perovskite compounds [14, 23, 24].

2.6 Piezoelectric Fatigue

Fatigue is a term most commonly associated with cyclic loading leading to mechanical failure of materials, but in the case of piezoelectric fatigue, the change in property, type of failure being considered, and the mechanisms that lead to deteriorating properties are

altogether different. Fatigue in piezoelectrics is generally explained as the reduction of polarization and strain with high cycling of an applied bipolar or unipolar electric field. The corresponding strain and polarization reduction are difficult to isolate due to the fact that the contributing mechanisms can be many and varied. For example, while micro-cracking (either within the bulk of the material or due to isolated delamination near-to and often parallel to the electrode) is an example of an extreme and permanent mechanism for fatigue, its presence is not necessary for fatigue to occur.

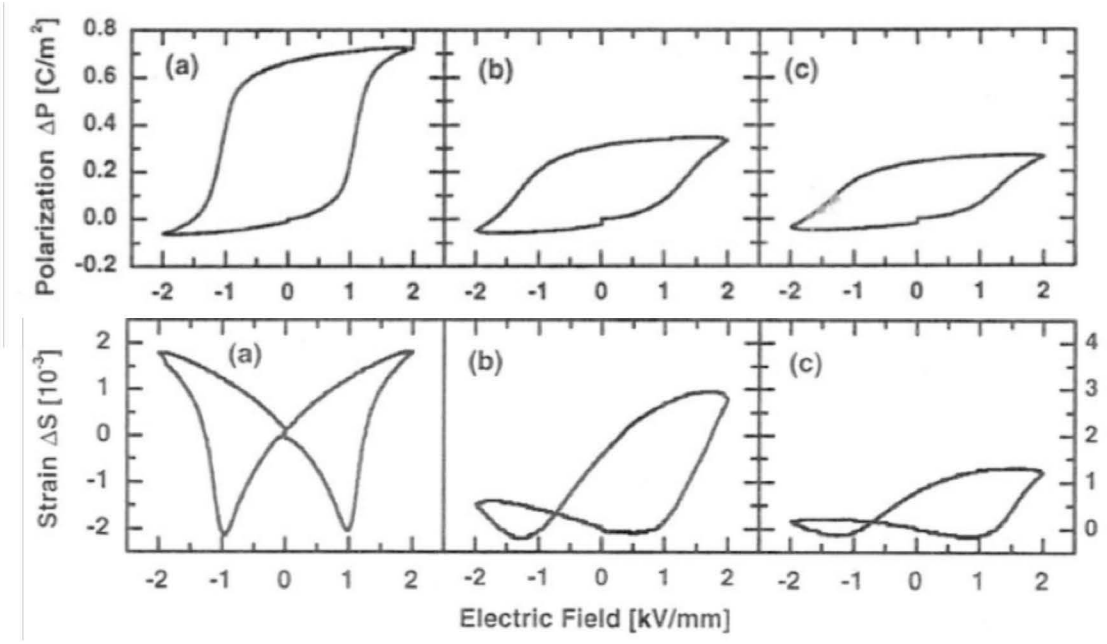

Fig. 2.7 *Bipolar fatigue affects on polarization and strain in bulk PZT after a) 0 b) $3x10^6$ and c) 10^8 cycles taken from [25].*

The two most studied types of fatigue are based on whether the applied field is unipolar or bipolar during cycling. While the two effects are related the manifestation of each is

not exactly the same. Two important fatigue-causing mechanisms have been identified and will be elaborated upon here. Aside from simply an observation of decrease in maximum polarization, both involve the separation of charge within the sample in the form of electronic or ionic carriers. This results in either a less-stable space charge-like bias field or an offset polarization yielding defect agglomerate type of behavior, respectively. These offsets are observable in P-E loops as represented by asymmetry in E_C and P_r with respect to the origin. In the largest study yet completed for fatigue of PZT, bulk PIC 151 was used for all testing. PIC 151 is a commercial PZT with Ni and Sb doping of the composition $Pb_{0.99}[Zr_{0.45}Ti_{0.47}(Ni_{0.33}Sb_{0.67})_{0.08}]O_3$ [25]. After fatigue under bipolar conditions at $2E_C$ for 10^8 cycles, a decrease of ~78.5% of the original value of P_{Max} is shown in Figure 2.7 above [25].

Importantly, for bulk PZT samples thus far investigated in the literature, severe fatigue is only observed when the applied field exceeds that of the coercive field for the material. For thin films of certain PZT compositions, however, fatigue has been observed at cycling fields as low as E_C levels [25]. Another important factor for thin films is the additional effect of substrate clamping, which results in remanent polarizations at around 30% P_s at high fields giving a more slanted hysteresis curve [25, 26]. This makes it more difficult to obtain accurate values of P_r and E_C for thin films. The number of cycles to failure is, regardless, similar in both bulk and thin film cases. The majority of the published research has been focused on the effects of bipolar fatigue and thus will largely make up the focus here.

2.6.1 Bipolar Fatigue

In bipolar fatigue, the permanent effects are tied to reduction in strain and switchable polarization simultaneously, implying a reduction of the mobility of 90° domain walls. Significant fatigue was found to consistently begin in the range of $2.5x10^5$ and $3x10^6$ cycles of applied fields at twice the coercive field level of the PZT in question [25]. There is another component to the fatigue effect that is quite apparent in Figure 2.5.1, the asymmetry of the degradation of the maximum strain observed. For these measurements, a thermal treatment was applied (4 hours at 400°C) between the cycling steps. The asymmetry persisted nonetheless.

There is a straightforward macroscopic explanation for the observed asymmetry. An offset polarization was defined by Nuffer *et al.* to explain the observed change in behavior [27]. This could be explained by Landau-Devonshire theory for electrostrictive materials, where strain is proportional to the square of total polarization. Technically, this is only fully applicable in cases of a single domain near the Curie point for the phase transition to the paraelectric phase. However, one must consider both the degradation of the total amount of switchable polarization and also the formation of an offset polarization, as both options could result in the reduced properties. As modeled by Lupascu *et al.*, a curve fit develops asymmetry only when an offset polarization is applied and not when combinations of two volume sets of switchable and "frozen", non-switchable polarizations within a material are considered for a given domain [25]. This indicates that an increasing polarization offset alone leads to the observed asymmetry.

In addition to this, bias or offset fields develop that are different from offset polarization. Offset fields still allows the domain system to move, and can be seen as the shift of the polarization hysteresis loop in one direction along the field axis. This can be observed due to just aging either under DC or without external loading conditions. It is common for a relatively minor offset field to develop automatically as a reduction in the energy of the system as a reaction to the spontaneous polarization generated upon cooling below the Curie temperature. The charge buildup that forms during this transition forms bias fields that tend to be located at grain boundaries or especially near electrodes. While oxygen vacancy diffusion from external sources could compensate this mechanism, ion diffusion through metal of electrodes is very small due to the large energetic barriers. Instead, a space charge region develops in these areas. But the resulting shift in the hysteresis is generally only seen in initial measurements, and is decreased upon subsequent measurements. Offset polarization, on the other hand, appears to arise from domains being pinned and no longer switching with the applied field. Defects forming immobile dipoles throughout the bulk alone is insufficient to cause the magnitude of offset polarization observed, as there would need to be $n=10^{21}$ cm^{-3} defects[25]. For this reason, it was instead proposed that some internal domain pinning mechanism must be in effect [28, 29].

Lupascu proposed that piezoelectric fatigue could be explained by a common mechanism that reduces switchable polarization and strain simultaneously by focusing on a mechanism that could possibly suppress 90° domain switching. These obstacles would inherently need to grow during the fatigue cycling process in order to make sense.

After $2E_C$ bipolar fatigue of the samples, increasing the applied field, E_{app}, from $2E_C$ to $4E_C$ one observes hysteresis loops restored to approximately full values of remanent and maximum polarization[30, 31]. Fatigue-lowered maximum and remanent polarization values are surpassed by the application of higher fields but the decreases are not removed permanently. Further measurements gave similarly reduced values when the field level was slowly stepped back down to $2E_C$, but now the P-E hysteresis was re-centered around the origin of the x-axis and S-E is once again fairly symmetric as seen in Figure 2.8 below.

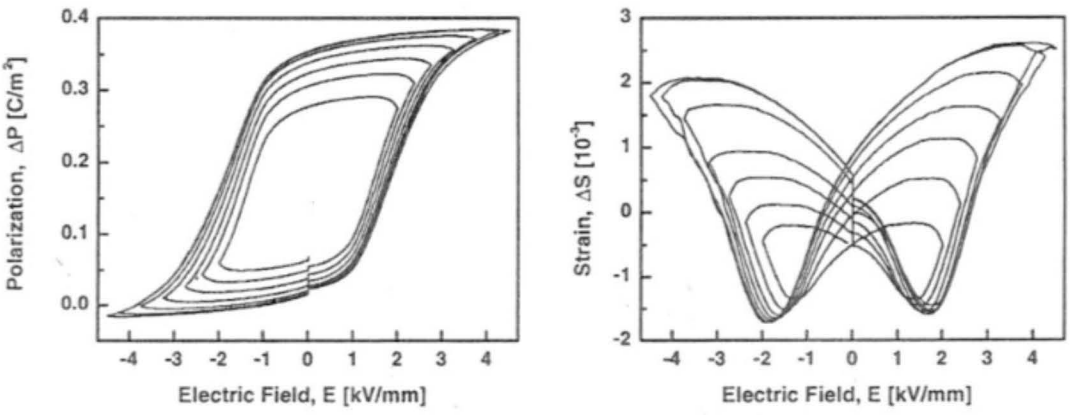

Fig. 2.8 *Post-fatigue hysteresis ($2x10^7$ cycles at $2E_C$) with E_{app} decreasing from 4 to 2 E_c taken from [25].*

Thermal annealing post fatigue was shown to be quite affective, yielding a maximum of 70% recovery of P_r under testing field levels after annealing 500°C for 1hr[25]. Higher temperatures yielded no greater change. In this case micro-cracking is one likely possible explanation for the remaining unrecovered losses.

From general observations of the degree of anisotropy in the strain hysteresis, a significant amount of information can be inferred. Large anisotropy is found in both the y and z-direction. Here, the axes are defined relative to applied fields matching those used in fatigue, i.e. the z direction. The defects acting as pinning mechanisms involved in the fatigue process must themselves be highly oriented within the bulk. It was found that fatigue is affecting specific domains for certain orientations of grains relative to the applied field.

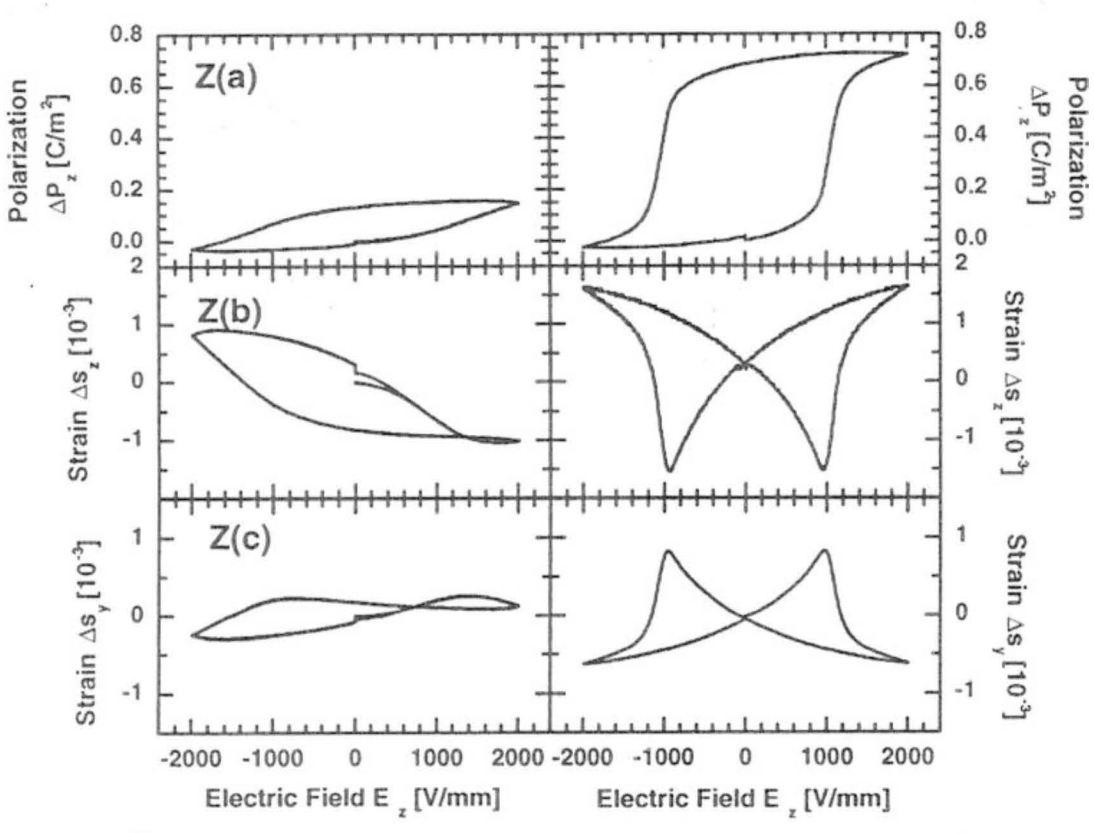

Fig. 2.9 *Polarization and strain after fatigue of 2x10⁷ cycles (left) and before fatigue (right) when fields are applied parallel to the fatigue direction (z-axis) taken from [25]*

In Figure 2.9 above it can be seen that maximum polarization, P_{Max} decreases by ~78.5% upon completion of $2x10^7$ cycles. Strain along the z-axis is also severely degraded and significant asymmetry has developed to the point where the hysteresis loses almost all of the characteristic butterfly shape seen in the right column.

After the measurements in the z- and y-directions were completed, the electrodes were ground off and reapplied and measurements were made along the x or y directions. It can be seen that polarization and strain hysteresis were symmetric with values nearing 80% and 70%, respectively, of the initial measurements along the original z direction (shown in Figure 2.10 for the new perpendicular electrode configuration, i.e. the "3" direction now being along the y-axis). The asymmetries associated with fatigue can still be observed, however, when measuring strain in the z-axis with respect to applied field in the y-axis.

This was similar to what was found in previous work with bulk PLZT (7/62.5/37.5) where the z-axis polarization hysteresis was found to decrease by approximately 75%, but the value was found to be virtually unaffected when new electrodes were created along the y-axis [31, 32].

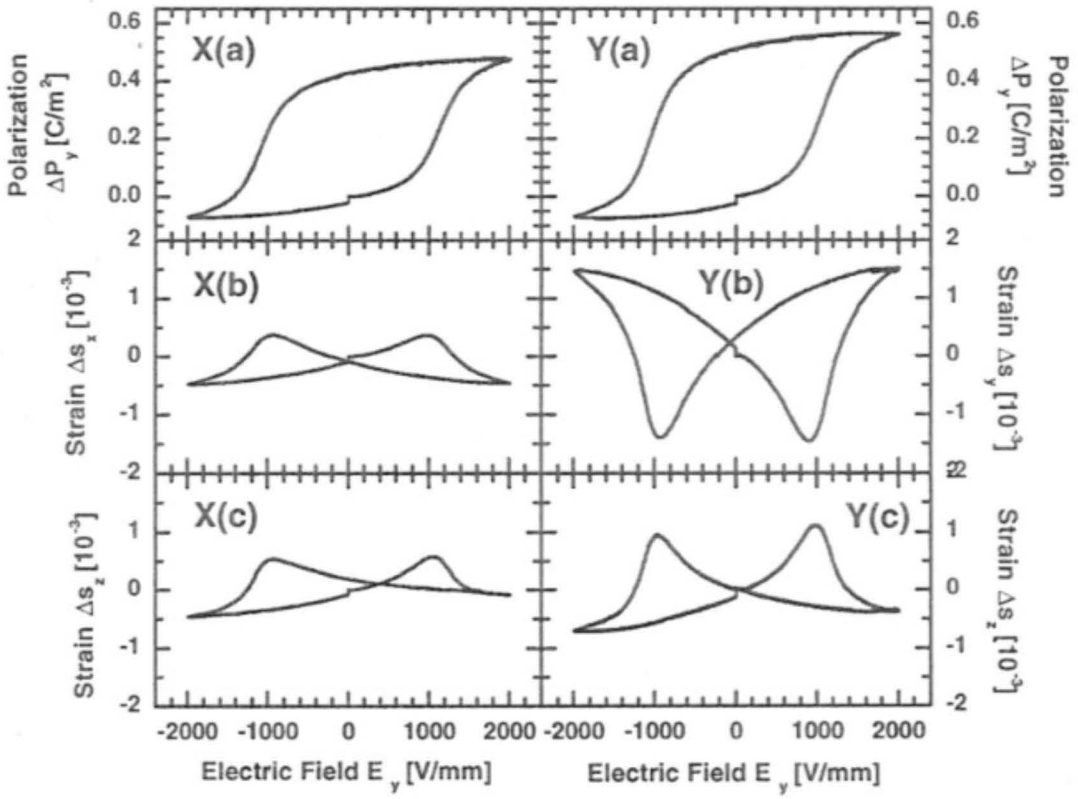

Fig. 2.10 *Polarization and strain after fatigue (2x10⁷ cycles) when fields are applied to new electrodes located normal to the fatigue direction taken from [25]*

From this it can be said that 90° domain switching is relatively unaffected by fatigue for both directions perpendicular to the cycling applied field, which is shown in regions X(c) and Y(c) in Figure 2.10 above. This shows that not all domains are participating in the fatigue of the switching process and that process is highly oriented based on the direction of the applied field used. Fatigue is being limited to a fraction of domains that are strongly affected by the applied field in a given grain.

2.6.2 Point Defect Agglomeration

"Screening, internal, and offset" fields and polarizations are all terms that have been used before to describe similar, internal field effects in materials [25]. But differences between motions and offsets of electronic and ionic carriers and their effects on piezoelectric properties exist and the terms need to be further clarified. Some of these terms have meanings that still allow domains to switch and only modifies the external applied field, while others will act to pin, clamp or 'freeze' domain motion. An offset polarization can only be said to have formed when the orientation of the effected domains is not random, for example. Shur *et al.* were the first to give a model for a volume fraction of non-switchable polarization, albeit without attributing a microscopic cause [33, 34]. The development of this hard agglomerates theory can also explain the restoration of polarization with higher applied fields if the agglomerates are represented as very largely increased, but not insurmountable, activation energies for domain switching. Lupascu proposed that the agglomerating species were oxygen vacancies and that the growth process was irreversible. The mean distance that oxygen vacancies travel within a single grain's lattice at room temperature is 100 nm after fatigue measurements, which is sufficient for the proposed agglomeration effect [25].

It is also reasonable to suppose that the grain boundaries become partially conducting due to diffusion of the Ag electrodes in to the bulk. Oxygen vacancies are drawn under applied electric fields and act to further weaken the predominantly PbO boundaries structurally. In the sample interior a lack of conduction paths means that charged defects agglomerate to planar structures inside the grains. This in turn causes the reduction of mobility of domain walls in the samples. Once a few of the ionic species

are gathered along the same plane, they act as a 180° domain boundary. Figure 2.11 represents one such domain within a single grain of polycrystalline PZT. Normally, oxygen vacancies within the domain do not have the necessary energy to move themselves to join the agglomerate. In Figure 2.11 b) the applied field is against the depolarizing field setup by the agglomerate. The growth process of these domains occurs especially rapidly under bipolar field conditions when the external applied field adds to the depolarizing field from the accumulated charged species, as seen in Figure 2.11 c). Note that the oxygen vacancy, $V_O^{\bullet\bullet}$, still move to the edges of the agglomerate so that growth is along the plane and it is not thickened in the direction parallel to the applied field.

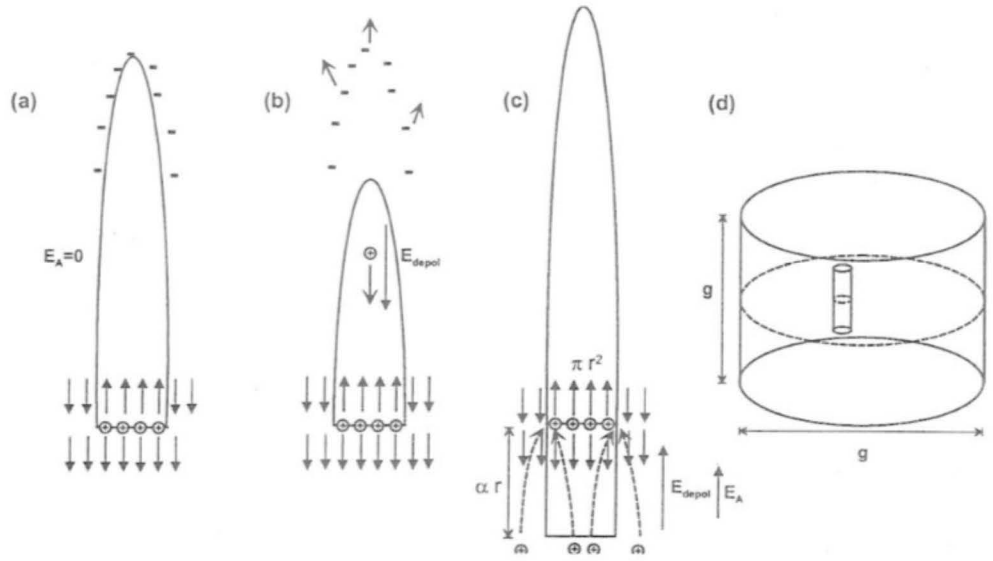

Fig. 2.11 *A 180° domain with an existing agglomerate(+) and space charges(-) and a) no applied field (b) downward pointing applied field (c) upward pointing applied field aligned with dipole field acts to grow of the agglomerate in-plane, and (d) the agglomerate capture range within a cylinder grain with dimensions, d, h= "g" taken from [25]*

The angle between defect agglomerates was observed via SEM (when etched with a HF/HCl solution for 60 seconds) to be on the {100} planes in the perovskite structure. From the agglomerate, any 90° domains that form will be 35.3° from it, or 54.7° in the rhombohedral case [25]. This results in a shear stress exerted on these domains, which given large enough agglomerates can force a shift from a rhombohedral to a tetragonal domain as observed via SEM after fatigue and as seen below in Figure 2.12.

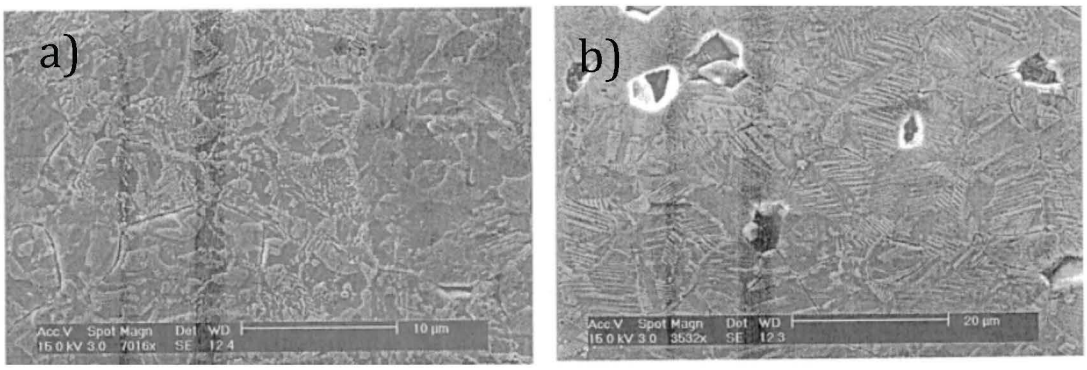

Fig. 2.12 *SEM images of domain structure a) before fatigue is rhombohedral and b) post-fatigue is tetragonal taken from [25]*

This switch from rhombohedral to tetragonal domains was shown to originate in the center of the samples and grow with increased fatigue cycling duration (at $2E_C$). Entire sample cross-sections were observed to have 100% conversion from rhombohedral to tetragonal-like domains [35]. This even includes regions directly under the electrodes, although transformation in this region seemed to have happened to a lower degree and at a later point in the fatigue process. Another possible explanation for domain transformation includes an increased ionization of local defects yielding a breakup of

larger domains into smaller ones [25]. Regardless, the domain structure is seen to be changing entirely upon completion of fatigue. It has also been shown via Atomic Force Microscopy imaging that a change from predominantly 180° domain walls to a dense 90° domain system with needle-like domains extending across the entire sample can be observed, as shown below in Figure 2.13. This is evidence of locking the domains and could explain the lack of domains fully switching after the corresponding 180° domain growth portion of the strain hysteresis loop, where 90° domains should form to enable switching.

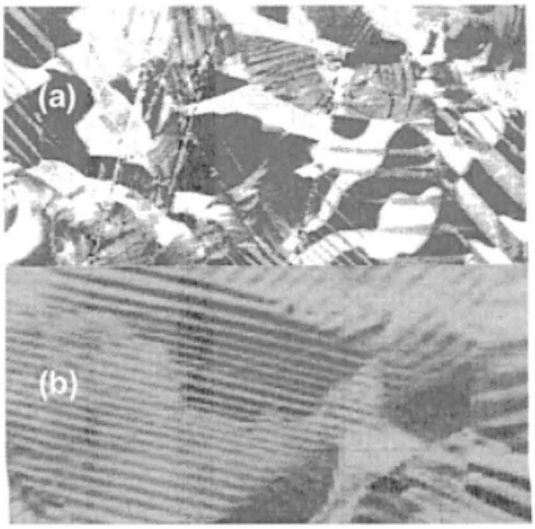

Fig. 2.13 *AFM images showing domain structure a) before and b) after 10^8 cycles of bipolar fatigue at $2E_C$ taken from [36]*

2.6.3 Unipolar Fatigue

For PZT samples, the effect of unipolar fatigue appears to be somewhat different than that seen in bipolar fatigue. In general, the loss of maximum polarization (-11%) and maximum strain (-4%) under unipolar fields after 10^9 cycles is lower than the losses in the bipolar case [37]. For bipolar measurements of these samples before and after fatigue, it has been observed that there is a less drastic change in symmetry for strain hysteresis, as seen in Fig. 2.14 b) and d). In fact, for this bipolar measurement there is a true reduction of strain only during negative applied fields. The positive applied field actually increases the observed strain. For the bipolar polarization hysteresis, very little change is observed.

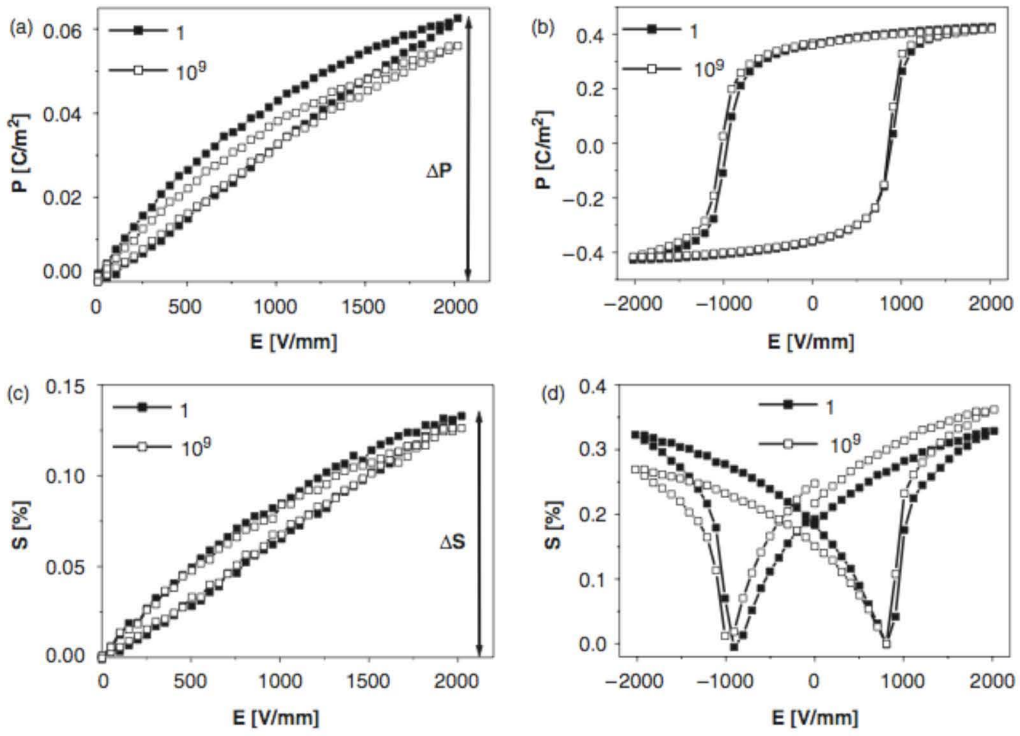

Fig. 2.14 *Unipolar and bipolar P-E (a,c) and S-E (b,d) hysteresis loops after initial and 10^9 cycles of unipolar fatigue taken from [38]*

The asymmetry developed in the strain seems to indicate the formation of a bias "poling" due to the cycling, which is similar to the bipolar case. It was posited that these slight decreases are due to a reduction of 180° domain switchability, but there does not seem to be a true degradation, just an imprint from an offset polarization. This effect is also different from the aforementioned offset field, which these samples also experienced. The offset field can be seen through the shift in the final bipolar measurements along the field axis as well, although it is somewhat minor in the polarization hysteresis here. Unipolar effects will be further explored in lead free systems for this project.

2.7 Lead-Free Perovskite Piezoelectrics

2.7.1 (K,Na)NbO_3-Based Systems

The KNN-based materials have been successfully modified using various A and B cations to enhance its piezoelectric properties, in some cases to levels approaching those of PZT. A pseudo ternary system was first formed between KNN, $LiTaO_3$, and $LiSbO_3$ by researchers at Toyota Inc in 2004 [39, 40]. That composition, $(K_{0.44}Na_{0.52}Li_{0.04})(Nb_{0.84}Ta_{0.10}Sb_{0.06})O_3$ was subsequently designated LF4 by the authors. For ease of use it will be referred to as LF4-1 throughout this work. It's Curie temperature was found to be T_C = 253°C and a plot of this along with a simple phase

diagram indicating d_{33} values can be found in Figure 2.15. In the textured case especially, but also in untextured LF4-1, it is seen that this new piezoelectric approaches comparable properties with PZT.

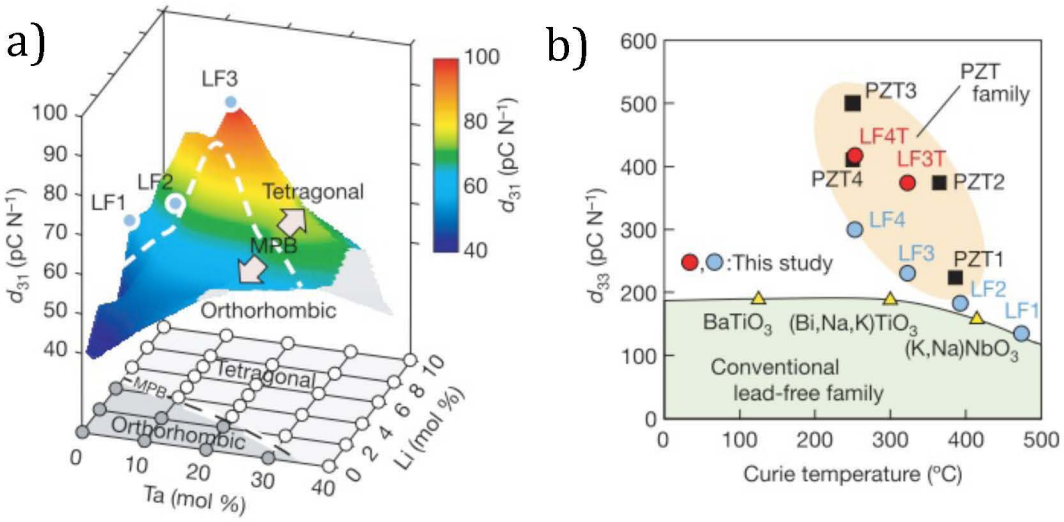

Fig. 2.15 *a) KNN-modified phase diagram showing piezoelectric properties and b) plotting current known piezoelectrics using Curie point versus d_{33} taken from [39]*

Several similar compositions have been investigated including those with only $LiTaO_3$ added, some with $AgTaO_3$, and some modified by $Ag(Sb_xTa_{1-x})O_3$ [41-43]. Although these all feature enhanced properties compared to KNN, this work is focused to optimal compositions found using only the six main cations found in the original LF4.

One such similar composition was independently developed with only very minor differences found in the amount of Ta and Sb added ($(K_{0.44}Na_{0.52}Li_{0.04})(Nb_{0.86}Ta_{0.10}Sb_{0.04})O_3$) and is referred to here as LF4-2 (T_C=326°C) [44]. Another study maintained constant amounts of the B-site cation and studied the effect of

the ratio of K to Na, which when optimized gave yet another similar composition of $(K_{0.38}Na_{0.58}Li_{0.04})(Nb_{0.91}Ta_{0.05}Sb_{0.04})O_3$ or LF4-3 (with T_C = 336°C) [45]. From these formulae it becomes apparent that changes in the ratio Nb:Sb results in a dramatic change in the Curie point. These compositions properties are summarized in Table 2.3 below.

Table 2.3 *Summary of previously optimized LF4 compositions compared to a commercially available PZT data summarized from [39, 44, 45]. *textured ceramic*

	PZT	LF4-1*	LF4-2	LF4-3
d_{31} [pC/N]	170	152	96	NA
d_{33} [pC/N]	410	416	NA	306
k_p	0.6	0.61	0.28	0.48
Curie Point [°C]	250	253	326	336

Further studies on LF4-2 compositions included doping with CuO and Fe_2O_3, with CuO showing enhanced sintering and better dielectric loss characteristics [44, 46]. Some secondary $K_4CuNb_8O_{23}$ phase was observed via X-ray diffraction (XRD) measurements. The best properties and came from dopant levels of 0.2 wt% CuO [44].

While these enhanced properties are well documented, there is very little research published regarding the effects of piezoelectric fatigue for lead-free ceramics in general and LF4 (KNN-based) materials in particular. Most currently published data shows enhanced fatigue-free behavior for bismuth layered structures, while simple perovskite materials have yet to be explored [47]. One other study has shown significant

improvement of fatigue properties for KNN when doped with $CaTiO_3$, but testing was limited to only 10,000 cycles in duration [48].

2.7.2 $(Bi_{0.5}Na_{0.5})TiO_3$ -$(Bi_{0.5}K_{0.5})TiO_3$ Solid Solutions:

Many other Pb-free piezoelectric reports have focused on Bi-based perovskites because Bi^{3+} has a similar electronic configuration to Pb^{2+} [49, 50]. Compounds such as $(Bi_{0.5}K_{0.5})TiO_3$ (BKT) and $(Bi_{0.5}Na_{0.5})TiO_3$ (BNT), and their solid solutions together or with $BaTiO_3$ have shown excellent piezoelectric properties as well [3, 4, 51-58].

Bismuth sodium titanate, BNT, has long been considered an excellent candidate to replace Pb-based materials, and BNT - related solid solutions have been studied extensively [4, 59, 60]. BNT has long been referenced as having a rhombohedral structure at room temperature with the transition from rhombohedral to tetragonal phase occurring at approximately 300 °C. The Curie temperature for BNT is 540 °C. Although it shows a relatively high remanent polarization P_r=38 μC/cm^2, unfortunately this can only be achieved at very high applied fields. This limitation of its pure state is necessarily tied to its extremely large coercive field, E_c = 73 kV/cm. This makes effective poling of BNT ceramics and subsequent large values for low field d_{33} quite challenging to obtain.

Bismuth potassium titanate, BKT, is another well-known non-lead ferroelectric with the perovskite structure. It has a tetragonal symmetry with a=0.391 nm and c=0.399 nm at room temperature and shows a relatively high Curie temperature,

T_c=380°C [61]. However a common problem reported with BKT, its poor sinterability, makes obtaining dense ceramic samples difficult when using conventional ceramic fabrication processes. Like BNT, extremely large applied fields are needed to achieve saturation in the polarization hysteresis. In hot pressed samples, saturation was found at E_{app}>100 kV/cm, which yielded a fairly large P_{max} = 33 and a P_r = 22.2 μC/cm^2. The coercive field for these materials, while lower than BNT, is still unsuitably large at 52.5 kV/cm [51].

As Figure 2.16 from Hiruma indicates, a morphotropic phase boundary (MPB) can be achieved when the rhombohedral and tetragonal perovskite phases are combined to form the BNT-BKT system [54]. This somewhat mimics the behavior of PZT, where the piezoelectric properties are optimized near the MPB composition of about 18-20 mol% of BKT added, but is not as stable with temperature. This system highlights the major advantage found when using BNT in solid solutions, namely that an MPB is relatively easily created when solid solutions are made with other perovskite materials with tetragonal symmetry such as $PbTiO_3$, $BaTiO_3$, and BKT [20].

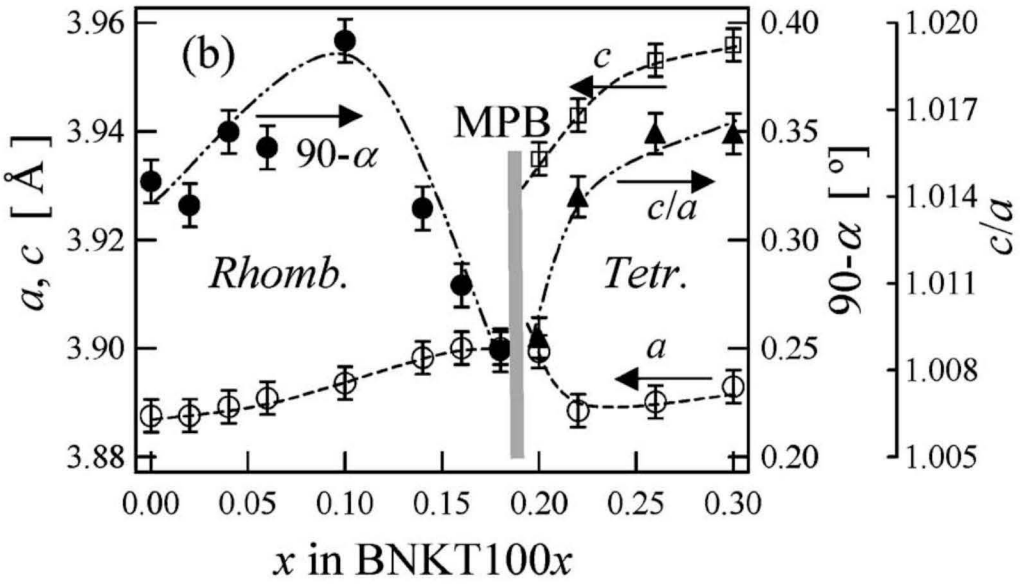

Fig. 2.16 *Binary phase diagram of xBKT-(1-x)BNT, taken from [60].*

The electrical properties of the BNT–BKT binary solid solution change significantly depending on the crystal structure of the system, as can be seen from the changes in width and height of the polarization hysteresis loops in Figure 2.17 [62]. The highest remanent polarization was found to be 38 $\mu C/cm^2$ at the MPB composition of 20 mol% of BKT. The compositions with tetragonal structure showed lower coercive field compared to rhombohedral, which makes sense because BKT itself has a generally lower coercive field. Piezoelectric properties are enhanced with d_{33} coefficients as high as 167 pC/N and coupling coefficient, k_{33}, as high as 0.56 [60]. Hiruma *et al.* have also investigated compositions the ternary system $(Bi_{0.5}K_{0.5})TiO_3$ (BKT) - $(Bi_{0.5}Na_{0.5})TiO_3$ (BNT) - $Bi_{0.5}Li_{0.5})TiO_3$ (BLT) [59, 60] in order to further improve these properties.

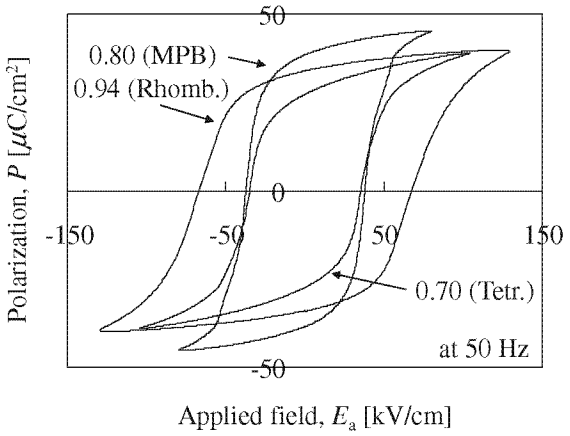

Fig. 2.17 *Hysteresis loops of (0.94, 0.8, 0.7) BNT – (0.06, 0.2, 0.3) BKT at RT taken from [51]*

2.7.3 $(Bi_{0.5}K_{0.5})TiO_3$ - $Bi(Zn_{1/2}Ti_{1/2})O_3$ Solid Solutions:

Another method of affecting the piezoelectric properties of BKT is to make solutions with other perovskite compounds that are normally unstable on their own at room temperature. In solutions with BKT, tolerance factors between 0.99 and 1.01 can be achieved when mixing with $Bi(Zn_{1/2}Ti_{1/2})O_3$, BZT.

The decision to investigate BZT was based on both theoretical and early experimental work on this system. The initial first principle calculations used the Density Functional Theory (DFT) methodology on BZT and found it to be highly tetragonal [63]. This led to Suchomel, *et al.* to prepare bulk samples of this material using high pressure (6GPa and 900°C for 1 hour) sintering that was followed by quenching. Intact dense bodied ceramics resulted and had lattice parameters found to be a = 3.82190(3)A and c =

4.62803(7)A. These completely phase pure materials give a c/a ratio as the highest observed for any d^0 B site Pb or Bi based perovskite [50]. No change in phase or microstructure was observed after a 400°C anneal. Powder and pellets were found to be stable up to 550°C via *in situ* synchrotron XRD with only slight changes in c/a ratio [50]. Above this, it was shown to decompose into bismuth titanate and other minor non-perovskite impurity phases. At the time of the initial publication there was no direct evidence of ferroelectricity in the system on its own, although it was somewhat implied by the structural results and dielectric data. This was mostly likely due to the fact that it can be nearly impossible to achieve a polarization hysteresis loop on such highly polarized materials due to the extraordinarily high switching fields required to reach the abnormally large coercive field of high c/a ratio materials. This is especially true in bulk ceramics. However, these strongly polarized materials can be suitable for enhancing tetragonality in single phase solid solutions with other perovskites. The $s^2/(d^{10}/d^0)$ cation combination in the $Bi(B'_{0.5}B''_{0.5})O_3$ perovskite structure allows for unusual coordination geometries that enhance polarization in the bulk and will be used in enhancing other lead-free binary and ternary solid solution perovskites.

Utilizing BZT in such a way allows it to be produced as a single phase by the simple mixed oxide route used for most ceramics. Huang *et al.* first reported the structure and electrical properties of (1-x) $(Bi_{1/2}K_{1/2})TiO_3$ - x $Bi(Zn_{1/2}Ti_{1/2})O_3$ solid solutions, or BKT – BZT [51, 61].It was also shown that forming a solid solution with BZT made large improvements to the density, dielectric, and piezoelectric properties of BKT, much like previous work in the BNT-BKT system [51, 54].

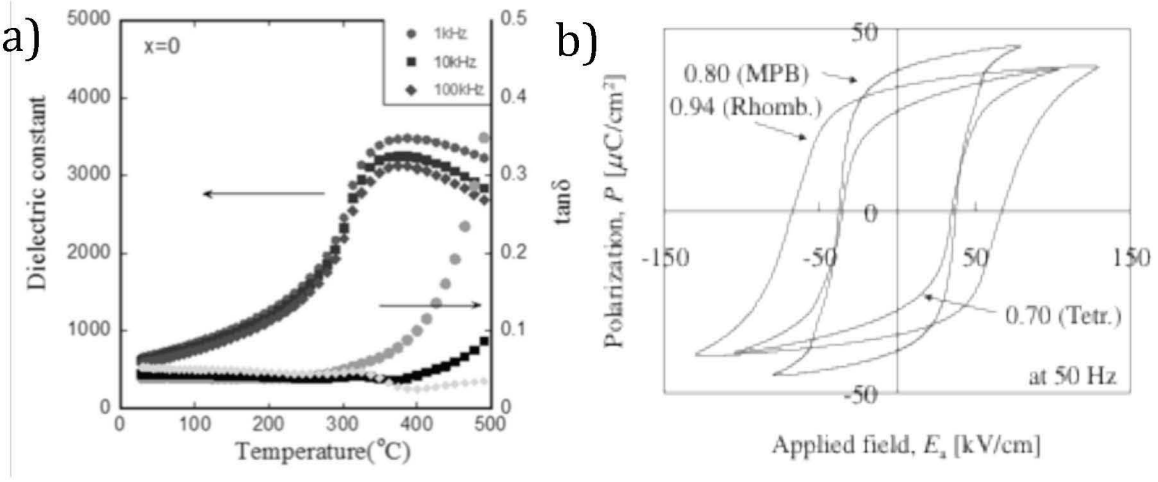

Fig. 2.18 *Dielectric properties of a) pure BKT (left) and b) 0.9 BKT – 0.1 BZT (right) taken from [61]*

X-ray diffraction of these BKT – BZT samples shows single phase, tetragonal symmetry were obtained for all samples up to a discovered solubility limit of 20 mol% BZT. Figure 2.18 shows the dielectric properties of pure BKT and 0.9 BKT – 0.1 BZT as a function of the temperature and frequency. Upon the addition of 10% BZT, the maximum dielectric constant increased and the dielectric spectra was broadened and shifted to the left (i.e. the T_C was lowered to ~300°C).

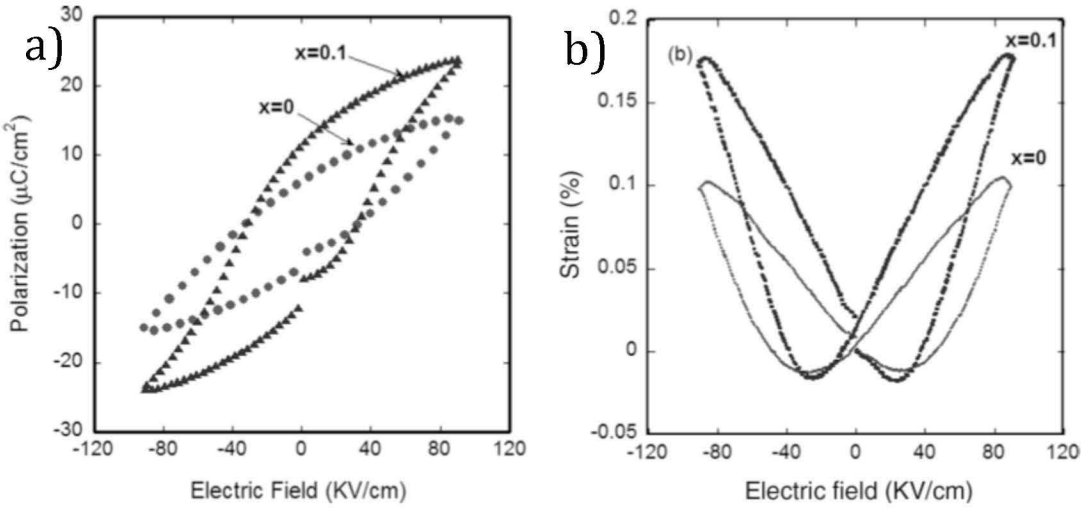

Fig. 2.19 *a) PE loops and b) strain hysteresis of pure BKT and 0.9 BKT – 0.1 BZT taken from [61]*

Figure 2.19 shows a comparison of P-E and S-E hysteresis loops between these same compositions. The P-E loops for both compositions were not fully saturated even at high applied fields (E_{app}>80 kV/cm). The remanent polarization P_r increased significantly from 6.1 μC/cm² to 11.8 μC/cm², but was not as high as in the BNT-BKT case [61]. The expected butterfly-shaped strain loops were observed with relatively low amounts of negative strain. Compared to pure BKT, the maximum strain of the 10% BZT material was significantly improved, matching the maximum and remanent polarization increases seen in the polarization hysteresis. Like in the KNN-based LF4 system very little work has yet been completed to understand the long-term reliability of the electrical properties of these systems.

2.8 References:

[1] R. E. Newnham, *Properties of Materials: Anisotropy, Symmetry, Structure*. Oxford, 2005.

[2] K. C. Kao, *Dielectric Phenomena in Solids*: Elsevier, 2004.

[3] V. A. Isupov, "Ferroelectric Na0.5Bi0.5TiO3 and K0.5Bi0.5TiO3 Perovskites and Their Solid Solutions," *Ferroelect. Review,* vol. 315, pp. 123-147, 2005.

[4] T. R. Shrout and S. J. Zhang, "Lead-free piezoelectric ceramics: Alternatives for PZT?," *J. Electroceram,* vol. 19, pp. 111-124, 2007.

[5] P. Curie, Curie, J, "Development by Pressure of Polar Electricity in Hemihedral Crystals with Inclined Faces," *Bulletin de la Societe Mineralique de France,* vol. 3, p. 90, 1880.

[6] S. O. Kasap, *Electronic materials and Devices*. New York: McGraw-Hill, 2002.

[7] A. Hussain, *et al.*, "Large electric-field-induced strain in Zr-modified lead-free Bi0.5(Na0.78K0.22)0.5TiO3 piezoelectricceramics," *Sens. Actuators, A,* vol. 158, pp. 84-89, 2010.

[8] B. Jaffe, Cook, W.R., and Jaffe, H., *Piezoelectric Ceramics*. New York: Academic Press, 1971.

[9] J. Valasek, "Piezo-Electric and Allied Phenomena in Rochelle Salt," *Physical Review,* vol. 17, p. 475, 1921.

[10] V. K. Pecharsky, Zavalij, P.Y. , *Fundamentals of Powder Diffraction and Structure Characterization of Materials*. Boston: Kluwer Academic, 2003.

[11] A. J. Moulson and J. M. Herbert, *Electroceramics: Materials, Properties, Applications*. Hoboken, NJ: John Wiley & Sons, Ltd., 2005.

[12] M. Ozgul, Trolier-Mckinstry, S., and Randall, C.A., "Fatigue induced effects on bipolar strain loops in PZN-PT piezoelectric single crystals," *J. Electroceram,* vol. 20, pp. 133-138, 2008.

[13] H. Sahota, "Simulation of butterfly loops in ferroelectric materials," *Coninuum Mech. Thermodyn.,* vol. 16, pp. 163-175, 2004.

[14] A. S. Bhalla, Guo, R., Roy, R., "The perovskite structure - a review of its role in ceramic science and technology.," *Material Research Innovatioins,* vol. 4, pp. 3-26, 2000.

[15] R. E. Cohen, "Origin of ferroelectricity in perovskite oxides," *Nature,* vol. 358, pp. 136-138, 1992.

[16] B.-q. Qin, *et al.*, "Preparation and Characterization of (1-x) BiInO<inf>3-xPbTiO3 ceramics," in *Applications of Ferroelectrics, 2007. ISAF 2007. Sixteenth IEEE International Symposium on*, 2007, pp. 616-617.

[17] A. A. Belik, *et al.*, "BiInO3: A Polar Oxide with GdFeO3-Type Perovskite Structure," *Chemistry of Materials,* vol. 18, pp. 1964-1968, 2006.

[18] R. Guo, *et al.*, "Origin of the High Piezoelectric Response in PbZr1-xTixO3," *Physical Review Letters,* vol. 84, p. 5423, 2000.

[19] V. M. Goldschmidt, *Naturwissenschaften* vol. 14, p. 477, 1926.

[20] R. E. Eitel, Randall, C.A., Shrout, T.R., Rehrig, P.W., Hackenberger, W., and Park, S.E., "New High Temperature Morphotropic Phase Boundary Piezoelectrics Based on Bi(Me)O3-PbTiO3 Ceramics," *Jpn. J. Appl. Phys.,* vol. 40, pp. 5999-6002, 2001.

[21] A. Halliyal, *et al.*, "Stability of Perovskite Phase in Pb(Zn1/3Nb2/3)O3and Other A(b'b'')O3Perovskites," in *Applications of Ferroelectrics. 1986 Sixth IEEE International Symposium on*, 1986, pp. 437-441.

[22] N. Wakiya, *et al.*, "Thermal stability of Pb(Zn1/3Nb2/3)O3 (PZN) and consideration of stabilization conditions of perovskite type compounds," *Materials Research Bulletin,* vol. 30, pp. 1121-1131, 1995.

[23] O. Muller, Roy, R., *The Major Ternary Structural Families,* . New York: Springer-Verlag, 1974.

[24] T. R. G. A. Halliyal, U. Umar and A. Safari, *IEEE 6th International Symposium on Application of Ferroelectrics,* vol. 437, 1986.

[25] D. C. Lupascu, *Fatigue in Ferroelectric Ceramics and Related Issues* vol. 61. Berlin: Springer, 2004.

[26] W. L. Warren, Dimos, D., Tuttle,, B.A., Pike, G.E., Schwartz, R.W., Clews, P.J. an dMcINtyre, D.C., "Polarization suppression in Pb(Zr,Ti)O3 thin films," *J. Appl. Phys.,* vol. 77, pp. 6695-6701, 1995.

[27] J. L. Nuffer, D.C., and Rodel, J., "Damage evolution in ferroelectric PZT induced by bipolar electric cycling.," *Acta. Mater.,* vol. 48, pp. 3783-3794, 2000.

[28] E. L. Colla, Tagantsev, A.K., Taylor, D.V., an dKholkin, A.L., "Fatigued state ofPt-{PZT}-PT system. ," *Integrated Ferroelectrics,* vol. 29, pp. 145-148, 1995.

[29] E. L. Colla, Taylor, D.V., Tagantsev, A.K., and Setter, N. , "Discrimination between bulk and interface scenarios for the suppression of the switchable polarization (fatigue) in Pb(Zr,Ti)O3 thin fims capacitors with Pt electrodes.," *Appl. Phys. Lett.,* vol. 72, pp. 2478-2480, 1998.

[30] C. Verdier, Lupascu, D.C., and Rodel, J., "Stability of defects in lead-zirconate-titanate after unipolar fatigue," *Appl. Phys. Lett.,* vol. 81, pp. 2596-2598, 2002.

[31] W. Pan, Yue, C.F., and Tosyali, O., "Fatigue of Ferroelectric Polarization and the Electric Field Induced Strain in Lead Lanthanum Zirconate Titanate Ceramics," *J. Am. Ceram. Soc.,* vol. 75, pp. 1534-1540, 1992.

[32] W. Pan, Yue, C.F., and Tuttle, B.A., "Ferroelectric Fatigue in modified bulk lead zirconate titanate ceramics and thin films," *Ceramic Transactions, Ferroelectric Films,* vol. 25, pp. 358-397, 1992.

[33] V. Y. Shur, Rumyantsev, E.L., Nikolaeva, E.V., Shishkin, E.I. and Baturin, I.S. , "Kinetic Approach to fatigue phenomena in ferroelectrics," *J. Appl. Phys.,* vol. 90, pp. 6312-6315, 2001.

[34] V. Y. Shur, Rumyantsev, E.L., Nikolaeva, E.V., Shishkin, E.I., Baturin, I.S., Ozgul, M., and Randall, C.A. , "Kinetics of fatigue effect," *Integrated Ferroelectrics,* vol. 33, pp. 117-132, 2001.

[35] J. F. Scott, "Fatigue as a phase transition.," *Integrated Ferroelectrics,* vol. 38, pp. 125-133, 2001.

[36] D. C. Lupascu, Rabe, U., "Cyclic cluster growth in ferroelectric perovskites," *Phys. Rev. Lett.,* vol. 89, p. 187601, 2002.

[37] N. Balke, Lupascu, D.C., Granzow, T., and Rodel, J., "Fatigue of Lead Zirconate Titanate Ceramics I: Unipolar and DC Loading," *J. Am. Ceram. Soc.,* vol. 90, pp. 1081-1087, 2007.

[38] N. Balke, Lupascu, D.C., Granzow, T., and Rodel, J., "Fatigue of Lead Zirconate Titanate Ceramics II: Sesquipolar Loading," *J. Am. Ceram. Soc.,* vol. 90, pp. 1088-1093, 2007.

[39] Y. Saito, *et al.*, "Lead-free piezoceramics," *Nature,* vol. 432, pp. 84-87, 2004.

[40] Y. Saito, *et al.*, "High Performance Lead-free Piezoelectric Material," *R&D Review of Toyota CRDL,* vol. 41, pp. 22-28, 2004.

[41] S. Zhang, *et al.*, "Piezoelectric properties in perovskite 0.948(K0.5Na0.5)NbO3-0.052LiSbO3 lead-free ceramics," *J. Appl. Phys.,* vol. 100, pp. 104108-1-6, 2006.

[42] Y. Wang, *et al.*, "Microstructure, dielectric, and piezoelectric properties of (Li, Ag, Ta) modified (K0.50Na0.50)NbO3 lead-free ceramics with high Curie Temperature," *J. Appl. Phys.,* vol. 102, pp. 054101-1-5, 2007.

[43] J. Wu, *et al.*, "Microstructure and electrical properties of (Li, Ag, Ta, Sb)-modified (K0.50Na0.50)NbO3 lead-free ceramics with good temperature stability," *J. Phys. D: Appl. Phys. ,* vol. 41, pp. 125405-1-6, 2008.

[44] E. Li, *et al.*, "Influence of CuO on the Structure and Piezoelectric Properties of the Alkaline Niobate-Based Lead-Free Ceramics," *J. Am. Ceram. Soc.,* vol. 90, pp. 1787-1791, 2007.

[45] J. Wu, *et al.*, "Effects of K/Na ratio on the phase structure and electrical properties of (KxNa0.96-xLi0.004)(Nb0.91Ta0.05Sb0.04)O3 lead-free ceramics," *Appl. Phys. Lett.,* vol. 91, pp. 252907-1-3, 2007.

[46] R. Zuo, *et al.*, "Dielectric and piezoelectric properties of Fe2O3-doped (Na0.5K0.5)0.96Li0.04Nb0.86Ta0.1Sb0.04O3 lead-free ceramics," *Journal of Physics and Chemistry of Solids,* vol. 69, pp. 1728-1732, 2008.

[47] Y. Ding, Liu, J.S., Qin, H.X., Zhu, J.S., and Wang, Y.N., "Why lanthanum-substituted bismuth titanate becomes fatigue free ferroelectric capacitor with platinum electrodes," *Appl. Phys. Lett.,* vol. 78, pp. 4175-4177, 2001.

[48] S. Zhang, *et al.*, "Mitigation of thermal and fatigue behvior in K0.5Na0.5NbO3-based lead free piezoceramics," *Appl. Phys. Lett.,* vol. 92, pp. 152904-1-3, 2008.

[49] P. S. Baettig, C.F., LeSar, R., Waghmare, U.V., and Spaldin, N.A., "Theoretical Prediction of New High-Performance lead-Free Piezoelectrics," *Chem. Mater.,* vol. 17, pp. 1376-1380, 2005.

[50] M. R. Suchomel, *et al.*, "Bi2ZnTiO6: A lead-free closed-shell polar perovskite with a calculated ionic polarization of 150 mu C cm(-2)," *Chemistry of Materials,* vol. 18, pp. 4987-4989, Oct 2006.

[51] Y. Hiruma, Aoyagi, R., Nagata, H. and Takenaka, T., "Ferroelectric and Piezoelectric Properties of (Bi1/2K1/2)TiO3 Ceramics," *Jpn. J. Appl. Phys.,* vol. 44, pp. 5040-5044, 2005.

[52] M. Nemoto, Nagata, H., Hiruma, Y., and Takenaka, T., "Fabrication and Piezoelectric Properties of Grain Oriented (Bi1/2K1/2)TiO3-BaTiO3 Ceramics," *Jpn. J. Appl. Phys.,* vol. 47, pp. 3829-3832, 2008.

[53] R. Ranjan, Dviwedi, A. , "Structure and dielectric properties of (Na0.50Bi0.50)1-xBaxTiO3: 0x0.10," *Sol. State Commun. ,* vol. 135, pp. 394-399, 2005.

[54] S. Zhao, Li, G., Ding, A., Wang, T., Yin, Q., "Ferroelectric and piezoelectric properties of (Na,K)0.5Bi0.5TiO3 lead free ceramics. ," *J. Phys. D: Appl. Phys.,* vol. 39, pp. 2277-2281, 2006.

[55] S. Zhang, Shrout, T.R., Nagata, H., Hiruma, Y., Takenaka, T. , "Piezoelectric properties in (K0.5Bi0.5)TiO3-(Na0.5Bi0.5)TiO3-BaTiO3 lead-free ceramics," *IEEE Trans. Ultrason. Ferroelectr. Freq. Control,* vol. 54, pp. 910-917, 2007.

[56] H. Nagata, Yoshida, M., Makiuchi, Y. and Takenaka, T., "Large Piezoelectric Constant and High Curie Temperature of Lead-Free Piezoelectric Ceramic Ternary System Based on Bismuth Sodium Titanate-Bismuth Potassium Titanate-

Barium Titanate near the Morphotropic Phase Boundary," *Jpn. J. Appl. Phys.,* vol. 42, pp. 7401-7403, 2003.

[57] T. Takenaka, Nagata, H., Hiruma, Y. , "Current Developments and Prospective of Lead-Free Piezoelectric Ceramics," *Jpn. J. Appl. Phys.,* vol. 47, pp. 3787-3801, 2008.

[58] T. Takenaka, Nagata, H., and Hiruma, Y., "Phase Transition Temperatures and Piezoelectric Properties of (Bi1/2Na1/2)TiO3-(Bi1/2K1/2)TiO3-Based Bismuth Perovskite Lead-Free Ferroelectric Ceramics," *IEEE Trans. Ultrason. Ferroelectr. Freq. Control* vol. 56, pp. 1595-1612, 2009.

[59] Y. Hiruma, Watanabe, T., Nagata, H. and Takenaka, T., "Piezelectric Properties of (Bi1/2Na1/2)TiO3-Based Solid Solutions," *Jpn. J. Appl. Phys.,* vol. 47, pp. 7659-7663, 2008.

[60] Y. Hiruma, Yoshii, K., Nagata, H., Takenaka, T., "Phase transition temperature and electrical properties of (Bi1/2Na1/2)TiO3-(Bi1/2A1/2)TiO3 (A=Li and K) lead-free ferroelectric ceramics.," *J. Appl. Phys.,* vol. 103, pp. 084121: 1-7, 2008.

[61] C. C. Huang, Naratip, V, Cann, D.P. , "Structure and ferroelectric properties of Bi(Zn(1/2)Ti(1/2))O3-(Bi(1/2)K(1/2))TiO3 perovskite solid solutions," *IEEE Trans. Ultrason. Ferroelectr. Freq. Control,* vol. 56, pp. 1304-1308, 2009.

[62] K. Yoshii, Hiruma, Y, Nagata, H., Takenaka, T., "Electrical properties and depolarization temperature of (Bi1/2Na1/2)TiO3-(Bi1/2K1/2)TiO3 lead-free piezoelectric ceramics.," *Jap. J. Appl. Phys. Part 1,* vol. 45, pp. 4493-4496, 2006.

[63] T. Qi, *et al.*, "First-principles investigation of the highly tetragonal ferroelectric material Bi(Zn_{1/2}Ti_{1/2})O_{3}," *Physical Review B,* vol. 79, p. 094114, 2009.

3 Materials and Methods

3.1 Materials Synthesis

For all samples prepared conventional solid-state synthesis methods were used. The general process flow consisted of 5 main steps. First six hours of high-energy vibratory milling was used for mixing the raw oxide or carbonate powders together. After drying these powders, high temperature calcination reactions were performed in alumina crucibles. Calcination temperatures were decided based on either processing known from previous literature, or they were determined empirically, with a starting point based on known reaction temperatures for binary or ternary end members and phase diagrams of the component materials. Post calcination, the powders were milled, as before, for six hours in order to obtain a fine particle size and then dried for at least 12 hours. For both milling steps, ethanol based slurries of ~15 vol% powder were used with cylindrical, high-density yttrium stabilized zirconia (YTZ) media (TOSOH corporation).

The calcined powders were next mixed with a 3 wt% solution of either Polyvinyl Butyral (PVB) or Paraloid (PL) binder, and then were uniaxially cold pressed into 12.7 mm pellets at a pressure of 150 MPa. Finally, following a 3 hour 400°C binder burnout, the pellets were sintered in sacrificial powders inside covered crucibles.

X-ray diffraction was used for phase identification between 20°–80° 2θ on polished sintered pellets (Bruker AXS D8 Discover). Additionally for compositions of the ternary BZT-BNT-BKT system, unpolarized Raman spectra were excited with the 514.5 nm line of an Ar laser and recorded with a Renishaw inVia micro-Raman spectrometer. The spectra were corrected to the Bose–Einstein temperature factor.

3.1.1 (K,Na)NbO_3 Based Systems:

For the compositions investigated in the KNN system, $(K_{0.44}Na_{0.52}Li_{0.04})(Nb_{0.84}Ta_{0.10}Sb_{0.06})O_3$ (LF4-1), $((K_{0.44}Na_{0.52}Li_{0.04})(Nb_{0.86}Ta_{0.10}Sb_{0.04})O_3)$ (LF4-2), and $(K_{0.38}Na_{0.58}Li_{0.04})(Nb_{0.91}Ta_{0.05}Sb_{0.04})O_3$ (LF4-3) were produced using starting powders of at least 99.9% purity ($LiCO_3$, $NaCO_3$, KCO_3, Nb_2O_5, Ta_2O_5, and Sb_2O_5). Calcinations were performed in covered crucibles at 780°C for 4 hours (LF4 - 1 and 2) or 850°C for 6 hours (LF4 -3). Sintering was done at 1135°C for 2 hours (LF4-1 and 2) or 1100°C for 3 hours (LF4-3). For subsequent fatigue testing of $(K_{0.44}Na_{0.52}Li_{0.04})(Nb_{0.86}Ta_{0.10}Sb_{0.04})O_3$ (LF4-2) and $((K_{0.44}Na_{0.52}Li_{0.04})(Nb_{0.86}Ta_{0.10}Sb_{0.04})O_3)$ + 0.2 wt% CuO were produced via the calcination method described above for LF4-2. The sintering was changed for LF4-2 + 0.2 wt% CuO to 1100°C for 3 hours.

3.1.2 Bi-based Systems

Ternary compositions of xBZT–0.4BKT–(0.6-x)BNT for x = 0.025, 0.05, 0.1, 0.15, and 0.20 were produced using starting powders (Bi_2O_3, TiO_2, ZnO, $NaCO_3$, and KCO_3) of >99.9% purity. Calcinations were performed in covered crucibles at 900–950°C for 6 hours. Sintering was performed at 1050–1100°C for 4 hours. These same conditions were used to make the x = 0.025 and 0.05 samples used in separate fatigue experiments.

Binary compositions based on $(1-x)(Bi_{0.5}Na_{0.5})TiO_3$-$xBi(Zn_{1/2}Ti_{1/2})O_3$ for x = 0.02, 0.04, 0.06, and 0.08 were likewise created using high purity (>99.9%) Bi_2O_3, $NaCO_3$, ZnO,

and TiO_2 powders as precursors. They were calcined at 900-975°C for 6 hours. Pellets were sintered at 1050-1100°C for 2-8 hours, with temperatures decreasing and time increasing as mol% BZT was increased.

3.2 Electrical Testing

Prior to electrical measurements, samples were polished to sub-millimeter thickness with smooth and parallel surfaces. Silver paste (Heraeus C1000) was fired on both sides in air at 650°C for 30 minutes. An Agilent 4284A LCR meter was used to measure the dielectric properties for a wide variety of frequencies and temperatures using a high temperature measurement cell (NorECS Probostat). Polarization hysteresis measurements were made using a Sawyer-Tower circuit-based system (Radiant Technology Premier II utilizing Vision software). Strain hysteresis measurements were taken with the same system in conjunction with an MTI Instruments 2100 Fotonic Sensor. When DC bias poling was needed, voltages were applied at elevated temperatures in a Si oil bath using a Delta 9023 (Delta Designs Inc) environmental chamber in the configuration shown in Fig. 3.1. High voltage was applied once the temperature of the oil had reached the set point temperature and was held typically for 30minutes. The voltage maintained until the chamber was cooled to at least 35°C.

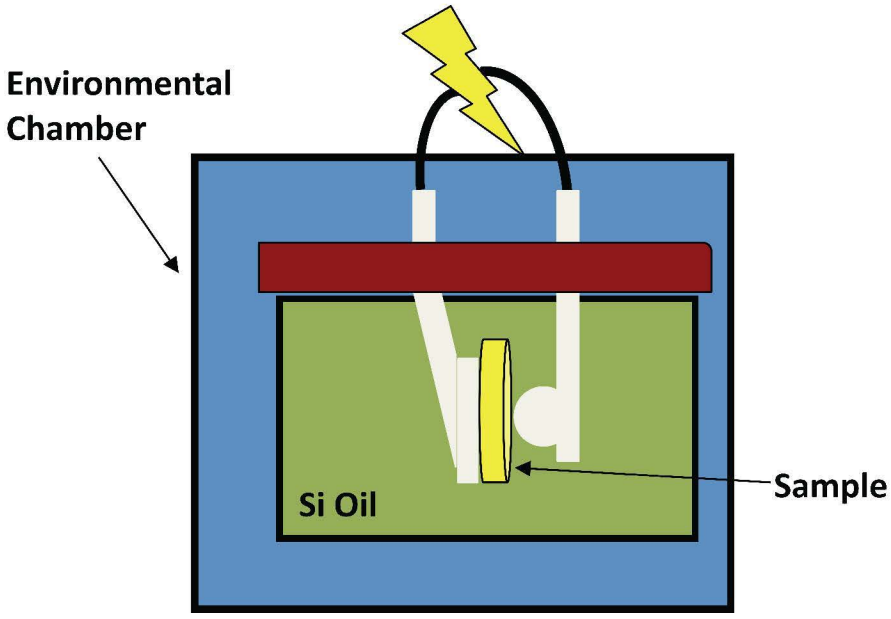

Fig. 3.1 *High temperature DC bias poling schematic*

3.3 Fatigue Testing

3.3.1 (K,Na)NbO_3 Based Systems:

For poling, dc biases of 40 kV/cm were used at room temperature for 10 minutes (LF4-2) or at 100°C for 30 minutes (LF4 + 0.2 wt% CuO). Unipolar fatigue effects were measured using a repeating triangular waveform applied in the same direction as that of the dc bias used in poling, at 10Hz or 50 Hz for either 18 kV/cm or 36 kV/cm ($1E_C$ and $2E_C$, respectively) for LF4-2 and 16 kV/cm or 30 kV/cm ($2E_C$ and $3E_C$, respectively) for LF4-2 + 0.2 wt% CuO. Fatigue testing was run for various cycle lengths ($1x10^5$, $1x10^6$, or $1x10^7$) with unipolar hysteresis measurements taken at every decade. Additionally, bipolar hysteresis measurements were taken before and after the fatigue of the CuO doped samples at multiple field levels.

3.3.2 Bi-based Systems

For the Bi-based ternary samples, the fatigue testing was performed on unpoled samples by applying a 10Hz bipolar triangular waveform at 50 kV/cm on both the 0.025 and 0.05 BZT samples. Additional testing was performed on 0.05BZT at $2E_C$ (20 kV/cm). The fatigue tests performed in this study were carried out under bipolar conditions because, as mentioned in the literature review, bipolar cycling results in more severe degradation of the polarization and electromechanical strain compared to unipolar cycling.

These tests were chosen to highlight any differences in fatigue behavior across the transition in behavior from "normal" ferroelectric response at 2.5%BZT, to the high electromechanical strain response of 5% BZT. The 2.5% BZT was tested at a field level of 50 kV/cm which amounts to approximately $2E_C$. These testing conditions are equivalent to fatigue tests carried out on PZT in order to allow for a basic comparison. The 5% BZT composition was tested at two different field levels, 20 kV/cm and 50 kV/cm. Since this material exhibits unconventional hysteresis behavior, these two field levels were chosen to provide different modes of comparison. The 20 kV/cm test is nominally equivalent to $2E_C$, although it is not fully accurate to define a coercive field in this way as it does not represent full switching in a conventional sense. Additionally, the fatigue test was carried out at 50 kV/cm so that a direct comparison could be made to 5%BZT composition. All three fatigue tests were carried out on three identical specimens and the results for each testing condition were very similar in each case.

4 Dielectric and Piezoelectric Properties of (K,Na)NbO_3-based Piezoelectric Ceramics

Eric A. Patterson and David P. Cann

Materials Science, School of Mechanical, Industrial and Manufacturing Engineering

Oregon State University

Corvallis, OR 97331

Published in July 2011 in

Journal of Advanced Dielectrics

Vol. 1, No. 3 (2011) 345-349

4.1 Abstract

Solid solutions based on Li, Ta, and Sb-doped $(K_{0.5}Na_{0.5})NbO_3$ (KNN) lead-free perovskite systems were created using standard solid state methods. X-ray diffraction was used to confirm that all compositions were single phase and to verify the phase transition from tetragonal to cubic at T_C = 302°C. The three compositions examined, originally developed by Y. Saito and E. Li, were shown to be strongly ferroelectric with sharp peaks in permittivity present at the Curie temperature. The optimum composition had loss tangent values below five percent up to 100 kHz at room temperature. Bipolar hysteresis measurements showed high values for both maximum polarization (25 and 21 μC/cm^2) and remanent polarizations (20 and 16 μC/cm^2) for undoped and 0.2 wt% CuO doped samples. Maximum strain values of greater than 0.23 percent were observed.

Key words: lead-free systems, piezoelectricity, dielectric, perovskite, ferroelectrics

4.2 Introduction

While lead-based piezoelectrics, primarily consisting of lead-zirconate-titanate (PZT) currently hold exemptions from European Union environmental standards, including RoHS, WEEE, and ELV, they can not be expected to be extended indefinitely. Therefore,

the search for lead-free alternatives to PZT has been of increased interest as companies endeavor to reduce their environmental impact.

Recent research in Pb-free piezoelectrics has been focused on a few commonly studied ferroelectric systems. The most common systems involve a binary system includes $(Bi_{0.5}K_{0.5})TiO_3$ (BKT), $(Bi_{0.5}Na_{0.5})TiO_3$ (BNT), or $(K_{0.5}Na_{0.5})NbO_3$ (KNN) combined with another perovskite end member of the form ABO_3, such as $BaTiO_3$ [*1, 2*]. The KNN-based materials have been successfully modified using various A and B cations to enhance their properties to levels approaching those of PZT. A pseudo-ternary was first formed between KNN, $LiTaO_3$, and $LiSbO_3$ by Saito *et al.* in 2004 [*3*]. That composition, $(K_{0.44}Na_{0.52}Li_{0.04})(Nb_{0.84}Ta_{0.10}Sb_{0.06})O_3$ was subsequently designated LF4 by the authors and for simplicity will be hereafter referred to as LF4-1. It's Curie point was found to be T_C = 253°C.

Several similar compositions have been investigated including those with only $LiTaO_3$ added, some with $AgTaO_3$, and some modified by $Ag(Sb_xTa_{1-x})O_3$ [*4-6*]. Although these all feature enhanced properties compared to KNN, the present study is limited to the compositions previously optimized in the literature, which approached the piezoelectric properties of PZT using only the six cations found in LF4-1.

Another similar composition was independently developed with slight differences found in the amount of Ta and Sb added ($(K_{0.44}Na_{0.52}Li_{0.04})(Nb_{0.86}Ta_{0.10}Sb_{0.04})O_3$) and is referred to here as LF4-2 (T_C =326°C) [*7*]. Different levels of CuO doping were studied for this composition, with enhanced sintering and a softening effect shown at CuO concentrations near 0.2 wt%. The final study investigated as focused on the effect of

K/Na ratio on the A-site, which when optimized gave $(K_{0.38}Na_{0.58}Li_{0.04})(Nb_{0.91}Ta_{0.05}Sb_{0.04})O_3$ or LF4-3 (with T_C = 336°C) [*8*]. From these formulae it becomes apparent that changes in the ratio Nb:Sb resulted in a dramatic change in the Curie point. The properties of these compositions are summarized below in Table 4.1 along with those of a commercially available PZT.

Table 4.1 *Summary of previously optimized LF4 compositions compared to a commercially available PZT, $[(Pb_{0.85}Ba_{0.15})_{0.9925}La_{0.005}]x(Zr_{0.52}Ti_{0.48})O_3$ [3, 7, 8].*

	PZT	LF4-1*	LF4-2	LF4-3
d_{31} (pC/N)	170	152	96	N/A
d_{33} (pC/N)	410	416	N/A	306
k_p	0.6	0.61	0.28	0.48
Curie T (°C)	250	253	326	336
Reference	Y. Saito	Y. Saito	E. Li	J. Wu

*Data represents measurements on textured ceramics

Further studies on LF4 compositions included doping with CuO, Fe_2O_3, or co-doping pure KNN with La_2O_3 and Fe_2O_3 to improve sintering in low pressure conditions and all showed an increase in piezoelectric coefficient [*7, 9, 10*]. Doping LF4-2 with CuO showed vastly improved sintering and better dielectric loss characteristics. Some secondary $K_4CuNb_8O_{23}$ phase, however, was previously observed via X-ray diffraction (XRD) measurements [*7*].

4.3 Experimental Method

All compositions (LF4-1, LF4-2, LF4-3) were reproduced via conventional solid-state synthesis methods. This includes using starting powders of at least 99.9% purity ($LiCO_3$, $NaCO_3$, KCO_3, Nb_2O_5, Ta_2O_5, and Sb_2O_5). Six hours of high energy vibratory milling was used for mixing and post-calcination grinding. Ethanol solutions of 15 vol% powder were used with high density YSZ media (corporation) during milling. Calcinations were performed in covered crucibles at 780°C for 4 hours (LF4 - 1 and 2) or 850°C for 6 hours (LF4 -3).

The calcined powders were mixed with a 3 wt% solution of Paraloid binder, and then were uniaxially cold pressed into 12.7 mm pellets at a pressure of 150 MPa. Following a 400°C binder burnout, the pellets were sintered in covered crucibles at 1135°C for 2 hours (LF4 - 1 and 2) or 1100°C for 3 hours (LF4 -3 and LF4-2 + CuO). A Bruker-AXS D8 x-ray diffractometer was used for phase identification in the 2θ scan range of 20°-80° for sintered pellets.

Prior to electrical measurements, samples were polished to sub-millimeter thickness with smooth and parallel surfaces. Silver paste (Heraeus C1000) was fired on both sides in air at 650°C for 30 minutes. An Agilent 4284A LCR meter was used to measure the dielectric properties for a wide variety of frequencies and temperatures using a high temperature measurement cell (NorECS Probostat). Hysteresis measurements were made using a Radiant Technology measurement set-up utilizing Vision software. Strain

hysteresis was also recorded using an interferometer probe in conjunction with the top electrode surface of the Radiant sample holder.

4.4 XRD and Dielectric Characterization

X-ray diffraction studies confirmed that all compositions exhibited the perovskite structure with no evidence of secondary phases to the detection limits of the instrument. Tetragonal symmetry was observed in all three cases with well-defined (00l) peak splitting, as seen in Fig. 4.1. Minimal peak shifting was observed between the various compositions. Additionally, when LF4-2 was synthesized with 0.2 wt% CuO added as a dopant to aid sintering. No secondary phases were observed within the limits of x-ray diffraction, despite previous reports to the contrary.

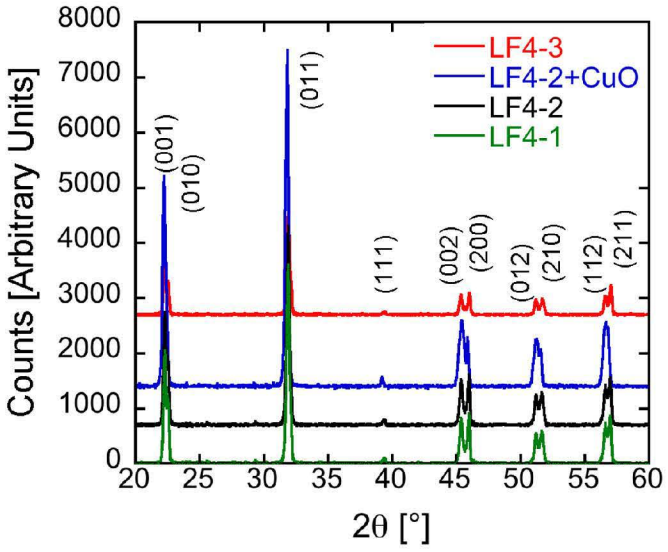

Fig. 4.1 *XRD data showing single-phase perovskite structure for all LF4 compositions investigated.*

In Fig. 4.2, the relative permittivity and loss tangent are shown for all three undoped LF4 compositions examined (at 10kHz). All exhibit strong ferroelectric behavior with sharp, well-defined peaks in permittivity at the Curie point, T_C. In all three cases, the Curie temperature was found to be slightly lower than the published values by varying degrees. A further slight downward shift to 302°C was observed upon the addition of 0.2 wt% CuO to LF4-2.

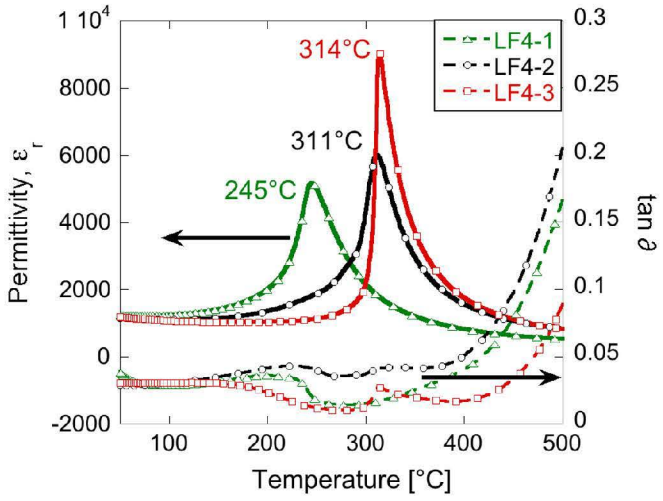

Fig. 4.2 *Dielectric properties of all three undoped LF4 compositions at 10 kHz*

Pure KNN has a T_C = 420°C and the compositional modifications in all three compounds shifts this downward depending upon the Nb content [4]. The compositions LF4-2 and LF4-3 have a significantly higher T_C (~311°C and ~314°C respectively) than LF4-1 due to their higher concentrations of Nb. All the compositions have room temperature permittivities close to 1200 and tan d values below 0.05 at room temperature. The lowest values of dielectric loss were those of LF4-2, so all further experiments were focused on this composition including the addition of CuO.

A more detailed plot of frequency dependence of the dielectric properties is shown for LF4-2 and LF4-2 with 0.2 wt% CuO in Fig. 4.3. The frequency dependence of the dielectric loss at room temperature data is plotted as an inset as well to emphasize the low loss values over a wide range of frequencies (tan d < 0.05 up to 100 kHz).

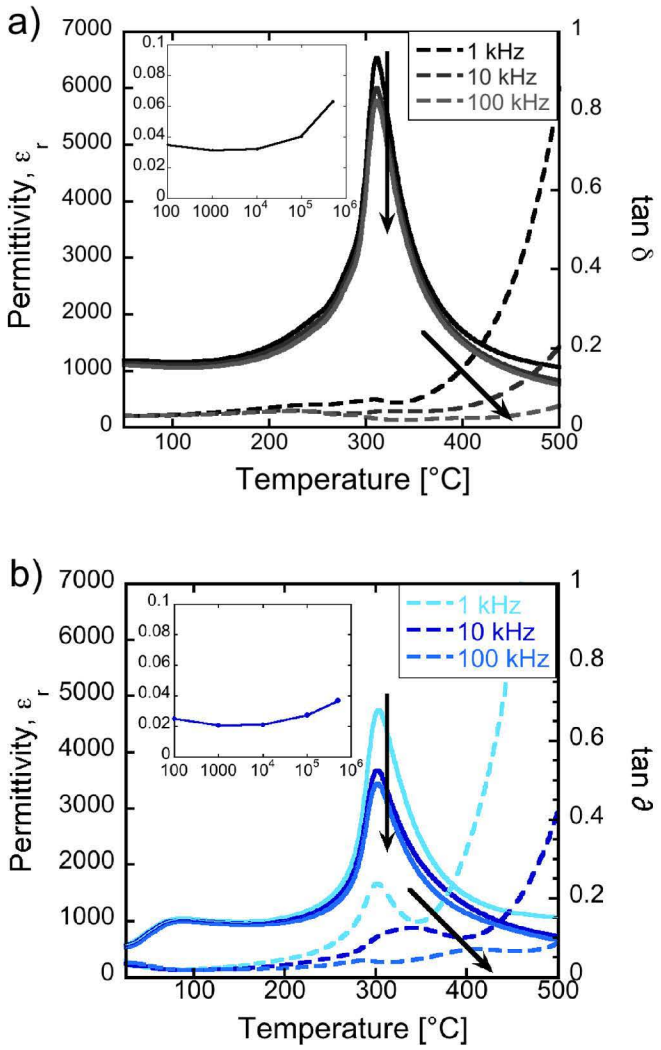

Fig. 4.3 *Frequency dependence of ε_r (solid lines) and tan d (dotted lines) as a function of temperature a) LF4-2 and b) LF4-2 + 0.2wt% CuO with arrows indicating increasing frequency. In both Figs., the inset shows tan d values at room temperature as function of frequency.*

The transition from tetragonal to cubic was further characterized for the CuO doped ceramics by XRD as a function of temperature. The collapse in the peak splitting is clearly observed at 300°C for both the (002) and (012) peaks as highlighted in Fig. 4.4 below.

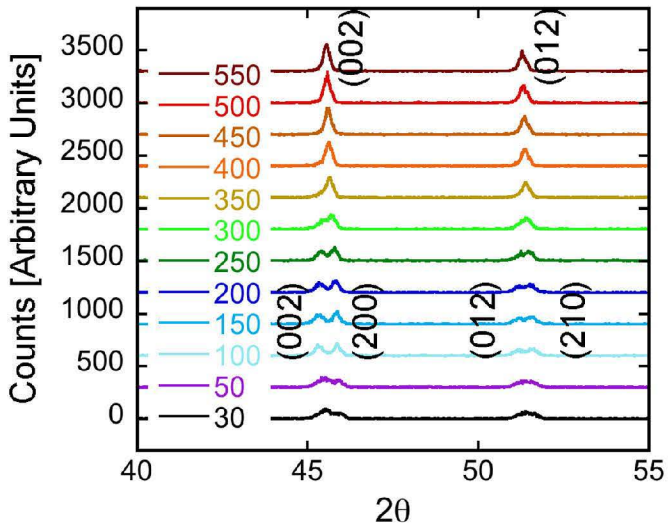

Fig. 4.4 *XRD vs. Temperature for LF4-2 + 0.2 wt% CuO with transition between tetragonal and cubic phase occurring at 300°C*

4.5 Piezoelectric Characterization

Polarization hysteresis loops measured at 1 Hz for LF4-2 ceramics show well-defined loops characteristic of a ferroelectric material with some degree of pinching that is a characteristic feature of the hysteresis behavior in many of the previously published results. The P_{MAX} for these samples was approximately 25 μC/cm² with the remanent polarization $P_r \sim 20$ μC/cm² as seen in Fig. 4.5. The coercive field for this specimen was approximately 18 kV/cm.

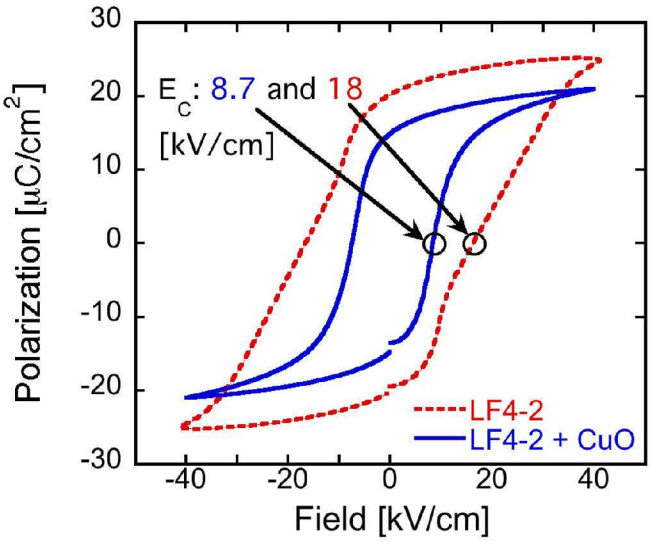

Fig. 4.5 *Typical bipolar hysteresis at 1 Hz for LF4-2 and LF4-2 +CuO with E_C highlighted*

The coercive field was dramatically reduced when CuO was added to the system, with $E_C \sim 8.7$ kV/cm. The loops are highly saturated though the maximum polarization was somewhat reduced compared to the undoped compositions. The various ferroelectric properties derived from the polarization hysteresis measurements, as well as low field piezoelectric properties are summarized in Table 2 and compared to those available in the literature for these compositions. The addition of CuO acts to make the samples more "hard" with the mechanical quality factor, Q_m, more than doubling. There is a corresponding decrease in the planar coupling coefficient, k_p, from 0.132 to 0.103 with the addition of CuO.

Table 4.2 *Summary of piezoelectric properties of optimized compositions compared to literature values [7]*

	LF4-2*	LF4-2	+CuO	+CuO*
P_{MAX} (μC/cm²)	22	25	21	20
P_r (μC/cm²)	17	20	15	16
E_C	36	16.5	8-10	25
k_p	-	0.132	0.103	-
Q_m	26	46.0	109.9	137

**Indicates data observed by E. Li, et al.*

Next, increasing field levels were applied (between 20 to 60 kV/cm) to CuO doped samples for both polarization and the corresponding strain hysteresis measurements as shown in Fig. 4.6.

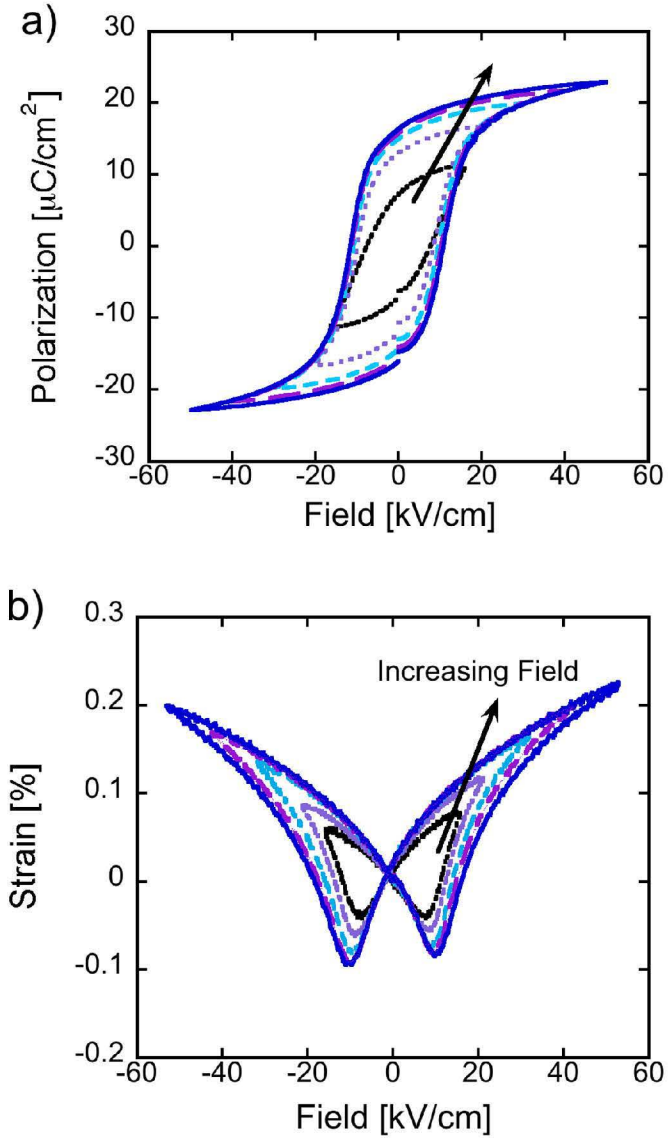

Fig. 4.6 *Typical bipolar hysteresis for a) polarization at 1 Hz and b) electromechanical strain at 0.1 Hz for LF4-2 + 0.2 wt% CuO under increasing applied fields. At 50 kV/cm, the effective d_{33}* was 450 pm/V.*

Highly symmetric butterfly-shaped strain loops were observed at all frequencies. Maximum strains of up to 0.23% were seen, in conjunction with high field d_{33}* values of

450-600 pm/V depending on applied field levels. Values of low field d_{33}, however, were found to range from 167-182 pC/N for samples poled under dc bias of 40 kV/cm at 100°C for 30 minutes. While these are smaller than the previously reported 416 pC/N of LF4-1 ceramics under unique texturing processing methods, they are still high compared to other known lead-free systems. It is also important to note that poling conditions are well-known for commercial PZT samples and yield d_{33} values that range anywhere from 400-600 pC/N depending on the use of hard and soft dopants [*3*]. Optimization of the poling conditions may enhance the low-field d_{33} values for the (K,Na)NbO_3-based ceramics in this study.

4.6 Conclusions

Single phase perovskite ceramics were synthesized for three variations of the lead-free (K,Na)NbO_3-based LF4 piezoelectric material. Analysis of their dielectric properties revealed strong ferroelectric behavior with T_C values similar to those previously published. For LF4-2, dielectric loss values were below 0.05 for frequencies up to 100 kHz. Ferroelectric hysteresis measurements showed remanent polarizations of 16 and 20 μC/cm^2 and maximum polarization values of 21 and 25 μC/cm^2 for LF4-2 plus CuO and LF4-2, respectively. The addition of a relatively small amount of 0.2 wt% CuO had the dramatic effect of decreasing E_C to approximately 8-10 kV/cm. These results match the mixed A and B site doping proposed in the work of Li, *et al.* [*7*]. The substitution of Cu into the A site acts to reduce oxygen vacancies and lower the coercive field, but the B site replacement makes the samples more "hard" with increased Q_m and decreased k_p values.

In general, the high field d_{33}^* (500-600 pm/V) and S_{Max} (~0.23%) values for these samples are very promising for future use in actuator devices.

4.7 Acknowledgements

The authors would like to thank Dr. Peter Mardilovich from Hewlett-Packard Co for his helpful comments.

4.8 References

1. V. A. Isupov, "Ferroelectric Na0.5Bi0.5TiO3 and K0.5Bi0.5TiO3 Perovskites and Their Solid Solutions," *Ferroelect. Review,* **315** 123-47 (2005).

2. T. R. Shrout and S. J. Zhang, "Lead-free piezoelectric ceramics: Alternatives for PZT?," *J. Electroceram,* **19** 111-24 (2007).

3. Y. Saito, H. Takao, T. Tani, T. Nonoyama, K. Takatori, T. Homma, T. Nagaya, andM. Nakamura, "Lead-free piezoceramics," *Nature,* **432** 84-87 (2004).

4. S. Zhang, R. Xia, T. R. Shrout, G. Zan, andJ. Wang, "Piezoelectric properties in perovskite 0.948(K0.5Na0.5)NbO3-0.052LiSbO3 lead-free ceramics," *J. Appl. Phys.,* **100** 104108-1-6 (2006).

5. Y. Wang, J. Wu, D. Xiao, J. Zhu, Y. Jin, J. Zhu, P. Yu, L. Wu, andX. Li, "Microstructure, dielectric, and piezoelectric properties of (Li, Ag, Ta) modified (K0.50Na0.50)NbO3 lead-free ceramics with high Curie Temperature," *J. Appl. Phys.,* **102** 054101-1-5 (2007).

6. J. Wu, D. Xiao, Y. Wang, W. Wu, B. Zhang, J. Zhu, Z. Pu, andQ. Li, "Microstructure and electrical properties of (Li, Ag, Ta, Sb)-modified (K0.50Na0.50)NbO3 lead-free ceramics with good temperature stability," *J. Phys. D: Appl. Phys.* , **41** 125405-1-6 (2008).

7. E. Li, H. Kakemoto, S. Wada, andT. Tsurumi, "Influence of CuO on the Structure and Piezoelectric Properties of the Alkaline Niobate-Based Lead-Free Ceramics," *J. Am. Ceram. Soc.,* **90**[6] 1787-91 (2007).

8. J. Wu, D. Xiao, Y. Wang, J. Zhu, L. Wu, andY. Jiang, "Effects of K/Na ratio on the phase structure and electrical properties of (KxNa0.96-xLi0.004)(Nb0.91Ta0.05Sb0.04)O3 lead-free ceramics," *Appl. Phys. Lett.,* **91** 252907-1-3 (2007).

9. R. Zuo, Z. Xu, andL. Li, "Dielectric and piezoelectric properties of Fe2O3-doped (Na0.5K0.5)0.96Li0.04Nb0.86Ta0.1Sb0.04O3 lead-free ceramics," *Journal of Physics and Chemistry of Solids,* **69**[7] 1728-32 (2008).

10. K.-I. Kakimoto, I. Masuda, andH. Ohsato, "Solid-Solution Structure and Piezoelectric Property of KNbO3 Ceramics Doped with Small Amounts of Elements," *Jap. J. Appl. Phys.,* **43**[9B] 6706-10 (2004).

5 Piezoelectric properties and unipolar fatigue behavior of KNN-based Pb-free piezoceramics

Eric A. Patterson and David P. Cann

Materials Science, School of Mechanical, Industrial and Manufacturing Engineering

Oregon State University

Corvallis, OR 97331

Published in September 2011 in

IEEE Transactions on Ultrasonics, Ferroelectrics, and Frequency Control

Vol. 58, No. 9, (2011) 1835-1841

5.1 Abstract

Single phase perovskite ceramics were synthesized of a Pb-free $(K_{0.44}Na_{0.52}Li_{0.04})(Nb_{0.86}Ta_{0.10}Sb_{0.04})O_3$ (LF4) piezoelectric material both with and without CuO as a dopant additive. Bipolar hysteresis measurements showed a relatively high remanent polarization (20 μC/cm², 16 μC/cm²) and maximum polarization (25 μC/cm², 21 μC/cm²) values were found for both undoped LF4 and 0.2 wt% CuO doped LF4 respectively. Unipolar fatigue behavior for this system was found to decrease strongly with increased applied testing fields and increased test durations. For undoped LF4, the maximum polarization values were stable after 10 cycles after testing for 100,000 cycles duration. For the CuO doped samples, increasing the testing field to $3E_C$ resulted in twice the decrease in P_{MAX} (-32%) compared to the $2E_C$ tests at 10^6 cycles (-17%). At $2E_C$ testing for CuO doping, polarization decreases continually through 10^7 cycles with the decreases in P_{MAX} and d_{33} both reaching a maximum (-22% and -30% respectively) after 10^7 cycles. In the CuO doped samples, the fatigue is exacerbated due to the influence of space charge on the increased number of defects present.

5.2 Introduction

Piezoelectric ceramics, particularly $PbZr_{1-x}Ti_xO_3$ (PZT), are the most widely used for key components in a wide variety of device applications, such as in underwater sonar systems, medical ultrasonic transducers, actuators for fuel injection, printers or positioning systems, pneumatic valves, gas igniters, and transformers [1, 2]. Lead-based piezoelectrics currently hold exemptions from all major European Union environmental

standards, including RoHS, WEEE, and ELV; they are not expected to be excluded indefinitely. These same regulations were in a large part responsible for driving the development of the Pb-free solders that are currently in use throughout the electronics industry. Therefore, the search for lead-free alternatives to lead-zirconate titanate (PZT) has been of increasing interest and gaining more attention as companies endeavor to reduce the impact of their products on the environment. In addition to the environmental reasons, PZT is also known to exhibit quite poor piezoelectric fatigue properties with relatively severe degradation in strain behavior after only a few millions of cycles of applied field [3-9].

Recent research in Pb-free piezoelectrics has been focused on a few commonly studied ferroelectric systems. The most common systems involve a binary system, which typically includes $(Bi_{0.5}K_{0.5})TiO_3$ (BKT), $(Bi_{0.5}Na_{0.5})TiO_3$ (BNT), or $(K_{0.5}Na_{0.5})NbO_3$ (KNN) with another ABO_3 perovskite, such as $BaTiO_3$ or one of the other starting components [10-11]. In this work, compositions from a lead-free ternary system based on KNN will be explored in order to further enhance these piezoelectric properties. Fatigue of these lead-free systems will also be evaluated in detail to determine if their behavior is as detrimental and if the mechanisms are the same as those found for PZT based systems.

5.3 $(K,Na)NbO_3$-Based Systems

The KNN-based materials have been successfully modified using various A and B cations to enhance its properties to levels approaching those of PZT. A pseudo ternary system was first formed between KNN, $LiTaO_3$, and $LiSbO_3$ by Saito *et al.* in 2004 [12-13]. That

composition, $(K_{0.44}Na_{0.52}Li_{0.04})(Nb_{0.84}Ta_{0.10}Sb_{0.06})O_3$ was subsequently designated LF4 by the authors. A general plot of various known perovskite-based piezoelectrics versus d_{33} was included and showed that even in the case of untextured samples, this new piezoelectric more closely approaches the properties found for PZT than the other common lead-free alternatives currently being explored.

Similar compositions also investigated included those with only $LiTaO_3$ added, some with $AgTaO_3$, and some modified by $Ag(Sb_xTa_{1-x})O_3$ [14-16]. While all exhibited enhanced properties, including d_{33} and P_r compared to the pure KNN system, this study is focused on optimized compositions found using only the six cations found in the original LF4 [12,17-18]. The second composition optimized resulted in only slight differences found in the amount of Ta and Sb added ($(K_{0.44}Na_{0.52}Li_{0.04})(Nb_{0.86}Ta_{0.10}Sb_{0.04})O_3$) and is referred to here as LF4-2 (with T_C = 326°C) [17]. Further studies on LF4-2 compositions included doping with CuO and Fe_2O_3, with CuO showing improved sintering and better dielectric loss characteristics [17,19]. Some secondary $K_4CuNb_8O_{23}$ phase, however, was observed via X-ray diffraction (XRD) measurements. This was proposed to function as a liquid phase sintering aid for this system. The best piezoelectric properties came from dopant levels of 0.2 wt% CuO [17].

While these enhanced properties are fairly well documented, there is very little research published regarding the effects of piezoelectric fatigue for lead-free ceramics in general and LF4 (i.e. KNN-based) compositions in particular. Most currently published data shows enhanced fatigue-free behavior for bismuth layered structures, while simple perovskite materials have yet to be explored [20]. One other study has shown significant

improvement of fatigue properties for KNN when doped with $CaTiO_3$, but testing was limited to only 10,000 cycles in duration [21].

5.4 Experimental Methods

Both compositions $(K_{0.44}Na_{0.52}Li_{0.04})(Nb_{0.86}Ta_{0.10}Sb_{0.04})O_3$ (LF4-2) and $((K_{0.44}Na_{0.52}Li_{0.04})(Nb_{0.86}Ta_{0.10}Sb_{0.04})O_3)$ + 0.2 wt% CuO added were produced via conventional solid state synthesis methods. This includes using starting powders of at least 99.9% purity (CuO, $LiCO_3$, $NaCO_3$, KCO_3, Nb_2O_5, Ta_2O_5, and Sb_2O_5). Six hours of high energy vibratory milling was used for mixing and post-calcination grinding. Ethanol solutions of ~15 vol% powder were used with high density yttrium stabilized zirconia (YTZ) media (TOSOH corporation) during milling. For these KNN based compositions, calcinations were performed in covered crucibles at 780°C for 4 hours.

The calcined powders were mixed with a 3 wt% solution of Paraloid (PL) binder, and then were uniaxially cold pressed into 12.8 mm pellets at a pressure of 150 MPa. Following a 3 hour 400°C binder burnout, the pellets were sintered in covered crucibles at 1135°C for 2 hours (LF4-2) or 1100°C for 3 hours (LF4-2 + 0.2 wt% CuO). X-ray diffraction (Bruker-AXS D8 Discover) was used for phase identification in the 2θ scan range of 20°- 80° for sintered pellets.

Prior to electrical measurements, samples were polished to sub-millimeter thickness with smooth and parallel surfaces. Silver paste (Heraeus C1000) was fired on both sides in air at 650°C for 30 minutes. A LCR meter (Agilent 4284A) was used to

measure the dielectric properties for a wide variety of frequencies and temperatures using a high temperature measurement cell (NorECS Probostat). Polarization and strain hysteresis measurements were made using a Sawyer-Tower circuit-based system (Radiant Technology Premier II utilizing Vision software).

For poling, dc biases of 40 kV/cm were used at room temperature for 10 minutes (LF4-2) or at 100°C for 30 minutes (LF4 + 0.2 wt% CuO). Unipolar fatigue effects were measured using a repeating triangular waveform applied in the same direction as that of the dc bias used in poling, at 10Hz or 50 Hz for either 18 kV/cm or 36 kV/cm ($1E_C$ and $2E_C$, respectively) for LF4-2 and 16 kV/cm or 30 kV/cm ($2E_C$ and $3E_C$, respectively) for LF4-2 + 0.2 wt% CuO. Fatigue testing was run for various cycle lengths ($1x10^5$, $1x10^6$, or $1x10^7$) with unipolar hysteresis measurements taken at every decade. Additionally, bipolar hysteresis measurements were taken before and after the fatigue of the CuO doped samples at multiple field levels.

5.5 Results and Discussion

Polarization hysteresis loops measured at 10 Hz for $(K_{0.44}Na_{0.52}Li_{0.04})(Nb_{0.86}Ta_{0.10}Sb_{0.04})O_3$ (LF4-2) ceramics showed well-defined loops characteristic of a ferroelectric material. The P_{MAX} for these samples was approximately 25 $\mu C/cm^2$ with the remanent polarization $P_r \sim 20\ \mu C/cm^2$, while the coercive field for these specimens was ~18 kV/cm. This was reduced by half when 0.2 wt% CuO was introduced to the system, with E_C =8.7 kV/cm at saturation field levels, yet the high polarization levels were maintained (P_{MAX} = 21, P_r = 16 $\mu C/cm^2$). Next, increasing field

levels were applied (between 20 to 60 kV/cm) to the CuO samples for both polarization and strain hysteresis measurements, which is shown in Fig. 5.1.

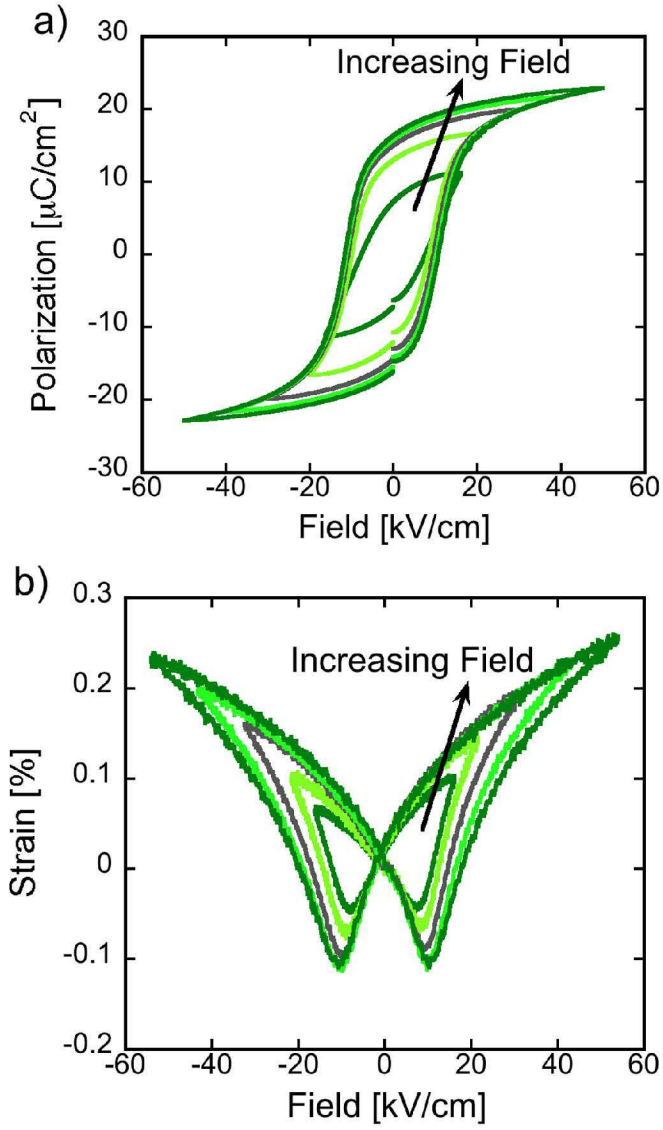

Fig. 5.1 *Typical bipolar hysteresis of LF4-2 + 0.2 wt% CuO ceramics for a) polarization and b) strain at increasing field levels (from 20 to 50 kV/cm) show a maximum strain of 0.26%*

Significantly, very symmetrical, butterfly shaped strain loops were observed at all frequencies and field levels used. Fully saturated loops first form at field levels between 40 and 50 kV/cm. Maximum strains of up to 0.26% were seen, in conjunction with high field d_{33}* values of 500-700 pm/V depending on the field applied. Values of low-field d_{33}, however, were only found to range from 167-182 pC/N. While these are smaller than the highest previously reported 416 pC/N of "textured" LF4 ceramics, they are still high compared to other known lead-free systems. Also, it should be noted that poled commercial PZT samples range anywhere from 400-600 pC/N depending on the levels of hard or soft dopants used [19].

After room temperature poling at 35 kV/cm, the unipolar fatigue characteristics of the undoped LF4-2 ceramics were evaluated out to 100,000 cycles. Figure 5.2 a) shows the unipolar hysteresis measurements at 18 kV/cm ($1E_C$) and Fig. 5.2 b) presents the data for samples fatigued at 36 kV/cm ($2E_C$). While some fatigue is observed, the majority of the loss in polarization occurs within the first 10-100 cycles. This is likely attributable to insufficient poling, as the domain structures appear to come to a stable equilibrium state after a small number of cycles that act to further pole the sample.

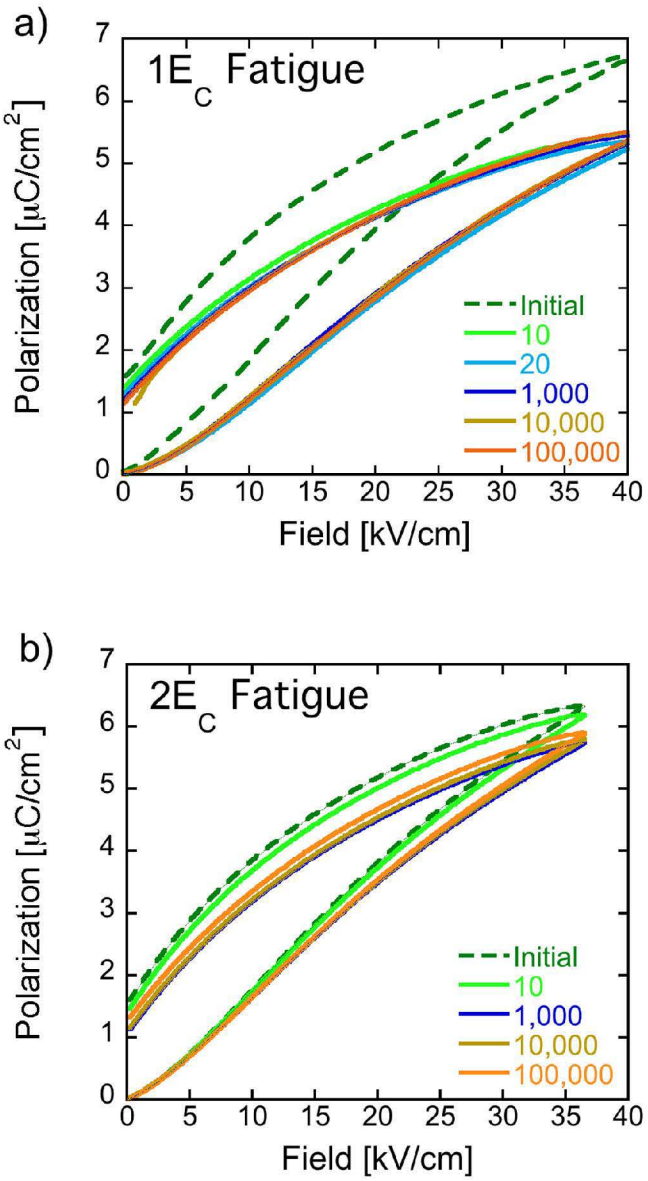

Fig. 5.2 *Fatigue behavior of undoped LF4-2 with a) 18 kV/cm ($1E_C$) and b) 36 kV/cm ($2E_C$) applied fields at 10 Hz for 10^5 cycles.*

For fatigue measurements performed at 18kV/cm ($1E_C$), after the first 10 cycles very little degradation in polarization is observed out to 100,000 cycles. For samples

fatigued at 36 kV/cm ($2E_C$), the polarization drop continues until after approximately 10 cycles were complete and arrived at a stable value. The magnitude of this decrease was approximately half that of the drop in P_{MAX} observed for fatigue tests at the 18 kV/cm ($1E_C$) level. This is made clearer in Fig. 5.5a, where P_{MAX} is plotted as a function of number of cycles. In general, samples that effectively had lower initial polarization and d_{33} values also experienced a correspondingly smaller drop in P_{MAX} after fatigue. In these samples the larger change in maximum polarization at the beginning of the fatigue test has more to do with the poling process than the fatigue process. The most important aspect of the fatigue characteristic is the stabilization of the polarization as higher numbers of cycles were reached.

Because the coercive field of the 0.2 wt% CuO doped samples was significantly lower than the undoped case, and based on what is known about the fatigue behavior of PZT at low field values, fatigue experiments at 16 and 30 kV/cm ($2E_C$ and $3E_C$) for the doped samples were chosen. It is difficult to normalize these fatigue tests between the undoped and 0.2 wt% CuO compositions because both the magnitude of the applied electric field and the coercive field are important semi-dependent parameters. The magnitude of the applied electric field is important since that is directly related to the energy that is introduced into the dielectric. However, the coercive field represents the energy required for domain motion, which is highly relevant to fatigue mechanisms.

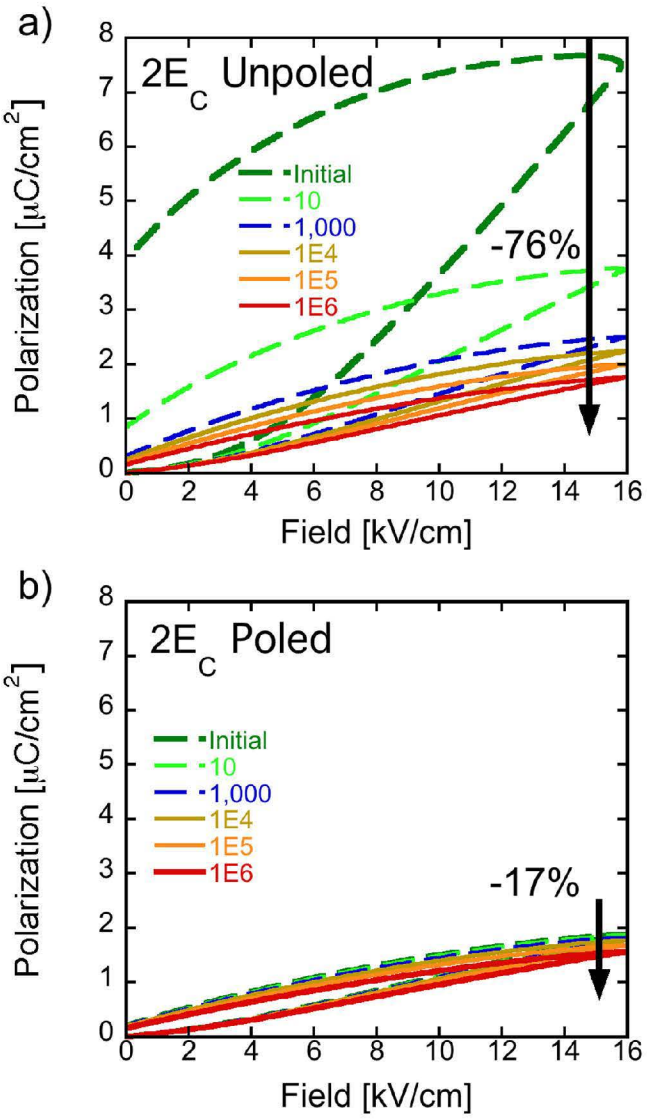

Fig. 5.3 *Unipolar fatigue behavior of 0.2 wt% CuO doped LF4-2 at $2E_C$ for 10^6 cycles with a) unpoled and b) poled ceramic samples*

In the first set of experiments on 0.2 wt% CuO LF4-2, samples were fatigued at 16kV/cm ($2E_C$) and 10 Hz for 10^6 cycles. Both samples poled at 100°C for 30 minutes at 40 kV/cm and one without any poling were examined. In the unpoled case, a much more significant drop in polarization was observed at the beginning of the test. This effect is very similar

to the large decrease in the maximum polarization that was observed in the undoped samples. In comparing the poled and unpoled 0.2 wt% LF4-2 specimens, if the data for the first 10-100 cycles of the unpoled sample are removed, the scale of the overall drop in P_{MAX} between the two are very similar, which can be seen in Fig. 5.3. This is not observed in the highly poled commercial PZT samples tested in previous studies, further confirming the importance of the poling on the overall fatigue of the sample.

In the case of 1 million cycle fatigue tests carried out on poled samples at 30 kV/cm ($\sim 3E_C$) applied field, the drop in P_{MAX} increases even further to 32%, nearly doubling the drop seen for the 16 kV/cm ($2E_C$) test at the 10^6 cycle mark. In separate tests, samples were examined out to 10^7 cycles at $2E_C$ (50 Hz applied triangular waveform). The trend observed matches the relative decrease observed in previous poled 16 kV/cm ($2E_C$) fatigue tests out to 10^6 cycles (~17%) and shows a further decrease in polarization out to 10^7 cycles (~22%) as expected. The unipolar hysteresis loops observed during these fatigue tests are shown in Fig. 5.4.

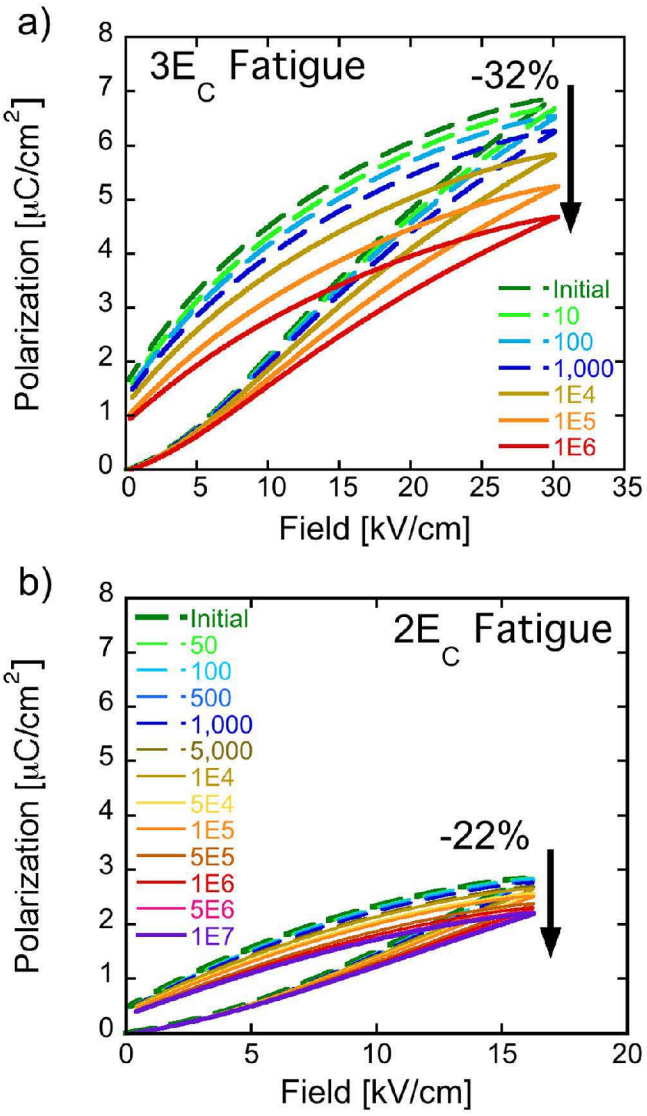

Fig. 5.4 *Unipolar fatigue behavior of 0.2 wt% CuO doped LF4-2 at a) $3E_C$ for 10^6 cycles (10 Hz) and b) $2E_C$ for 10^7 cycles (50 Hz)*

For the CuO doped samples, the trend is clearly different than for the undoped LF4, which can be seen in Fig. 5.5. The maximum polarization does not reach a constant value at increased cycles, but rather exhibits a steady decrease as a function of cycles applied, even out to 10 million cycles. Also, increasing the testing field levels from 18 to 30 kV/cm

($2E_C$ to $3E_C$) further increased the degradation of the polarization, as shown in Fig. 5.5b. While additions of 0.2 wt% CuO enhanced the piezoelectric properties in general, they simultaneously appeared to worsen the fatigue properties in this system. If Cu^{2+} was acting as an acceptor, more oxygen vacancy species should be present and fatigue would be worsened according to previous models [4-5, 7-9]. However, a hardening effect was not observed as the E_C decreased with the addition of CuO. This suggests a more complicated mechanism or simply a different explanation for fatigue may be necessary for lead-free systems.

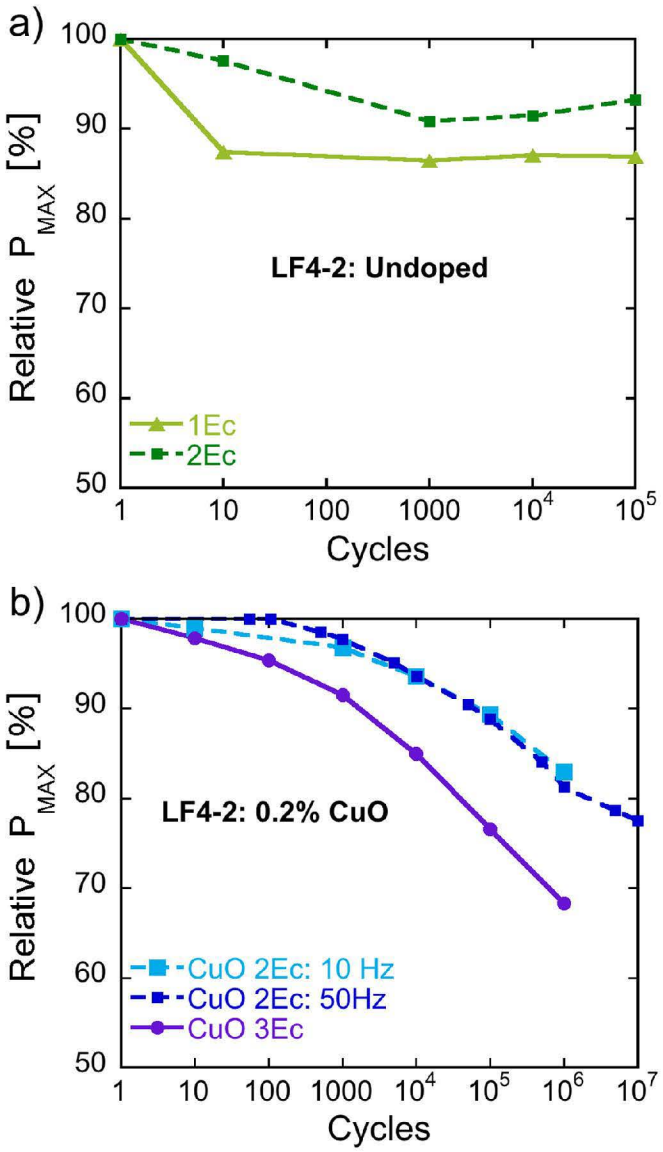

Fig. 5.5 *Maximum polarization vs. number of poling cycles at 10 Hz for a) undoped and b) 0.2 wt% CuO doped samples*

Another comparison can be made between the bipolar polarization and strain hysteresis measurements taken before and after the unipolar fatigue was complete. In Fig. 5.6 a) bipolar loops at the cycling field are shown, while Fig. 5.6 b) shows bipolar loops at

saturation voltages. For the change in the polarization plots, the 0.2 wt% CuO doped LF4-2 samples shows a significant departure from PZT behavior, with the final values being significantly higher than the initial, rather than simply slightly lower [3,5,9]. This can be explained by the fact that the initial hysteresis of the commercial PZT were for poled samples, whereas the initial bipolar measurements for the doped LF4 were not poled to prevent influence of bipolar fields on the unipolar tests. A more fully poled sample gives a larger proportion of switchable domains and higher saturation polarizations. So if only a very slight degradation in polarization is occurring similar to that of the unipolar fatigued PZT case, it is most likely being obscured by the much larger magnitude increase of polarization from the poling process. This further emphasizes the importance that optimized poling conditions, such as those already well established for commercial PZT, have on the fatigue properties of piezoelectrics.

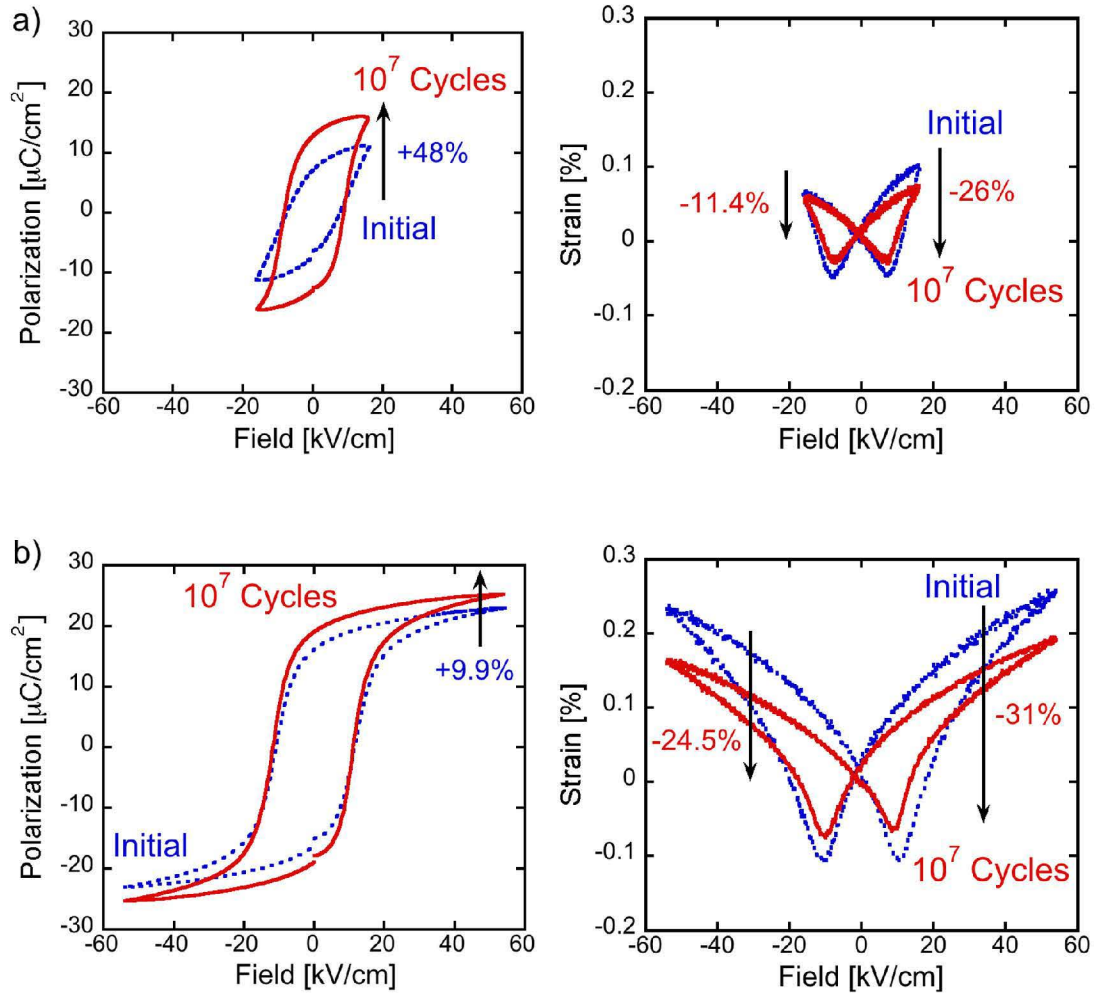

Fig. 5.6 *Polarization and Strain Hysteresis for 0.2 wt% CuO doped LF4-2 samples before and after fatigue at 16kV/cm ($2E_C$) for 10^7 cycles at a) fatigue cycling field levels (16kV/cm) and b) saturation field levels (50 kV/cm)*

From the change in strain hysteresis, it is clear that the decrease in strain is not uniform for positive and negative applied fields. At both the testing and saturation field levels, the positive applied field side of the strain curve clearly decreased to a greater extent. In the unipolar fatigue of PZT, there was not a true degradation of strain but rather an imprint

from an offset polarization, causing the positive maximum strain value to be increased and the negative maximum strain value to decrease. In the 0.2 wt% CuO doped LF4-2 system, while a slight increase in symmetry is observed, it is the result of an overall decrease in maximum strain for both positive and negative bias, thus showing a true degradation of strain more similar to the type observed in bipolar fatigue of PZT.

The effects of fatigue on the piezoelectric coefficient of the undoped system were observed as an increase in the value of d_{33} for both $1E_C$ level fatigue tests (173 to 186 pC/N) and $2E_C$ level fatigue tests (145 to 164 pC/N) due to the large effective poling experienced by these systems under unipolar conditions. For the 0.2 wt% CuO doped samples, a very clear decrease in d_{33} is observed as these samples were more completely poled before testing. For fatigue out to 1 million cycles, the sample fatigued at $2E_C$ experienced $\Delta\ d_{33} \sim$ -21 pC/N, while the $3E_C$ fatigued sample experienced a sharper decrease of $\Delta\ d_{33} \sim$ -32 pC/N. The 0.2 wt% CuO doped samples fatigued at $2E_C$ for 10^7 cycles showed an even larger drop in d_{33} (-45 pC/N) was seen, which was approximately double that of the 10^6 cycle fatigue test. The trends in d_{33} value measured for both undoped and doped LF4-2 are plotted together in Fig. 5.7.

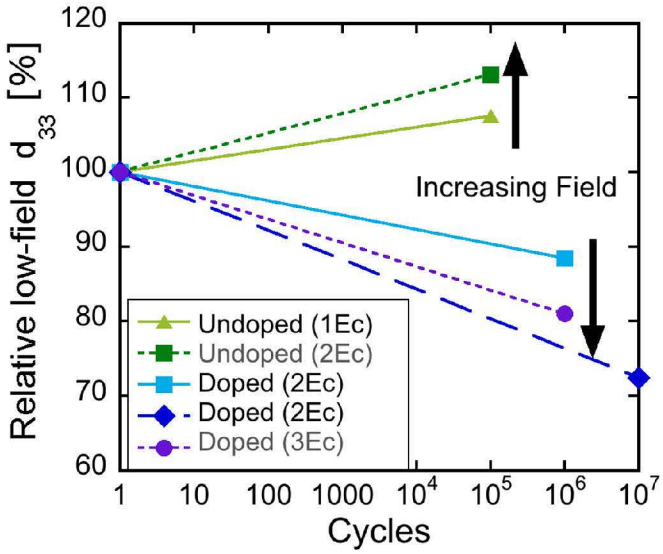

Fig. 5.7 *Effective change in low field d_{33} as a function of applied field during fatigue and total number of cycles applied for all sample types*

5.6 Conclusions

Single phase perovskite ceramics were synthesized for two variations of the Pb-free LF4 piezoelectric material. Bipolar hysteresis showed relatively high remanent polarization (20 μC/cm², 16 μC/cm²) and maximum polarization (25 μC/cm², 21 μC/cm²) values were found for both undoped LF4-2 and 0.2 wt% CuO doped LF4-2 respectively. Unipolar fatigue behavior for this system is clearly very dependent on applied field during testing and the initial poling conditions. For undoped LF4-2, after minor initial decreases the polarization becomes stable after 10 cycles for testing of 100,000 cycles duration with an overall increase of piezoelectric coefficient. For the CuO doped samples, increasing the testing field to $3E_C$ resulted in twice the decrease in P_{MAX} (-32%) compared to the $2E_C$ tests at 10^6 cycles (-17%). At $2E_C$ testing for CuO doping,

polarization decreases continually through 10^7 cycles with the decreases in P_{MAX} and d_{33} both reaching a maximum (-22% and -30% respectively) after 10^7 cycles. Further analysis and SEM work is warranted to determine the exact nature of the defect mechanism responsible for inducing this difference in behavior.

5.7 References

[1] R. E. Newnham, *Properties of Materials: Anisotropy, Symmetry, Structure*. Oxford, 2005.

[2] K. C. Kao, *Dielectric Phenomena in Solids*: Elsevier, 2004.

[3] N. Balke, H. Kungl, T. Granzow, D.C. Lupascu, M.J. Hoffman, and J. Rödel, "Bipolar Fatigue Caused by Field Screening in Pb(Zr,Ti)O3 Ceramics." *J. Am. Ceram. Soc.* **90**(12): 3869-3874, 2007.

[4] N. Balke, D.C. Lupascu, T. Granzow, and J. Rödel, "Fatigue of Lead Zirconate Titanate Ceramics I: Unipolar and DC Loading." *J. Am. Ceram. Soc.* **90**(4): 1081-1087, 2007.

[5] D.C. Lupascu, Fatigue in Ferroelectric Ceramics and Related Issues. Berlin, Springer, 2004.

[6] W. Pan, C.F. Yue, and O. Tosyali, "Fatigue of Ferroelectric Polarization and the Electric Field Induced Strain in Lead Lanthanum Zirconate Titanate Ceramics." *J. Am. Ceram. Soc.* **75**(6): 1534-1540, 1992.

[7] C. Verdier, D.C. Lupascu, and J. Rödel, "Unipolar fatigue of ferroelectric lead zirconate titanate." *J. Eur. Ceram. Soc.* **23**: 7, 2003.

[8] C. Verdier, D.C. Lupascu, and J. Rödel "Stability of defects in lead-zirconate-titanate after unipolar fatigue." *Appl. Phys. Lett.* **81**(14): 2596-2598, 2002.

[9] N. Balke, H. Kungl, T. Granzow, D.C. Lupascu, M.J. Hoffman, and J. Rödel, "Bipolar Fatigue Caused by Field Screening in Pb(Zr,Ti)O3 Ceramics." *J. Am. Ceram. Soc.* **90**(12): 3869-3874, 2007.

[10] V. A. Isupov, "Ferroelectric Na0.5Bi0.5TiO3 and K0.5Bi0.5TiO3 Perovskites and Their Solid Solutions," *Ferroelect. Review,* vol. 315, pp. 123-147, 2005.

[11] T. R. Shrout, and S.J. Zhang, "Lead-free piezoelectric ceramics: Alternatives for PZT?," *J. Electroceram,* vol. 19, pp. 111-124, 2007.

[12] Y. Saito, H. Takao, T. Tani, T. Nonoyama, K. Takatori, T. Homma, T. Nagaya, and M. Nakamura, "Lead-free piezoceramics," *Nature,* vol. 432, pp. 84-87, 2004.

[13] Y. Saito, *et al.*, "High Performance Lead-free Piezoelectric Material," *R&D Review of Toyota CRDL,* vol. 41, pp. 22-28, 2004.

[14] S. Zhang, R. Xia, T.R. Shrout, G. Zan, and J. Wang, "Piezoelectric properties in perovskite 0.948(K0.5Na0.5)NbO3-0.052LiSbO3 lead-free ceramics," *J. Appl. Phys.,* vol. 100, pp. 104108-1-6, 2006.

[15] Y. Wang, J. Wu, D. Xiao, J. Zhu, Y. Jin, J. Zhu, P. Yu, L. Wu, and X. Li, "Microstructure, dielectric, and piezoelectric properties of (Li, Ag, Ta) modified (K0.50Na0.50)NbO3 lead-free ceramics with high Curie Temperature," *J. Appl. Phys.,* vol. 102, p. 054101, 2007.

[16] J. Wu, D. Xiao, Y. Wang, W. Wu, B. Zhang, J. Zhu, Z. Pu, and Q. Li, "Microstructure and electrical properties of (Li, Ag, Ta, Sb)-modified (K0.50Na0.50)NbO3 lead-free ceramics with good temperature stability," *J. Phys. D: Appl. Phys. ,* vol. 41, p. 125405, 2008.

[17] E. Li, H. Kakemoto, S. Wada, T. Tsurumi, "Influence of CuO on the Structure and Piezoelectric Properties of the Alkaline Niobate-Based Lead-Free Ceramics," *J. Am. Ceram. Soc.,* vol. 90, pp. 1787-1791, 2007.

[18] J. Wu, D. Xiao, Y. Wang, J. Zhu, L. Wu, and Y. Jiang, "Effects of K/Na ratio on the phase structure and electrical properties of (KxNa0.96-xLi0.004)(Nb0.91Ta0.05Sb0.04)O3 lead-free ceramics," *Appl. Phys. Lett.,* vol. 91, p. 252907, 2007.

[19] R. Zuo, *et al.*, "Dielectric and piezoelectric properties of Fe2O3-doped (Na0.5K0.5)0.96Li0.04Nb0.86Ta0.1Sb0.04O3 lead-free ceramics," *Journal of Physics and Chemistry of Solids,* vol. 69, pp. 1728-1732, 2008.

[20] Y. Ding, J.S. Liu, H.X. Qin, J.S. Zhu, and Y.N. Wang, "Why lanthanum-substituted bismuth titanate becomes fatigue free ferroelectric capacitor with platinum electrodes," *Appl. Phys. Lett.,* vol. 78, pp. 4175-4177, 2001.

[21] S. Zhang, R. Xia, H. Hao, H. Liu, and T.R. Shrout, "Mitigation of thermal and fatigue behavior in K0.5Na0.5NbO3-based lead free piezoceramics," *Appl. Phys. Lett.,* vol. 92, p. 152904, 2008.

6 Electromechanical Strain in $Bi(Zn_{1/2}Ti_{1/2})O_3$–$(Bi_{1/2}Na_{1/2})TiO_3$–$(Bi_{1/2}K_{1/2})TiO_3$ Solid Solutions

Eric A. Patterson and David P. Cann

Materials Science, School of Mechanical, Industrial and Manufacturing Engineering

Oregon State University

Corvallis, OR 97331

Jan Pokorny and Ian M. Reaney

Department of Materials Science and Engineering

University of Sheffield

Sheffield S1 3JD, UK

Published on May 10, 2012:

Journal of Applied Physics

111 (9), 094105-094105 (2012)

6.1 Abstract

Solid solutions ceramics of the $Bi(Zn_{0.5}Ti_{0.5})O_3$–$(Bi_{0.5}K_{0.5})TiO_3$–$(Bi_{0.5}Na_{0.5})TiO_3$ ternary system for < 20 mol% BZT were created and confirmed to be single phase using X-ray diffraction. The dielectric dispersion showed decreasing T_{max} of the dielectric spectrum with a broadening of the transition with increasing BZT content. At 2.5 BZT–40 BKT–57.5 BNT, a secondary transition commonly observed for MPB BNT–BKT was observed. The ferroelectric behavior of the system was characterized by a transition where the polarization hysteresis showed a severe pinching effect on remanent polarization (20.8 μC/cm^2 at 2.5% BZT) as BZT contents was increased (P_r = 2.3 μC/cm^2 at 20% BZT). Similarly, as the temperature increased to 175°C, the remanent polarization of the 2.5% BZT composition significantly reduced to 2.1 μC/cm^2. The onset of this transition corresponds to the lower temperature frequency dispersion observed in the dielectric spectrum. The strain hysteresis experienced analogous transition to the polarization, with a change in shape from typical ferroelectric butterfly to a complete loss of negative strain as BZT concentration increased. Maximum strain values of 0.33% were observed at 5-40-55 accompanied by a large d_{33}^* = 547 pm/V.

6.2 Introduction

Much recent research has focused on the development of Bi-based piezoelectrics as environmentally compatible alternatives to lead zirconate titanate (PZT) since the Bi^{3+}, like the Pb^{2+} ion, is highly polarizable due to a lone electron pair [1, 2]. Compounds such as $(Bi_{0.5}K_{0.5})TiO_3$ (BKT) and $(Bi_{0.5}Na_{0.5})TiO_3$ (BNT), and their solid solutions with $BaTiO_3$ and

other tetragonal perovskites exhibit usable piezoelectric properties [3-12] and are considered as candidates to replace Pb-based materials [11, 13, 14]. BNT has recently been shown to have a monoclinic (Cc) rather than rhombohedral (R3c) structure at room temperature, and although it shows a relatively high remanent polarization P_r=38 μC/cm^2, such values can only be achieved at very high applied fields due to its extremely large coercive field, E_c = 73-75 kV/cm [12, 15, 16]. BKT is tetragonal but also requires a large field [E_{app} > 100 kV/cm] to yield its maximum polarization (P_{max} = 33 μC/cm^2) and also has an unsuitably large E_C = 52.5 kV/cm [3]. Thus effective poling of BKT and BNT ceramics is challenging with large d_{33} values difficult to obtain at low fields.

BKT–BNT is one of the closest PbO-free materials in behavior to PZT, with optimum piezoelectric performance in the vicinity of an MPB between R3c and tetragonal (P4mm) phases [17] with P_r = 38 μC/cm^2, piezoelectric coefficient, d_{33} = 167 pC/N, and electromechanical coupling coefficient, k_{33} = 0.56 [14]. It has proved relatively easy to form solid solutions of BNT–BKT with other perovskites such as $BaTiO_3$ and $(Bi_{0.5}Li_{0.5})TiO_3$ (BLT) in which an MPB may be located, examples of which may be found in refs [18]. More recently, attention has focused on forming solid solution of BNT–BKT with end members that are unstable in ambient, such as $Bi(Zn_{1/2}Ti_{1/2})O_3$. Huang *et al.* first reported the structure and electrical properties of $(1-x)\,(Bi_{1/2}K_{1/2})TiO_3 - x\,Bi(Zn_{1/2}Ti_{1/2})O_3$ solid solutions (BKT–BZT) [19] and demonstrated that BZT improved the density, dielectric, and piezoelectric properties of BKT [3, 19]. P_r (11.8 μC/cm^2) for BKT–BZT was not as high as in

the BNT–BKT system, but the maximum strain, S_{MAX} = 0.15%, was significantly improved over that practically achieved in pure BKT [3, 6, 19].

In this contribution, the ternary BNT–BKT–BZT solid solutions are explored. Starting compositions were chosen based on the reported properties of 0.1 BZT–0.9 BKT [19]. Ternary space was first mapped by varying the K/Na ratio, in accordance with the formula, 0.1 BZT–(0.9–*z*) BKT–(*z*) BNT. Subsequently, composition space was explored by fixing BKT at 0.4 and the varying the BZT/BNT ratio according to the formula, *x* BZT – (0.4) BKT – (0.6–*x*) BNT. For convenience, all compositions are referred to by their mole percentage of *X*–*Y*–*Z* to indicate *X*%BZT–*Y*%BKT–*Z*%BNT throughout this article.

6.3 Experimental Methods

Compositions in the BZT–BKT–BNT ternary system were produced via conventional solid state synthesis, using starting powders (Bi_2O_3, TiO_2, ZnO, $NaCO_3$, and KCO_3) of > 99.9% purity. Six hours of high energy vibratory milling using yttrium stabilized zirconia milling media in ethanol was utilized for mixing and post-calcination grinding. Calcinations were performed in covered crucibles at 900–950°C for 6 hours followed by a second six hour vibratory milling step.

The milled, calcined powders were mixed with 3 wt% solution of Paraloid (PL) binder, and then uniaxially cold pressed into 12.8 mm pellets at a pressure of 150 MPa. Sintering was performed at 1050–1100°C for 4 hours. X-ray diffraction was used for

phase identification between 20°–80° 2θ on polished sintered pellets (Bruker AXS D8 Discover).

Prior to electrical measurements, samples were polished to sub-millimeter thickness and high-temperature silver paste (Heraeus C1000) was fired on both sides in air at 650°C for 30 minutes. An LCR meter (Agilent 4284A) was used to measure the dielectric properties for a wide variety of frequencies and temperatures using a high temperature measurement cell (NorECS Probostat). Hysteresis measurements were made using a sawyer-tower circuit-based Radiant Technology Premier II ferroelectric test system utilizing Vision software. Strain hysteresis measurements were taken with the same system in conjunction with an MTI Instruments 2100 Fotonic Sensor. Unpolarized Raman spectra were excited with the 514.5 nm line of an Ar laser and recorded with a Renishaw inVia micro-Raman spectrometer. The spectra were corrected to the Bose–Einstein temperature factor.

6.4 Results and Discussion

All peaks in X-ray diffraction data could be indexed according to a single perovskite phase for all compositions with < 20% BZT as shown in Fig. 6.1. All ceramics achieved typically < 95% of the theoretical density at sintering temperatures below 1100°C. All compositions in this study exhibited splitting of the {h00} peaks, characteristic of tetragonal symmetry but as the mole fraction of BZT increased the c/a ratio increased slightly from 1.014 at 2.5 mol% BZT to 1.017 at 20 mol% BZT. Similarly, for 10% BZT compositions, the c/a ratio barely decreased as the temperature increased from 1.012 at

room temperature to 1.014 at 200°C. For compositions with > 20% BZT, multiple phases were observed, with the assemblage dominated by perovskite and $Bi_4Ti_3O_{12}$.

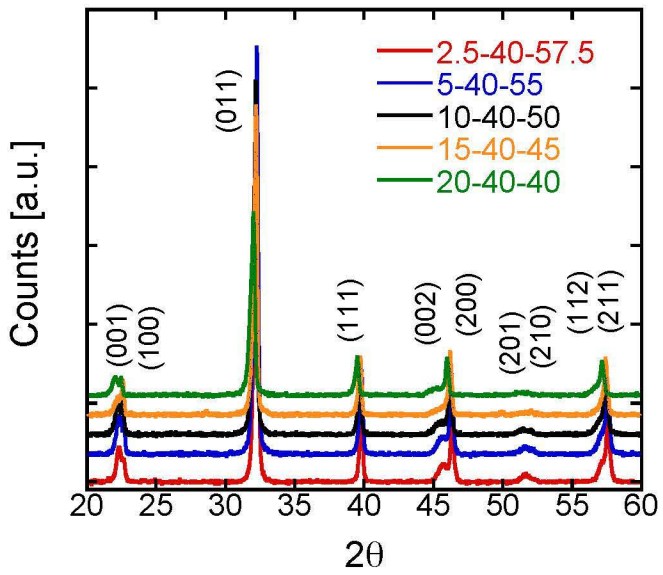

Fig. 6.1 *XRD patterns as a function of 2θ for the indicated compositions (%BZT–%BKT–%BN) with peaks indexed.*

The dielectric spectra for all compositions as a function of BZT concentration at 10 kHz are shown in Fig. 6.2a. The dielectric maximum (T_{max}) for each composition is indicated. The data for these BZT solid solutions look somewhat similar to those for the BNT–BKT or BNT–BT binary solid solutions, with a broad maximum located between 250°C to 350°C [5, 6, 12]. Generally, as the amount of BZT increased, T_{max} shifted to lower temperatures. In addition, with increased BZT, the transition became increasingly diffuse, and the maximum permittivity decreased. A secondary transition could be

clearly resolved for compositions with 2.5% BZT, Fig. 6.2b. At higher BZT concentrations, the low temperature transition cannot be identified as the overall dielectric spectra between room temperature and T_{max} became highly dispersive. The maximum permittivity and sharpest transition peak are found for 2.5% BZT with a T_{max} = 322°C.

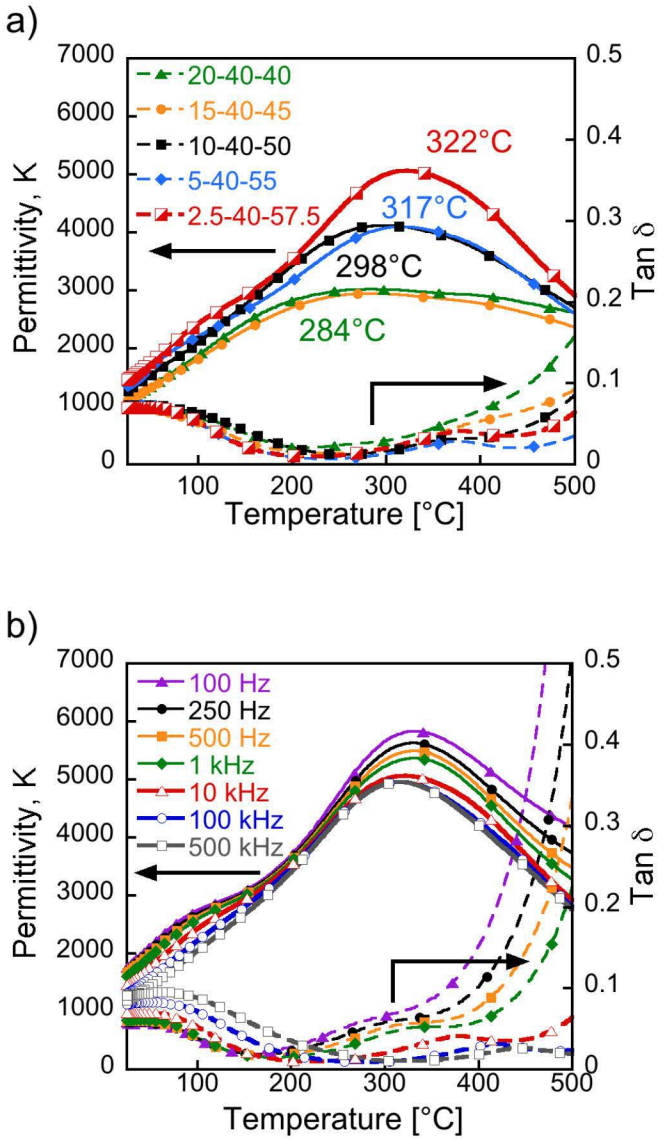

Fig. 6.2 *a) Dielectric properties as a function of temperature at 10 kHz for the indicated compositions (%BZT–%BKT–%BNT) and b) frequency dispersion of the dielectric properties of the composition 2.5 BZT–40 BKT–57.5 BNT.*

In the binary BKT–BNT system, compositions with > 20 mol% BKT favor tetragonal symmetry at room temperature. In the ternary compounds in this study, based on *x* BZT–(0.4) BKT–(0.6–*x*) BNT, tetragonal distortions were clearly observed in XRD data for

2.5 mol% BZT. In Raman data obtained on a range of BZT (Fig. 6.3), compositions with up to 15 mol% BZT showed a characteristic doublet at approx. 300 cm^{-1} at room temperature typical of tetragonal symmetry, in agreement with the XRD data. With increasing BZT concentration, the lower-wavenumber peak weakens in intensity. On heating compositions with 2.5% BZT, the doublet transforms gradually into a broad single mode at approx. 320°C in agreement with T_{max} in the dielectric data shown in Fig. 6.2. However, no structural anomalies were observed in the Raman or XRD data as a function of temperature that would correspond to the weak broad transition in the dielectric data at approx. 200°C. In the binary BKT–BNT system, the broad peak in permittivity observed near 200°C has been attributed to the emergence of either a tetragonal P4mm phase (Teranishi *et al.*) or to a pseudo-cubic phase (Hiruma *et al.*) from a rhombohedral phase at room temperature. High temperature XRD data obtained on materials in this study were largely inconclusive, however the Raman data disagree with the interpretation of Teranishi *et al.* since the structure remains tetragonal until approximately T_{max}. The broad anomaly at 200°C remains to be elucidated but is likely a weak non-symmetry breaking relaxation not uncommon in oxides with such complex crystal chemistry.

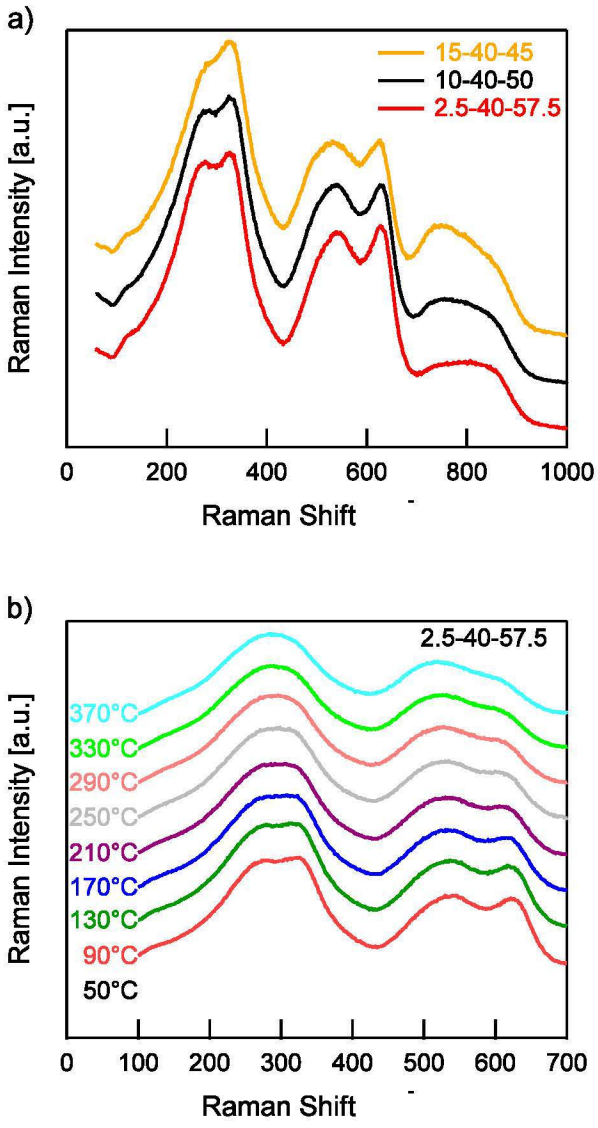

Fig. 6.3 *Raman Spectroscopy data for a) tetragonal 2.5%, 10% and 15% BZT compositions at room temperature and b) showing the tetragonal to cubic transition of 2.5–40–57.5 with increasing temperature.*

The polarization hysteresis behavior of the 2.5% BZT composition strongly resembled the behavior of a normal ferroelectrics with large remanent and maximum polarization values of $P_r = 20.8\ \mu C/cm^2$ and $P_{MAX} = 30.5\ \mu C/cm^2$, respectively. The coercive field

(E_C = 22.0 kV/cm) of these samples is also considerably reduced compared to the MPB compositions in the BKT–BNT binary, which are typically on the order of 40 kV/cm or larger [20]. The piezoelectric properties changed dramatically as the amount of BZT was increased to > 5 mol%, above which the remanent polarization decreased significantly. These "pinched" hysteresis loops become more severe for all subsequent compositions. At 10% BZT the maximum polarization begins to decrease, and by 20% BZT the loops start to exhibit pseudo-linear behavior with P_{MAX} = 18.2 μC/cm^2 and a negligible remanent polarization. The corresponding P–E and S–E hysteresis loops are shown in Fig. 6.4a and 6.4b, respectively.

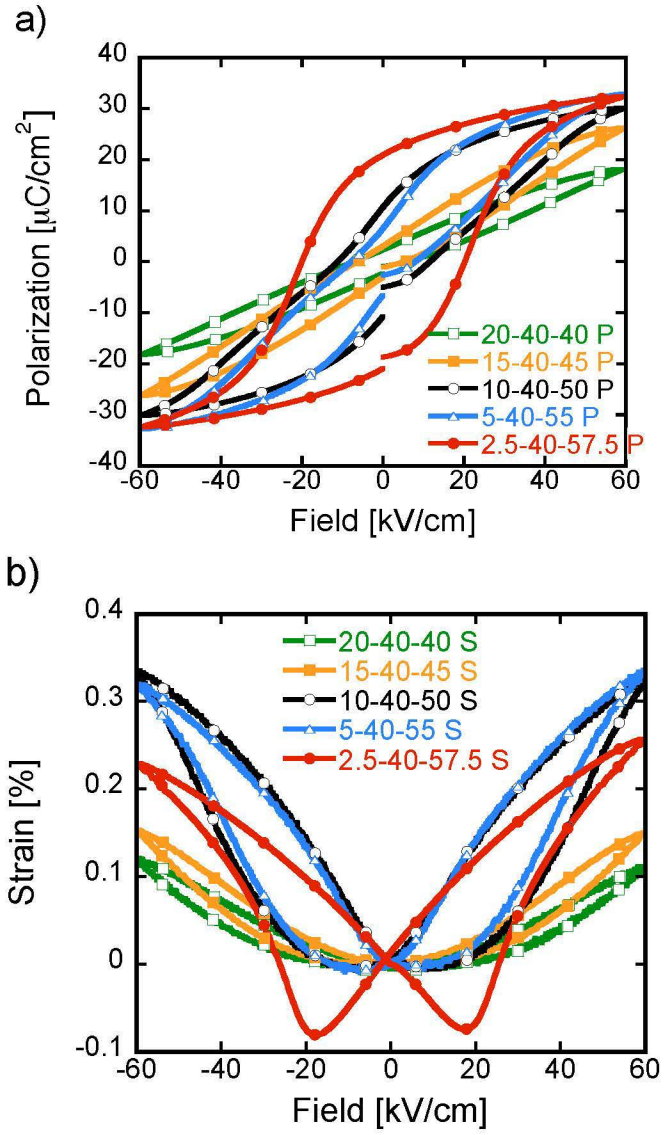

Fig. 6.4 *a) Polarization and b) electromechanical strain as a function of the applied electric field for compositions with a varying amount of BZT.*

Consistent with polarization data, the electromechanical strain data also changed as a function of BZT concentration. For compositions with 2.5% BZT, the strain data exhibited a classic "butterfly" shape with approximately –0.8% negative strain, typical of

domain switching for a ferroelectric. The maximum strain, S_{MAX} = 0.22-0.25% and corresponded to a high-field effective d_{33}* of 408 pm/V. For 10–40–50 and 5–40–55 compositions showed $S_{MAX} \approx 0.33\%$ and were correlated with a high-field d_{33}* of 547 pm/V. For all samples with > 5% BZT, however, no negative strain was observed. The electromechanical strain generally decreased in magnitude and become more parabolic and hysteretic as the concentration of BZT further increased. The strain hysteresis for the 20% BZT composition was low, with the most narrow, parabolic shape and an $S_{MAX} \approx 0.13\%$. These parabolic strain characteristics are similar to the electrostrictive behavior observed in relaxor ferroelectrics [21].

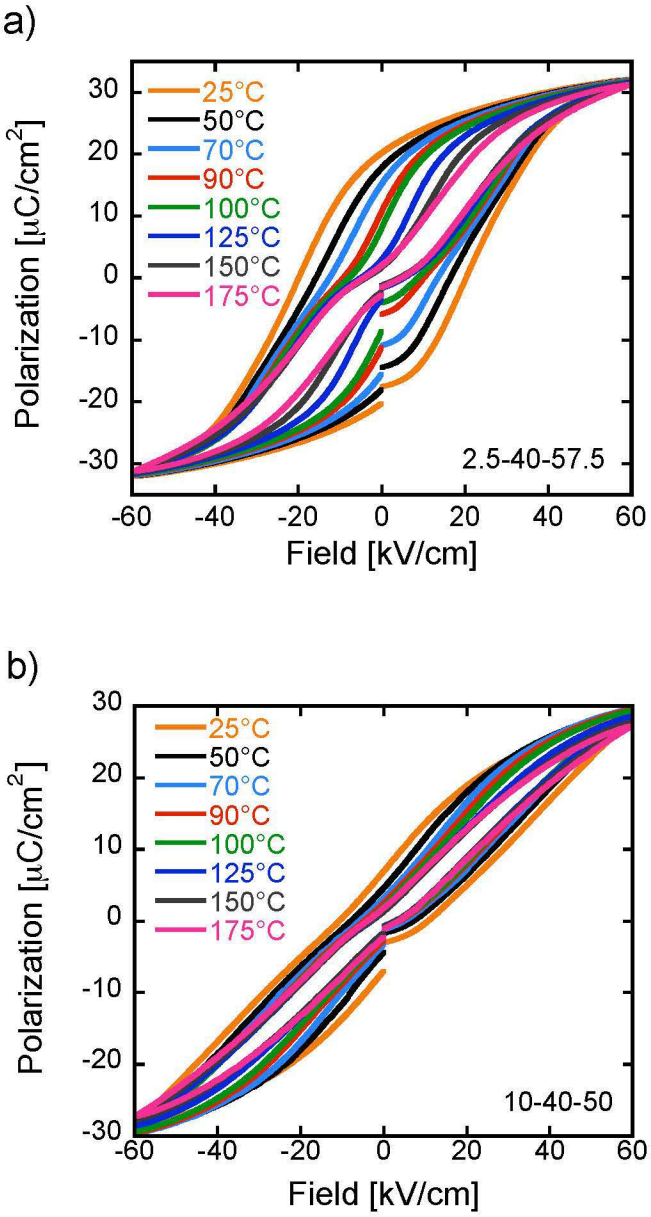

Fig. 6.5 *Saturated polarization hysteresis as a function of temperature for a) 2.5–40–57.5 and b) 10–40–50 ceramics, measured at 1 Hz.*

Polarization hysteresis behavior was also investigated as a function of temperature and is shown in Fig. 6.5. As the temperature increased, the composition with 2.5% BZT

exhibited a narrowing of the hysteresis loops, with a significant decrease in the coercive field. Above 70°C, in addition to the decrease in coercive field, the loops became pinched, resulting in a massive reduction in remanent polarization to 2.0 μC/cm^2 at 175°C. This pinching is similar to the effect of adding higher levels of BZT observed at room temperature. The temperature at which this pinching initiates corresponds to the onset of the frequency dispersion in the dielectric response at around 200°C. Fig. 6.5 b) demonstrates a further reduction in the remanent polarization observed in the already pinched loops of the 10–40–50 composition, but the magnitude of this decrease is not as severe as in the 2.5% BZT composition.

Ternary diagrams showing S_{Max} and d_{33}* for all compositions measured are displayed in Fig. 6.6. The maximum values in both cases are near the 10–40–50 for the 10% BZT compositions and 5–40–55 for the 40% BNT compositions. The maximum values for the high-field piezoelectric coefficient are shifted noticeably towards the BKT-rich end of the diagram compared to the location of the MPB in the binary system at 20 BKT–80 BNT. The largest S_{Max} of 0.33% values are nearly twice that of the stable binary compositions for BKT–BZT and also result from lower applied field levels [19]. The d_{33}* values are nearly twice those previously reported for BNT–BKT (291 pm/V) or BNT–BT (240 pm/V) and are comparable to other high strain compositions of BNT–BT–KNN (385–560 pm/V) recently published. [11, 12, 17, 22].

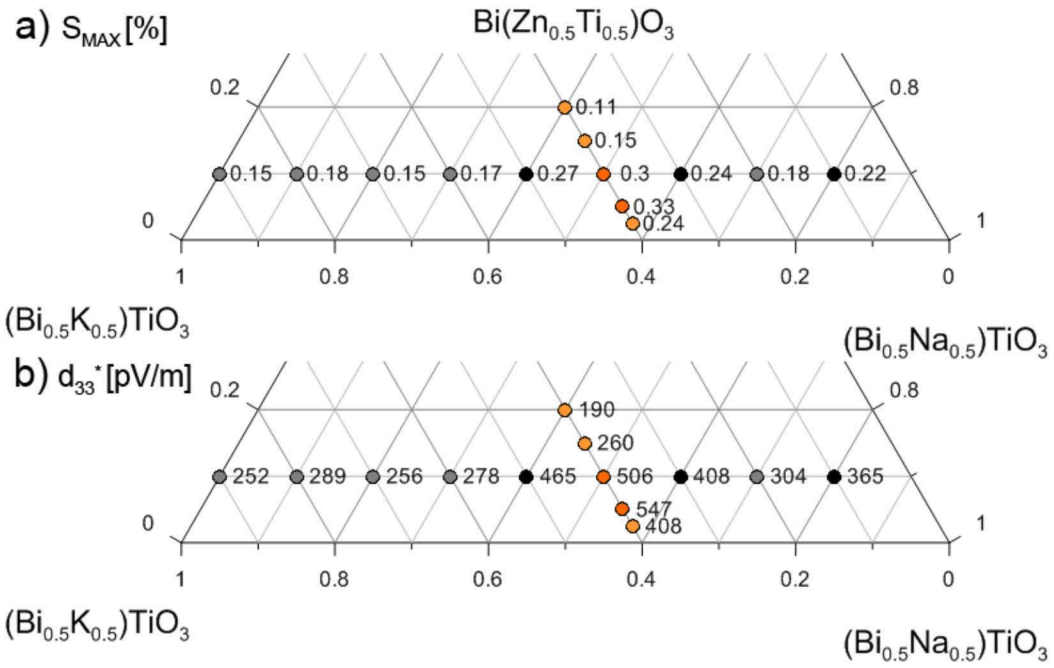

Fig. 6.6 *a) S_{Max} [%] and b) d_{33}* [pm/V] values plotted on the BZT–BKT–BNT phase diagram.*

The transition in hysteresis behavior is schematically illustrated in Fig. 6.7. The polarization hysteresis type follows the scheme utilized by Hiruma *et al.* for similar BNT-based solid solutions. The diagram shows that fully saturated polarization hysteresis behavior dominates at low BZT concentrations and low temperatures. As the temperature increases there is first a transition from ferroelectric to "pinched" loops with a significant reduction in remanent polarization and coercive field. This is followed by a transition to a pseudo-linear behavior at compositions above 10% BZT or temperatures above 100–150°C up to a solubility limit of 20% BZT. Finally, above 300–350°C compositions are paraelectric.

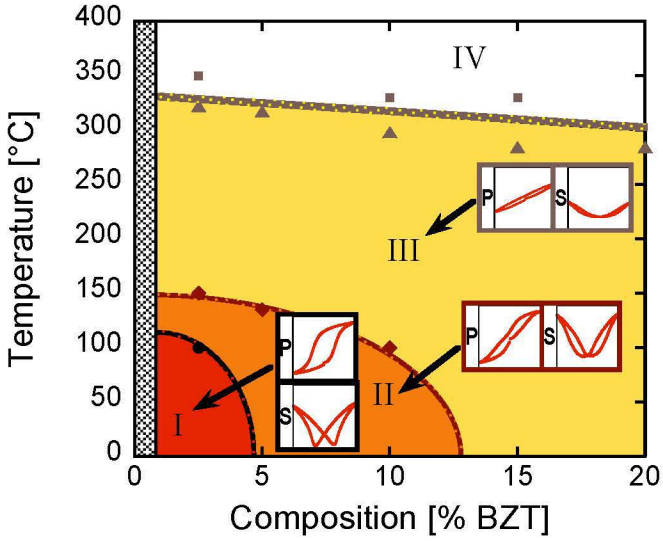

Fig. 6.7 *Phase diagram for BZT–BNT–BKT as a function of temperature showing transition in hysteresis behaviors up to the solubility limit of 20 mol% BZT. The circles and diamonds correspond to data taken from hysteresis measurements (● and u). The squares and triangles correspond to T_{max} values taken from Raman spectroscopy (n) and dielectric data (▲).*

6.5 Conclusions

Single phase ceramics were fabricated in the BZT–BKT–BNT ternary system for < 20mol% BZT and the dielectric and piezoelectric properties investigated. T_{max} of the dielectric spectrum steadily decreased with a corresponding broadening of the transition as BZT concentration increased. At 2.5 BZT–40 BKT–57.5 BNT, a secondary transition commonly observed for MPB BNT–BKT was observed. The polarization hysteresis showed ferroelectric behavior at 2.5% BZT with high remanent polarization of 20.8 μC/cm². At 20% BZT, the hysteresis of the samples becomes severely pinched, with negligible P_r (2.3 μC/cm²). Similarly, as the temperature increased to 175°C, the

remanent polarization of the 2.5% BZT composition drastically reduced to 2.1 μC/cm^2. The onset of this transition corresponds to the lower temperature frequency dispersion observed in the dielectric spectrum. The strain hysteresis also changed shape as BZT concentration increased with the typical ferroelectric butterfly gradually losing any negative strain and widening to a parabolic shape. Maximum strain values of 0.33% were observed at 5–40–55 accompanied by a large d_{33}^* = 547 pm/V.

The author (EP) would like to acknowledge the support of Dr. Peter Mardilovich for his helpful comments.

6.6 References

1. P. S. Baettig, C.F., LeSar, R., Waghmare, U.V., and Spaldin, N.A., "Theoretical Prediction of New High-Performance lead-Free Piezoelectrics," *Chem. Mater.,* **17** 1376-80 (2005).

2. M. R. Suchomel, A. M. Fogg, M. Allix, H. J. Niu, J. B. Claridge, andM. J. Rosseinsky, "Bi2ZnTiO6: A lead-free closed-shell polar perovskite with a calculated ionic polarization of 150 mu C cm(-2)," *Chemistry of Materials,* **18**[21] 4987-89 (2006).

3. Y. Hiruma, Aoyagi, R., Nagata, H. and Takenaka, T., "Ferroelectric and Piezoelectric Properties of (Bi1/2K1/2)TiO3 Ceramics," *Jpn. J. Appl. Phys.,* **44**[7A] 5040-44 (2005).

4. M. Nemoto, Nagata, H., Hiruma, Y., and Takenaka, T., "Fabrication and Piezoelectric Properties of Grain Oriented (Bi1/2K1/2)TiO3-BaTiO3 Ceramics," *Jpn. J. Appl. Phys.,* **47**[5] 3829-32 (2008).

5. R. Ranjan, Dviwedi, A. , "Structure and dielectric properties of (Na0.50Bi0.50)1-xBaxTiO3: 0x0.10," *Sol. State Commun. ,* **135**[6] 394-99 (2005).

6. S. Zhao, Li, G., Ding, A., Wang, T., Yin, Q., "Ferroelectric and piezoelectric properties of (Na,K)0.5Bi0.5TiO3 lead free ceramics. ," *J. Phys. D: Appl. Phys.,* **39**[10] 2277-81 (2006).

7. S. Zhang, Shrout, T.R., Nagata, H., Hiruma, Y., Takenaka, T. , "Piezoelectric properties in (K0.5Bi0.5)TiO3-(Na0.5Bi0.5)TiO3-BaTiO3 lead-free ceramics," *IEEE Trans. Ultrason. Ferroelectr. Freq. Control,* **54**[5] 910-17 (2007).

8. V. A. Isupov, "Ferroelectric Na0.5Bi0.5TiO3 and K0.5Bi0.5TiO3 Perovskites and Their Solid Solutions," *Ferroelect. Review,* **315** 123-47 (2005).

9. H. Nagata, Yoshida, M., Makiuchi, Y. and Takenaka, T., "Large Piezoelectric Constant and High Curie Temperature of Lead-Free Piezoelectric Ceramic Ternary System Based on Bismuth Sodium Titanate-Bismuth Potassium Titanate-Barium Titanate near the Morphotropic Phase Boundary," *Jpn. J. Appl. Phys.,* **42**[Part 1, No. 12] 7401-03 (2003).

10. T. Takenaka, Nagata, H., Hiruma, Y. , "Current Developments and Prospective of Lead-Free Piezoelectric Ceramics," *Jpn. J. Appl. Phys.,* **47**[5] 3787-801 (2008).

11. T. R. Shrout and S. J. Zhang, "Lead-free piezoelectric ceramics: Alternatives for PZT?," *J. Electroceram,* **19** 111-24 (2007).

12. T. Takenaka, Nagata, H., and Hiruma, Y., "Phase Transition Temperatures and Piezoelectric Properties of (Bi1/2Na1/2)TiO3-(Bi1/2K1/2)TiO3-Based Bismuth Perovskite Lead-Free Ferroelectric Ceramics," *IEEE Trans. Ultrason. Ferroelectr. Freq. Control* **56**[8] 1595-612 (2009).

13. Y. Hiruma, Watanabe, T., Nagata, H. and Takenaka, T., "Piezelectric Properties of (Bi1/2Na1/2)TiO3-Based Solid Solutions," *Jpn. J. Appl. Phys.,* **47**[9] 7659-63 (2008).

14. Y. Hiruma, Yoshii, K., Nagata, H., Takenaka, T., "Phase transition temperature and electrical properties of (Bi1/2Na1/2)TiO3-(Bi1/2A1/2)TiO3 (A=Li and K) lead-free ferroelectric ceramics.," *J. Appl. Phys.,* **103**[8] 084121: 1-7 (2008).

15. B. Jaffe, Cook, W.R., and Jaffe, H., "Piezoelectric Ceramics." Academic Press: New York, (1971).

16. E. Aksel, J. S. Forrester, J. L. Jones, P. A. Thomas, K. Page, andM. R. Suchomel, "Monoclinic crystal structure of polycrystalline Na(0.5)Bi(0.5)TiO(3)," *Applied Physics Letters,* **98**[15] (2011).

17. K. Yoshii, Hiruma, Y, Nagata, H., Takenaka, T., "Electrical properties and depolarization temperature of (Bi1/2Na1/2)TiO3-(Bi1/2K1/2)TiO3 lead-free piezoelectric ceramics.," *Jap. J. Appl. Phys. Part 1,* **45**[5B] 4493-96 (2006).

18. R. E. Eitel, Randall, C.A., Shrout, T.R., Rehrig, P.W., Hackenberger, W., and Park, S.E., "New High Temperature Morphotropic Phase Boundary Piezoelectrics Based on Bi(Me)O3-PbTiO3 Ceramics," *Jpn. J. Appl. Phys.,* **40**[Part 1. No. 10] 5999-6002 (2001).

19. C. C. Huang, Naratip, V, Cann, D.P. , "Structure and ferroelectric properties of Bi(Zn(1/2)Ti(1/2))O3-(Bi(1/2)K(1/2))TiO3 perovskite solid solutions," *IEEE Trans. Ultrason. Ferroelectr. Freq. Control,* **56**[7] 1304-08 (2009).

20. A. Sasaki, T. Chiba, Y. Mamiya, andE. Otsuki, "Dielectric and Piezoelectric Properties of (Bi0.5Na0.5)TiO3-Bi0.5K0.5TiO3 Systems," *Japanese Journal of Applied Physics,* **38**[Copyright (C) 1999 Publication Board, Japanese Journal of Applied Physics] 5564-67 (1999).

21. J. Kling, X. Tan, W. Jo, H.-J. Kleebe, H. Fuess, andJ. Rödel, "In Situ Transmission Electron Microscopy of Electric Field-Triggered Reversible Domain Formation in Bi-Based Lead-Free Piezoceramics," *Journal of the American Ceramic Society,* **93**[9] 2452-55 (2010).

22. S.-T. Zhang, A. B. Kounga, E. Aulbach, H. Ehrenberg, andJ. Rodel, "Giant strain in lead-free piezoceramics Bi0.5Na0.5TiO3-BaTiO3-K0.5Na0.5NbO3 system," *Appl. Phys. Lett.,* **91**[11] 112906 (2007).

7 Relaxor to Ferroelectric Transitions in $(Bi_{1/2}Na_{1/2})TiO_3$ – $Bi(Zn_{1/2}Ti_{1/2})O_3$ Solid Solutions

Eric A. Patterson and David P. Cann

Materials Science, School of Mechanical, Industrial and Manufacturing Engineering

Oregon State University

Corvallis, OR 97331

Article first published online: 3, July 2012

Journal of the American Ceramic Society

Early view, 1–5 (2012)

7.1 Abstract

Recently, $(Bi_{1/2}Na_{1/2})TiO_3$ solid solutions have been found to exhibit excellent dielectric and piezoelectric properties. In this study, the dielectric and ferroelectric properties of $(1-x)(Bi_{1/2}Na_{1/2})TiO_3$-$xBi(Zn_{1/2}Ti_{1/2})O_3$ (BNT-BZT) solid solutions were investigated. Up to a solubility limit of 8% BZT, distortions to the parent cubic perovskite phase were observed in the diffraction data through splitting of the (001), (011), and (111) reflections. At low concentrations of BZT, the material behaves very much like a conventional ferroelectric, with well-saturated loops with high remanent polarization (P_r ~ 35 $\mu C/cm^2$). As the BZT content increased, the dielectric behavior displays characteristics of relaxor behavior. Polarization hysteresis data at elevated temperatures and a thermal hysteresis in the dielectric maximum are evidence for a relaxor to ferroelectric transition.

7.2 Introduction

In the search for Pb-free piezoelectric materials, the perovskites compound bismuth sodium titanate, (BNT)[1-5], has been studied extensively since its discovery in 1961. Several recent review papers provide an excellent summary of its dielectric and piezoelectric properties. [6-8] At room temperature it is stabilized in a *R3c* rhombohedral perovskite structure [9, 10], although it has recently been argued that they are better characterized by *Cc* monoclinic symmetry. [11, 12] Upon heating, BNT undergoes a phase transition with a broad dielectric maximum close to 300°C. The ferroelectric (FE)

properties of BNT are characterized by large remanent polarizations ($P_r \sim 40$ μC/cm^2) with large coercive fields ($E_C > 60$ kV/cm). [13, 14]

More commonly, researchers have employed solid solutions with BNT to enhance its dielectric and piezoelectric properties. For example, the solid solution with $(Bi_{0.5}K_{0.5})TiO_3$ (BKT) shows vastly improved sinterability using conventional ceramic fabrication processes and a morphotropic phase boundary (MPB) near 80BNT-20BKT with optimum piezoelectric properties. [6, 7, 13, 15-18] At this MPB composition, the remanent polarization, piezoelectric coefficient and coupling coefficients were found to be $P_r = 38$ μC/cm^2, $d_{33} = 167$ pC/N, and $k_{33} = 0.56$, respectively. [15]

Solid solutions with BNT have shown interesting properties including $BaTiO_3$ (BT)[18-22], (K,Na)NbO_3 (KNN)[23,24], and many other binary and ternary compositions. [25-36] In BNT-BT solid solutions, complex phase equilibria behavior occurs over the compositional range 6-10 mol% BT between tetragonal, rhombohedral and pseudocubic phases. In the vicinity of 6 mol% BT, the dielectric and piezoelectric properties are pronounced with d_{33} values approaching 125 pC/N.[18] Upon heating, however, the material undergoes a phase transition to a non-polar phase which results in depolarization and the loss of piezoelectric properties at temperatures as low as 150°C.[18]

Similar results have been observed in solid solutions between BNT and KNN. From the work of Kounga *et al.*, at 7 mol% KNN there is an MPB between a rhombohedral FE phase and a tetragonal anti-ferroelectric (AFE) phase.[23] Optimal d_{33} and electromechanical coupling coefficients (k_p) were recorded near this MPB. Interestingly, large field-induced strains with significant hysteresis were observed for compositions

beyond the MPB in the AFE phase. In this and the similar BNT-BT-KNN system, the large strains were attributed to a reversible AFE-FE phase transition. [23, 37]

This work will focus on the dielectric and ferroelectric properties of the solid solution between BNT and $Bi(Zn_{1/2}Ti_{1/2})O_3$ (BZT). The end member BZT is not a stable perovskite at room temperature and 1 atm pressure, but previous work has shown that it can form solid solutions with stable perovskite end members such as BT, BKT, and $PbTiO_3$. [38-44] The properties of these BZT-based solid solutions have shown excellent properties. With high permittivities (ε_r > 1000), large field induced strains with d_{33}* values as high as 500 pm/V, and excellent high temperature properties.[45,46,47]

7.3 Experimental Methods

A conventional mixed oxide method was used to prepare the compositions based on $(1-x)(Bi_{0.5}Na_{0.5})TiO_3$-$xBi(Zn_{1/2}Ti_{1/2})O_3$. High purity (>99%) Bi_2O_3, $NaCO_3$, ZnO, and TiO_2 powders were used as precursors. The powders were mixed and ground by using a vibratory milling machine for 6 hours. After drying the mixture in an oven for at least 12 hours, the powder, which was contained in an alumina crucible, was calcined at 900-975°C for 6 hours. Before making a pellet, the calcined powder was milled again by vibratory milling for 6 hours to obtain a fine particle size. Pellets were uniaxially cold pressed and sintered in sacrificial powders at 1050-1100°C for 2-8 hours, with temperatures decreasing and time increasing as mol% BZT was increased. X-ray diffraction was used to confirm the presence of a single perovskite phase. Prior to electrical measurements, samples were polished to sub-millimeter thickness and high-

temperature silver paste (Heraeus C1000) was fired on both sides in air at 650°C for 30 minutes. An LCR meter (Agilent 4284A) was used to measure the dielectric properties for a wide variety of frequencies and temperatures using a high temperature measurement cell (NorECS Probostat). Hysteresis measurements were made using a Sawyer-Tower circuit based ferroelectric measurement set-up (Radiant Technology) utilizing Vision software.

7.4 Results

All of the compositions were sintered to relatively high densities (r > 95% theoretical density) at relatively low sintering temperatures (T ≤ 1100°C). Consistent with prior results on BZT solid solutions, it is likely that BZT acts as a sintering aid in some manner. Analysis of x-ray diffraction data revealed that a single perovskite phase was present for all compositions with BZT concentrations below a solubility limit of approximately 8% BZT where a weak reflection from a parasitic bismuth titanate phase appears. For simplicity, all peak indices are referenced relative to the pseudocubic perovskite unit cell as shown in Fig. 7.1.

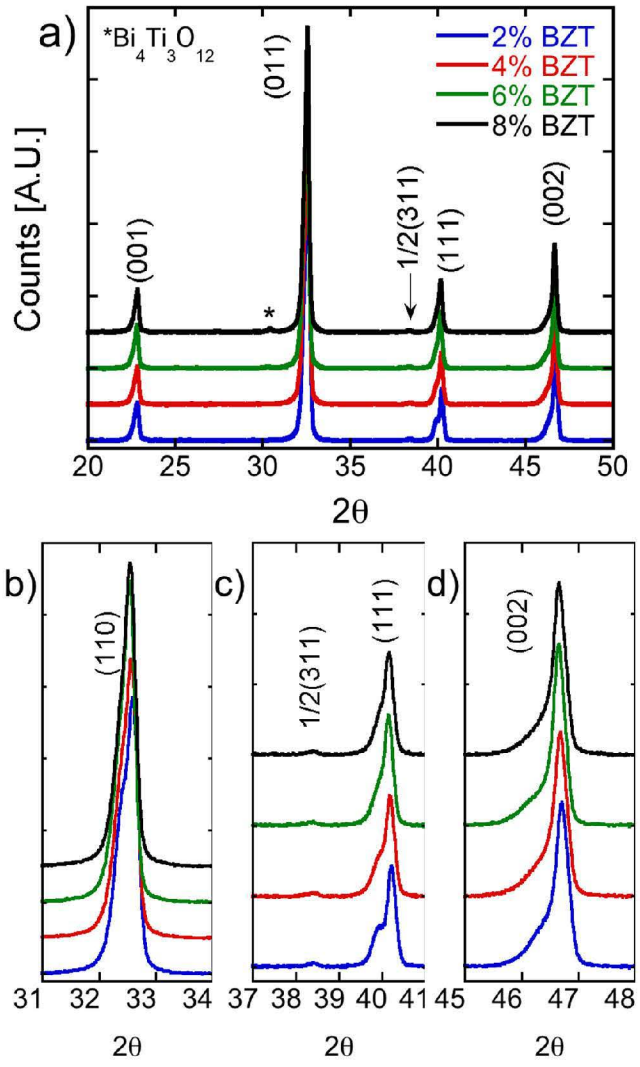

Fig. 7.1 *X-ray diffraction data on a) (1-x)BNT-xBZT solid solutions, with close ups on the splittings in the b) (110), c) superlattice and (111), and d) (002) reflections.*

Peak splittings were observed in the (001), (011), and (111) peaks as well as the higher order peaks. These results are considerably different than the XRD results on similar compositions by Zhang *et al.* which assigned rhombohedral symmetry to compositions with BZT concentrations greater than x=0.375.[41] This is likely due to minor differences in the processing conditions and starting materials. The observation of multiple peak

splittings was observed in the BNT-KNN system where it was attributed to the coexistence of tetragonal and rhombohedral phases.[23] No obvious trends in the relative amounts of rhombohedral or tetragonal distortions were observed over the range of compositions from 2 to 8 mol% BZT. Alternatively, the distortions observed at these peaks in pure BNT have been attributed to *Cc* monoclinic symmetry.[11] In addition, the XRD clearly shows evidence of ($^3/_2$ $^1/_2$ $^1/_2$) superlattice peaks, which were most prevalent in compositions with 2% and 4% BZT. The same superlattice peaks were also reported in pure BNT powders from crushed, sintered samples. [11,41]

The dielectric properties as a function of temperature of the BNT-BZT ceramic (upon cooling) is shown in Fig. 7.2. There is a broad dielectric maximum with similar characteristics to other BNT-based solutions. The temperature at which the relative permittivity is maximum (T_{max}) is largely independent of composition varying over the narrow range of 333 to 345°C. Below the dielectric maximum, all compositions exhibit a dielectric dispersion that is less pronounced above T_{max}.

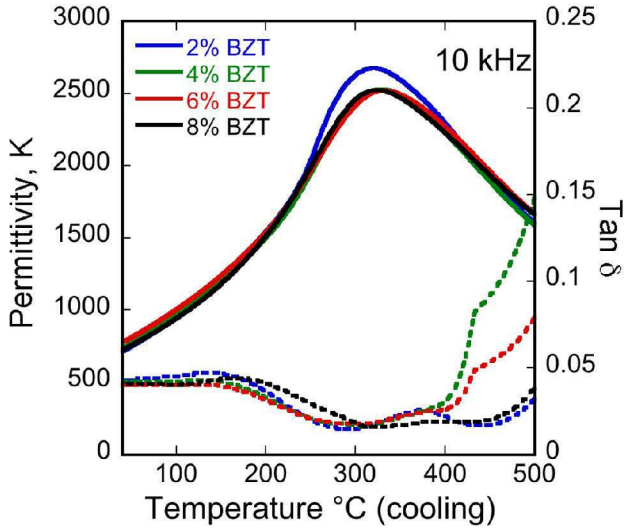

Fig. 7.2 *Dielectric properties at 10 kHz of (1-x)BNT-xBZT ceramics as a function of temperature (data taken on cooling).*

Most interestingly, all of the compositions exhibit significantly different dielectric spectra on heating versus cooling. As shown in Fig. 7.3, T_{max} shifts to lower temperatures on cooling (ΔT_{max} = 12-14°C) and the decrease in permittivity below T_{max} is less sharp. The dielectric properties upon cooling eventually converge as room temperature is approached.

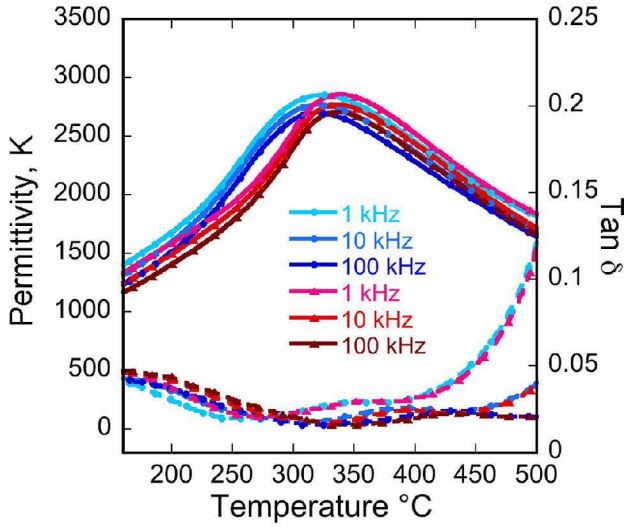

Fig. 7.3 *Dielectric spectra of 96BNT-4BZT on heating (triangles) and cooling (circles) at frequencies of 1, 10, and 100 kHz.*

Behavior of this nature is sometimes observed in poled specimens, which after depoling, exhibit a different dielectric spectra upon cooling. The samples in this study were virgin samples that were not subjected to any poling or any prior electrical measurements. Furthermore the same experiment was repeated for the 4 mol% BZT composition and the data obtained on both heating and cooling data were identical to the results from the initial run shown in Fig. 7.3.

The polarization hysteresis measurements conducted on the BNT-BZT samples are shown in Fig. 7.4. At low BZT concentrations, the hysteresis loops show full saturation with a strong remanent polarization as high as 35 $\mu C/cm^2$.

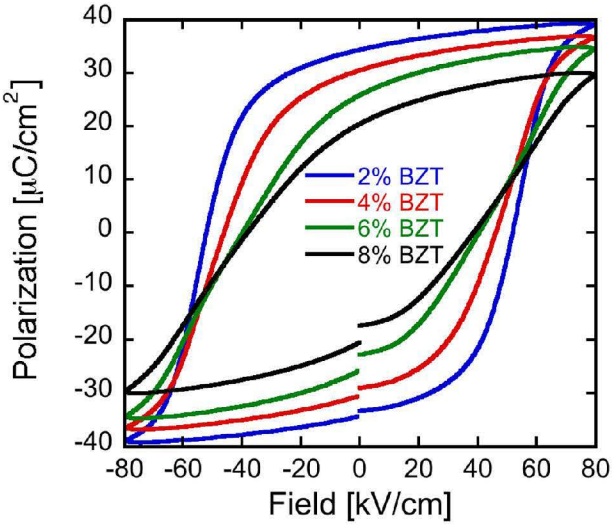

Fig. 7.4 *Polarization hysteresis measurements on (1-x)BNT-xBZT ceramics taken at room temperature at 1 Hz.*

Immediately after the polarization hysteresis measurements these samples exhibited low-field d_{33} values of between 40 to 80 pC/N, which confirms the presence of domain alignment without prior application of a dc bias. As the BZT content increased the loops began to take on relaxor-like characteristics with a decrease in the coercive field and a decrease in the remanent polarization as the BZT content increased. This is similar to other results seen in BZT solid solutions, for example in the work of Zhang[41] and Wang.[43] However the pinching of the remanent polarization shows no signs of a double-loop configuration as has been seen in other systems.[45]

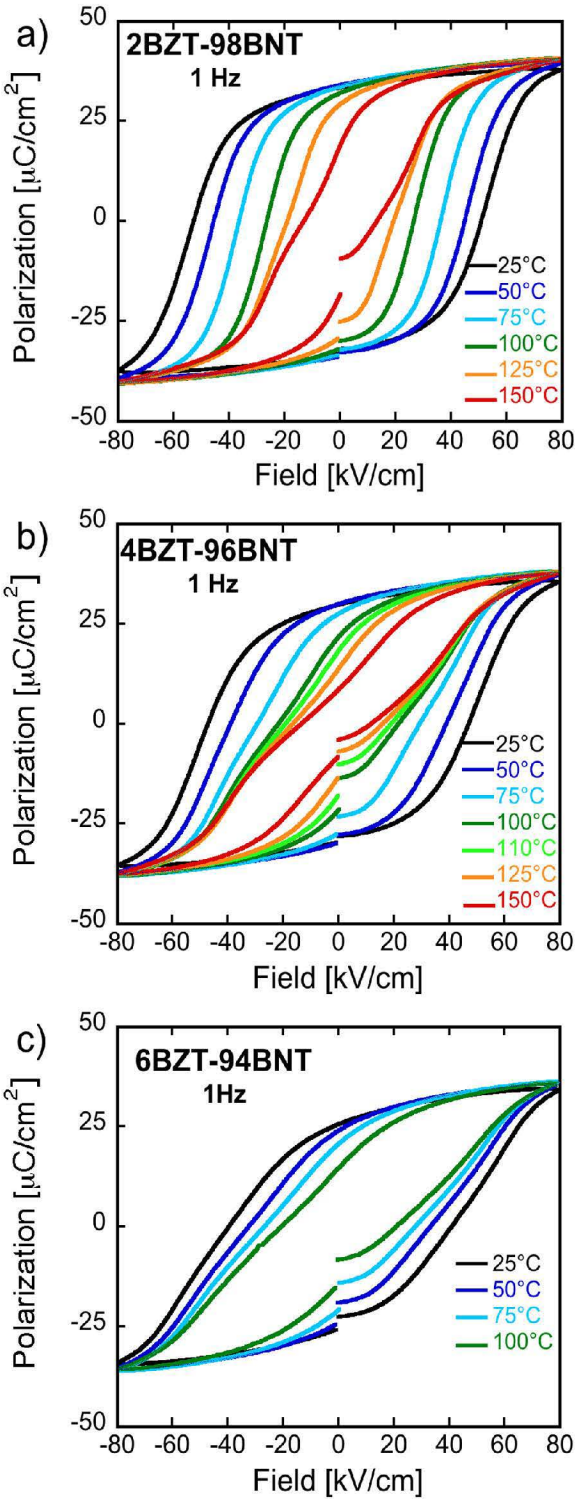

Fig. 7.5 *Polarization hysteresis measurements taken on a) 98BNT-2BZT, b) 96BNT-4BZT and c) 94BNT-6BZT ceramics at elevated temperatures at 1 Hz.*

Polarization hysteresis measurements at elevated temperatures are shown in Fig. 7.5. At 2 mol% BZT, a clear decrease in the coercive field was noted as the temperature increased with no loss in saturation or remanent polarization until approximately 150°C. At 150°C, a significant loss in remanent polarization (i.e. "pinching") was observed with a clear double-loop character. Above an electric field of 40 kV/cm, the polarization at 150°C converged to the same maximum polarization value as the room temperature data. The data for the 4 mol% BZT composition showed a similar trend, with the onset of the pinching occurring at 100°C. Finally, at 6 mol% BZT, the hysteresis loops were less saturated and were characterized by a more gradual loss of remanent polarization starting at temperatures above 75°C.

7.5 Discussion

Hysteresis loops characterized by temperature dependent pinching have been observed in a number of ferroelectric and relaxor ferroelectric materials. In ferroelectric materials this behavior is attributed to aging processes that are tied to interactions between domain walls and charged defects. [48,49] The features shown in Fig. 7.5 are also similar to observations in relaxor materials such as PLZT 8/36/65,[50,51] $Pb(Sc_{1/2}Nb_{1/2})O_3$[52], and $Ba(Ti_{0.7}Zr_{0.3})O_3$. [53,54] A recent report by Jo *et al.* illustrated a similar hysteresis behavior in BNT with 6 mol% $BaTiO_3$.[55] Jo's analysis attributes the observed behavior in BNT-6BT to relaxor behavior where the transition observed in the hysteresis data is simply a relaxor-to-ferroelectric transition. This analysis would seem to apply to the hysteresis behavior

observed in the present work as shown in Fig. 7.5 for BNT-BZT as well as the previously observed hysteresis behavior of pure BNT and MPB compositions in the binary system BNT-BKT.[5,56] This also bears some similarities to the work of Dittmer *et al.*[45] on the ternary system based on BZT added to the MPB composition 0.8BNT-0.2BKT. Interestingly, however, the ternary BNT-BKT-BZT compositions showed no evidence of splitting in the {200} or {111} reflections while in the present work the there is clear evidence of splitting in both {200} and {111} reflections in unpoled ceramics of all compositions with no discernable trend with BZT content.[45,55] In BNT-6BT as well as for 2%BZT-BNT-BKT, these same peak splittings can be induced under an applied electric field.[55,57,58]

The results in this work have many similarities to the phase transitions seen in disordered $Pb(Sc_{1/2}Nb_{1/2})O_3$ (PSN). [52] A thermal hysteresis in the transition temperature on the order of 10°C was observed which is comparable to the hysteresis shown in Fig. 7.3 in this work. In PSN, this observation along with differential scanning calorimetry data was attributed to a first-order relaxor to normal ferroelectric phase transition. In PSN, this transition is clearly seen in the relative permittivity as a function of temperature. However, in BZT-BNT there is no clear signature in the dielectric data however the thermal hysteresis and the relaxor to ferroelectric transition seen in the high temperature polarization hysteresis data BZT-BNT system are clearly linked. This may be due to the greater structural and chemical complexity in BZT-BNT compared to PSN.

The transition in polarization hysteresis behavior is schematically illustrated in Fig. 7.6. The transition temperatures were estimated from the polarization hysteresis data and from dielectric measurements.

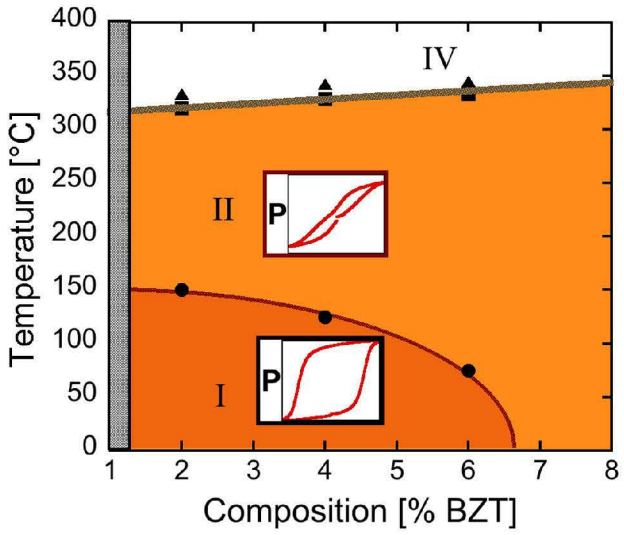

Fig. 7.6 *Schematic diagram showing the transition in polarization hysteresis behavior. The circles correspond to data taken from hysteresis measurements (●). The squares and triangles correspond to T_{max} values taken from dielectric data on cooling (■) and heating (▲).*

The diagram shows that fully saturated polarization hysteresis behavior dominates at low BZT concentrations and low temperatures. As the temperature increases there is a transition to relaxor behavior with characteristic pinched loops. As the BZT content increased that transition temperature decreased such that for 8% BZT the loops are poorly saturated. Room temperature polarization measurements conducted at 0.1 Hz show higher remanent and saturation polarization values than data taken at 1 Hz. This was especially prominent for solid solutions with higher BZT content. Furthermore, in

the 6 and 8 mol% BZT specimens, consecutive hysteresis measurements at 1 Hz led to increased remanent and saturation polarization values. These time-dependent results were much less apparent but still measureable in the 2% and 4% BZT compositions. These time or cycle dependent polarization data and the hysteretic nature of the dielectric data in Fig. 7.3 suggest that the kinetics are very slow.

7.6 Conclusions

In this work, the dielectric and ferroelectric properties of BNT-BZT solid solutions were investigated. Diffraction data on all of the specimens showed no significant secondary phases up to approximately 8 mol% BZT and clear peak splitting of the (001), (011), and (111) reflections. At low concentrations of BZT, the material behaves very much like a conventional ferroelectric, with well-saturated loops with high remanent polarization (P_r ~ 35 μC/cm^2). As the BZT content increased, the remanent polarization and coercive field decreased and the hysteresis data were characterized by features consistent with relaxor behavior. Temperature dependent hysteresis measurements showed that, on heating, the remanent polarization decreased significantly and the data showed double-loop characteristics. This finding, along with the observation of thermal hysteresis in the dielectric maximum, indicates the presence of a relaxor to ferroelectric transition in this material. These results include many common characteristics with similar perovskite systems that exhibit a relaxor to ferroelectric transition.

7.7 References

1. G. A. Smolenskii, V. A. Isupov, A. I. Agranovskaya, and N. N. Krainik, "New Ferroelectrics of Complex Composition IV. ," *Sov. Phys. Solid State,* **2** 2651 (1961).

2. C. S. Tu, I. G. Siny, and V. H. Schmidt, "Sequence of dielectric anomalies and high-temperature relaxation behavior in (Na1/2Bi1/2)TiO3," *Physical Review B,* **49**[17] 11550-59 (1994).

3. J. Suchanicz, A. Jeżowski, and R. Poprawski, "Low-Temperature Thermal and Dielectric Properties of Na0.5Bi0.5TiO3," *physica status solidi (a),* **169**[2] 209-15 (1998).

4. K. Roleder, I. Franke, A. M. Glazer, P. A. Thomas, S. Miga, and J. Suchanicz, "The piezoelectric effect in (Na0.5Bi0.5)TiO3 ceramics," *Journal of Physics: Condensed Matter,* **14**[21] 5399 (2002).

5. Y. Hiruma, H. Nagata and T. Takenaka, "Thermal depoling process and piezoelectric properties of bismuth sodium titanate ceramics " *J. Appl. Phys.,* **105** 084112 (2009).

6. S. Zhao, G. Li, A. Ding, T. Wang, and Q. Yin, "Ferroelectric and piezoelectric properties of (Na,K)0.5Bi0.5TiO3 lead free ceramics. ," *J. Phys. D: Appl. Phys.,* **39**[10] 2277-81 (2006).

7. V. A. Isupov, "Ferroelectric Na0.5Bi0.5TiO3 and K0.5Bi0.5TiO3 Perovskites and Their Solid Solutions," *Ferroelect. Review,* **315** 123-47 (2005).

8. T. R. Shrout and S. J. Zhang, "Lead-free piezoelectric ceramics: Alternatives for PZT?," *J. Electroceram,* **19** 111-24 (2007).

9. J. Suchanicz and J. Kwapulinski, "X-ray diffraction study of the phase transitions in Na0.5Bi0.5TiO3," *Ferroelectrics,* **165**[1] 249-53 (1995).

10. G. O. Jones and P. A. Thomas, "Investigation of the structure and phase transitions in the novel A-site substituted distorted perovskite compound Na0.5Bi0.5TiO3," *Acta Crystallographica Section B,* **58**[2] 168-78 (2002).

11. E. Aksel, J. S. Forrester, J. L. Jones, P. A. Thomas, K. Page, and M. R. Suchomel, "Monoclinic crystal structure of polycrystalline (Na0.5Bi0.5)TiO3," *Applied Physics Letters,* **98**[15] (2011).

12. E. Aksel, J. S. Forrester, B. Kowalski, J. L. Jones, and P. A. Thomas, "Phase transition sequence in sodium bismuth titanate observed using high-resolution x-ray diffraction," *Applied Physics Letters,* **99**[22] 222901 (2011).

13. T. Takenaka, H. Nagata, and Y. Hiruma, "Phase Transition Temperatures and Piezoelectric Properties of (Bi1/2Na1/2)TiO3-(Bi1/2K1/2)TiO3-Based Bismuth

Perovskite Lead-Free Ferroelectric Ceramics," *IEEE Trans. Ultrason. Ferroelectr. Freq. Control* **56**[8] 1595-612 (2009).

14. B. Jaffe, W.R. Cook, and H. Jaffe, "Piezoelectric Ceramics." Academic Press: New York, (1971).

15. Y. Hiruma, K. Yoshii, H. Nagata, and T. Takenaka, "Phase transition temperature and electrical properties of (Bi1/2Na1/2)TiO3-(Bi1/2A1/2)TiO3 (A=Li and K) lead-free ferroelectric ceramics.," *J. Appl. Phys.,* **103**[8] 084121: 1-7 (2008).

16. A. Sasaki, T. Chiba, Y. Mamiya, and E. Otsuki, "Dielectric and Piezoelectric Properties of (Bi0.5Na0.5)TiO3-(Bi0.5K0.5)TiO3 Systems," *Japanese Journal of Applied Physics,* **38**, 5564 (1999).

17. Y.-R. Zhang, J.-F. Li, B.-P. Zhang, and C.-E. Peng, "Piezoelectric and ferroelectric properties of Bi-compensated (Bi1/2Na1/2)TiO3-(Bi1/2K1/2)TiO3 lead-free piezoelectric ceramics," *Journal of Applied Physics,* **103**[7] 074109 (2008).

18. T. Takenaka, K. Maruyama, and K. Sakata, "(Bi1/2Na1/2)TiO3-BaTiO3 System for Lead-Free Piezoelectric Ceramics," *Jpn. J. Appl. Phys.,* **30**[9B] 2236-39 (1991).

19. R. Ranjan and A. Dviwedi, "Structure and dielectric properties of (Na0.5Bi0.5)1-xBaxTiO3: 0≤x≤0.1," *Sol. State Commun.* , **135**[6] 394-99 (2005).

20. Z. Luo, T. Granzow, J. Glaum, W. Jo, J. Rödel, and M. Hoffman, "Effect of Ferroelectric Long-Range Order on the Unipolar and Bipolar Electric Fatigue in Bi1/2Na1/2TiO3-Based Lead-Free Piezoceramics," *Journal of the American Ceramic Society,* **94**[11] 3927-33 (2011).

21. Z. Luo, J. Glaum, T. Granzow, W. Jo, R. Dittmer, M. Hoffman, and J. Rödel, "Bipolar and Unipolar Fatigue of Ferroelectric BNT-Based Lead-Free Piezoceramics," *Journal of the American Ceramic Society,* **94**[2] 529-35 (2011).

22. M. Ehmke, J. Glaum, W. Jo, T. Granzow, and J. Rödel, "Stabilization of the Fatigue-Resistant Phase by CuO Addition in (Bi1/2Na1/2)TiO3–BaTiO3," *Journal of the American Ceramic Society,* **94**[8] 2473-78 (2011).

23. A. B. Kounga, S.-T. Zhang, W. Jo, T. Granzow, and J. Rodel, "Morphotropic phase boundary in (1-x)Bi0.5Na0.5TiO3 - xK0.5Na0.5NbO3 lead-free piezoceramics," *Applied Physics Letters,* **92**[22] 222902-02-3 (2008).

24. H. Ishii, H. Nagata, and T. Takenaka, "Morphotropic Phase Boundary and Electrical Properties of Bisumuth Sodium Titanate-Potassium Niobate Solid-Solution Ceramics," *Jpn. J. Appl. Phys.,* **40** 3 (2001).

25. C. Zhou and X. Liu, "Dielectric and piezoelectric properties of bismuth-containing complex perovkite solid solution of Bi1/2Na1/2TiO3-Bi(Mg2/3Nb1/3)O3," *J. Mater. Sci,* **43** 1016-19 (2008).

26. Y. Hiruma, H. Nagata, and T. Takenaka, "Phase diagrams and electrical properties of (Bi1/2Na1/2)TiO3-based solid solutions," *Journal of Applied Physics,* **104**[12] 124106 (2008).

27. K. Sakata and Y. Masuda, "Ferroelectric and antiferroelectric properties of (Na0.5Bi 0.5)TiO3-SrTiO3 solid solution ceramics," *Ferroelectrics,* **7** 347 (1974).

28. X. X. Wang, X. G. Tang, and H. L. W. Chan, "Electromechanical and ferroelectric properties of (Bi1/2Na1/2)TiO3-(Bi1/2K1/2)TiO3-BaTiO3 lead-free piezoelectric ceramics," *Applied Physics Letters,* **85**[1] 91-93 (2004).

29. H. Nagata, M. Yoshida, Y. Makiuchi and T. Takenaka, "Large Piezoelectric Constant and High Curie Temperature of Lead-Free Piezoelectric Ceramic Ternary System Based on Bismuth Sodium Titanate-Bismuth Potassium Titanate- Barium Titanate near the Morphotropic Phase Boundary," *Jpn. J. Appl. Phys.,* **42**[Part 1, No. 12] 7401-03 (2003).

30. J. Shieh, K. C. Wu, and C. S. Chen, "Switching characteristics of MPB compositions of (Bi0.5Na0.5)TiO3-BaTiO3-(Bi0.5K0.5)TiO3 lead-free ferroelectric ceramics," *Acta Materialia,* **55**[9] 3081-87 (2007).

31. J. Yoo, D. Oh, Y. Jeong, J. Hong, and M. Jung, "Dielectric and piezoelectric characteristics of lead-free Bi0.5(Na0.84K0.16)0.5TiO3 ceramics substituted with Sr," *Materials Letters,* **58**[29] 3831-35 (2004).

32. X. Y. Wang, C. L. Wang, M. L. Zhao, J. F. Wang, K. Yang, and J. C. Li, "Ferroelectric properties of lithia-doped (Bi0.95Na0.75K0.20)0.5Ba0.05TiO3 ceramics," *Materials Letters,* **61**[18] 3847-50 (2007).

33. S.-T. Zhang, L. Wang, Y.-F. Chen, and A. B. Kounga, "Phase Characteristics and Piezoelectric Properties in the Bi0.5Na0.5TiO3–BaTiO3–K0.5Na0.5NbO3 System," *Journal of the American Ceramic Society,* **93**[6] 1561-64 (2010).

34. J. E. Daniels, W. Jo, J. Rodel, V. Honkimaki, and J. L. Jones, "Electric-field-induced phase-change behavior in (Bi0.5Na0.5)TiO3-BaTiO3-(K0.5Na0.5)NbO3: A combinatorial investigation," *Acta Materialia,* **58**[6] 2103-11 (2010).

35. Y. J. Dai, S. Zhang, T. R. Shrout, and Z. W. Zhang, "Piezoelectric and Ferroelectric Properties of Li-Doped (Bi0.5Na0.5)TiO3-(Bi0.5K0.5)TiO3-BaTiO3 Lead-Free Piezoelectric Ceramics," *J. Am. Ceram. Soc.,* **93**[4] 1108-13 (2010).

36. P. Jarupoom, E. Patterson, B. Gibbons, G. Rujijanagul, R. Yimnirun, and D. Cann, "Lead-free ternary perovskite compounds with large electromechanical strains," *Applied Physics Letters,* **99**[15] (2011).

37. S.-T. Zhang, A. B. Kounga, E. Aulbach, H. Ehrenberg, and J. Rodel, "Giant strain in lead-free piezoceramics Bi0.5Na0.5TiO3-BaTiO3-K0.5Na0.5NbO3 system," *Appl. Phys. Lett.,* **91**[11] 112906 (2007).

38. C.-C. Huang and D. P. Cann, "Phase transitions and dielectric properties in Bi(Zn1/2Ti1/2)O3 - BaTiO3 perovskite solid solutions," *Journal of Applied Physics,* **104**[2] 024117 (2008).

39. M. R. Suchomel and P. K. Davies, "Enhanced tetragonality in (x)PbTiO3-(1-x)Bi(Zn1/2Ti1/2)O3 and related solid solution systems," *Applied Physics Letters,* **86**[26] 262905 (2005).

40. C. C. Huang, N. Vittayakorn, D.P. Cann, "Structure and ferroelectric properties of Bi(Zn1/2Ti1/2)O3-(Bi1/2K1/2)TiO3 perovskite solid solutions," *IEEE Trans. Ultrason. Ferroelectr. Freq. Control,* **56**[7] 1304-08 (2009).

41. S.-T. Zhang, F. Yan, and B. Yang, "Morphotropic phase boundary and electrical properties in (1−*x*)Bi0.5Na0.5TiO3−*x*Bi(Zn0.5Ti0.5)O3 lead-free piezoceramics," Journal of Applied Physics , **107**, 114110 (2010).

42. Y. Oshima, Y. Kitanaka, Y. Noguchi, and M. Miyayama, "Materials design and characterization of (Bi1/2Na1/2)TiO3-Bi(*B',B"*)O3 ceramics," *Key Engineering Materials*, **445**, pp. 59-62, (2010).

43. L. Wang, J.H.Cho, Y.S. Sung, M.H. Kim, T.K. Song, S.S. Kim, and B.C. Choi, "'Dielectric and Piezoelectric Properties of Lead-free BaTiO3-Bi(Zn0.5Ti0.5)O3 and (Bi0.5Na0.5)TiO3-Bi(Zn0.5Ti0.5)O3 Ceramics," *Ferroelectrics*, **380**:1, pp. 177-182, (2009).

44. R. Muanghlua, S. Niemcharoen, W.C. Vittayakorn, N. Tungsitivisetkul, P. Chinwaro, A. Ruangphanit, N. Chaiyo, and N. Vittayakorn, *Ferroelectrics,* **383**:1, pp. 1-7, (2009).

45. R. Dittmer, W. Jo, J. Daniels, S. Schaab, and J. Rödel, "Relaxor Characteristics of Morphotropic Phase Boundary (Bi1/2Na1/2)TiO3–(Bi1/2K1/2)TiO3 Modified with Bi(Zn1/2Ti1/2)O3," *Journal of the American Ceramic Society,* **94**[12] 4283-90 (2011).

46. N. Raengthon and D. P. Cann, "High temperature electronic properties of BaTiO3 – Bi(Zn1/2Ti1/2)O3 – BiInO3 for capacitor applications," *Journal of Electroceramics,* **28** pp. 165-171 (2012).

47. N. Raengthon and D.P. Cann, "Dielectric relaxation in BaTiO3-Bi(Zn1/2Ti1/2)O3 ceramics," *Journal of the American Ceramic Society (in press)* DOI: 10.1111/j.1551-2916.2011.05018.x (2012).

48. M. I. Morozov and D. Damjanovic, "Hardening-softening transition in Fe-doped Pb(Zr,Ti)O3 ceramics and evolution of the third harmonic of the polarization response," *Journal of Applied Physics,* **104**[3] 034107-07-8 (2008).

49. G. Robert, D. Damjanovic, and N. Setter, "Preisach modeling of ferroelectric pinched loops," *Applied Physics Letters,* **77**[26] 4413-15 (2000).

50. V. Y. Shur, B. L. Rumyantsev, G. G. Lomakin, O. V. Yakutova, D. V. Pelegov, A. Sternberg, and M. Kosec, "AC Switching of Relaxor PLZT Ceramics," *Ferroelectrics,* **314**[1] 245-53 (2005).

51. S. Schaab and T. Granzow, "Temperature dependent switching mechanism of (Pb0.92La0.08)(Zr0.65Ti0.35)O3 investigated by small and large signal measurements," *Applied Physics Letters,* **97**[13] 132902 (2010).

52. F. Chu, I. M. Reaney, and N. Setter, "Spontaneous (zero-field) relaxor--to--ferroelectric-phase transition in disordered Pb(Sc1/2Nb1/2)O3," *Journal of Applied Physics,* **77**[4] 1671-76 (1995).

53. Z. Yu, C. Ang, R. Guo, and A. S. Bhalla, "Piezoelectric and strain properties of Ba(Ti1 - xZrx)O3 ceramics," *Journal of Applied Physics,* **92**[3] 1489-93 (2002).

54. Z. Yu, C. Ang, R. Guo, and A. S. Bhalla, "Ferroelectric-relaxor behavior of Ba(Ti0.7Zr0.3)O3 ceramics," *Journal of Applied Physics,* **92**[5] 2655-57 (2002).

55. W. Jo, S. Schaab, E. Sapper, L. A. Schmitt, H.-J. Kleebe, A. J. Bell, and J. Rodel, "On the phase identity and its thermal evolution of lead free (Bi1/2Na1/2)TiO3-6 mol% BaTiO3," *Journal of Applied Physics,* **110**[7] 074106 (2011).

56. K. T. P. Seifert, W. Jo, and J. Rodel, "Temperature-Insensitive Large Strain of (Bi1/2Na1/2)TiO3-(Bi1/2K1/2)TiO3-(K1/2Na1/2)NbO3 Lead-Free Piezoceramics," *J. Am. Ceram. Soc.,* **93**[5] 1392-96 (2010).

57. J. Daniels, W. Jo, J. Rödel, and J.L. Jones, " Electric-field-induced phase transformation at a lead-free morphotropic phase boundary: Case study in a 93%(Bi0.5Na0.5)TiO3–7% BaTiO3 piezoelectric ceramic," *Applied Physics Letters,* **95**, 032904 (2009).

58. W. Jo, J.E. Daniels, J.L. Jones, X. Tan, P.A. Thomas, D. Damjanovic, and J. Rödel, "Evolving morphotropic phase boundary in lead-free (Bi0.5Na0.5)TiO3–7% BaTiO3 piezoceramics," *Journal of Applied Physics*, **109**, 014110 (2011).

8 Bipolar Piezoelectric Fatigue of $Bi(Zn_{0.5}Ti_{0.5})O_3$ - $(Bi_{0.5}K_{0.5})TiO_3$ -$(Bi_{0.5}Na_{0.5})TiO_3$ Pb-free Ceramics

Eric A. Patterson and David P. Cann

Materials Science, School of Mechanical, Industrial and Manufacturing Engineering

Oregon State University

Corvallis, OR 97331

Published online on 26 July 2012

Applied Physics Letters

101, 042905 (2012)

8.1 Abstract

The piezoelectric fatigue behavior of Pb-free ceramics based on solid solutions of $Bi(Zn_{0.5}Ti_{0.5})O_3$ -$(Bi_{0.5}K_{0.5})TiO_3$ -$(Bi_{0.5}Na_{0.5})TiO_3$ was characterized at 50 kV/cm after 10^6 bipolar cycles . Ferroelectric compositions containing 2.5% $Bi(Zn_{0.5}Ti_{0.5})O_3$ exhibited only minor losses in maximum strain (~ 10%). In compositions with 5% $Bi(Zn_{0.5}Ti_{0.5})O_3$ that exhibit large electric field-induced strains, the electromechanical strain actually increased 4%, exhibiting essentially fatigue free behavior. This finding demonstrates that these materials have excellent potential for demanding high cycle applications such as microelectromechanical systems actuators.

8.2 Background

The search for lead-free alternatives to lead-zirconate titanate (PZT) continues to gain more attention as companies endeavor to reduce the impact of Pb-containing materials on the environment. Compounds such as $(Bi_{0.5}K_{0.5})TiO_3$ (BKT) and $(Bi_{0.5}Na_{0.5})TiO_3$ (BNT), and their solid solutions with $BaTiO_3$ (BT) or $KNaNbO_3$ (KNN) and other tetragonal perovskites exhibit promising piezoelectric properties [1-10] and are considered as possible candidates to replace Pb-based materials[9, 11, 12]. One promising system achieves a large normal ferroelectric response, BNT-BT, through a mechanism tied to phase coexistence and an enhanced capacity for domain texturing associated with relaxor behavior similar to La-modified PZT[13, 14]. In the closely related ternary system (BNT-BT-KNN), an anomalous large electromechanical strain approaching 0.4%

develops in association with a phase transition from pseudocubic to tetragonal symmetry[15-17].

Another common method has been forming solid solutions of BNT–BKT with end members that are unstable in ambient processing conditions, such as $Bi(Mg_{1/2}Ti_{1/2})O_3$ or $Bi(Ni_{1/2}Ti_{1/2})O_3$[18]. Previously it was shown that when BNT-BKT is combined with increasing concentrations of $Bi(Zn_{1/2}Ti_{1/2})O_3$ (BZT), a transition from normal ferroelectric behavior to a material with large electric field induced strains was observed[19, 20]. The higher BZT containing compositions are characterized by large hysteretic strains (> 0.3%) with no negative strains that might indicate domain switching. Polarization hysteresis measurements show pinched loops with low or negligible remanent polarizations that yield relatively small low field d_{33} values. The Bi-based systems, generally, have shown complex poling behavior and it has been difficult to achieve repeatable low-field, piezoelectric coefficients (d_{33}).

In addition to the environmental concerns driving this work, PZT is also known to exhibit poor piezoelectric fatigue properties with relatively severe degradation in strain behavior after only a few millions of cycles of applied field [21-26]. In bipolar fatigue studies for PZT, the permanent effects are tied to reduction in strain and switchable polarization simultaneously, implying a reduction of the mobility of domain walls. Significant fatigue was found begin in the range of $2.5x10^5$ and $3x10^5$ cycles of applied fields at twice the coercive field level [21, 23, 27]. A clear asymmetry of the degradation of the maximum strain on positive versus negative applied voltage was observed as another important component of the fatigue effect. Due to the dominating presence of oxygen

vacancies in perovskite ferroelectrics, a defect agglomeration model was proposed to explain the pinning of domain walls and the induced polarization offset necessary to explain both fatigue effects seen in PZT [23, 27].

It should be noted completely electrostrictive rhombohedral phases of lanthanum doped PZT behavior were shown to be fatigue free up to 10^6 cycles[23, 24]. More recently morphotropic phase boundary (MPB) compositions of 94BNT-6BT have been investigated for piezoelectric fatigue at twice the coercive field ($2E_C$) for 10^6 cycles. In this case, fatigue in the bipolar case was highly accelerated and largely developed within the first 100-1,000 cycles. After 1,000 cycles, the polarization dropped by 47.4% of the initial value and E_C began to increase [28]. However for most Pb-free ceramics, very little fatigue data is available. The total decrease in strain (~36%) was not nearly as large or asymmetric as for PZT [28]. The addition of CuO acted to stabilize the rhombohedral phase into a tetragonal phase and improved the fatigue characteristics without negatively impacting the piezoelectric response [29].

8.3 Experimental Methods

Ceramics of xBZT–0.4BKT–(0.6-x)BNT were produced via conventional solid state synthesis, for x = 0.025 and 0.05. Starting powders of (Bi_2O_3, TiO_2, ZnO, $NaCO_3$, and KCO_3) with > 99.9% purity were milled for six hours using high-energy vibratory milling. Calcinations were performed in covered crucibles at 900–950°C for 6 hours followed by a second six hour vibratory milling step.

The milled, calcined powders were mixed with 3 wt% solution of Paraloid (PL) binder and uniaxially pressed into 12.8 mm pellets at a pressure of 150 MPa. Sintering

was performed at 1050 or 1100°C for 4 hours. Prior to electrical measurements, samples were polished to sub-millimeter thickness and high-temperature silver paste (Heraeus C1000) was fired on both sides in air at 650°C for 30 minutes. Hysteresis measurements were made using a sawyer-tower circuit-based Radiant Technology Premier II ferroelectric test system utilizing Vision software. Strain hysteresis measurements were taken in conjunction with an MTI Instruments 2100 Fotonic Sensor. The fatigue testing was performed on unpoled samples by applying a 10Hz bipolar triangular waveform at 50 kV/cm on both the 0.025 and 0.05 BZT samples. Additional testing was performed on 0.05BZT at $2E_C$ (20 kV/cm). The fatigue tests performed in this study were carried out under bipolar conditions because it has been shown in the literature that bipolar cycling results in more severe degradation of the polarization and electromechanical strain compared to unipolar cycling.[23]

These tests were chosen to highlight any differences in fatigue behavior across the transition in behavior from "normal" ferroelectric response at 2.5%BZT, to the high electromechanical strain response of 5% BZT. The two different polarization and strain hysteresis behaviors for these compositions are demonstrated in Figure 1(a) and 1(b), respectively. In this work, only the bipolar fatigue characteristics of these two compositions were analyzed. The 2.5% BZT was tested at a field level of 50 kV/cm which amounts to approximately $2E_C$. These testing conditions are equivalent to fatigue tests carried out on PZT which allows for a basic comparison.[21] The 5% BZT composition was tested at two different field levels, 20 kV/cm and 50 kV/cm. Since this material exhibits unconventional hysteresis behavior as shown in Fig. 8.1, these two field levels were chosen to provide different modes of comparison. The 20 kV/cm test is nominally

equivalent to $2E_C$, though admittedly it is not fully accurate to define a coercive field in this way as it does not represent full switching in a conventional sense. Additionally, the fatigue test was carried out at 50 kV/cm so that a direct comparison could be made to previous work. All three fatigue tests were carried out on three identical specimens and the results for each testing condition were very similar in each case. The data traces included in the figures correspond to a representative sample and the numerical data in this letter represent the average of all tests at a given condition.

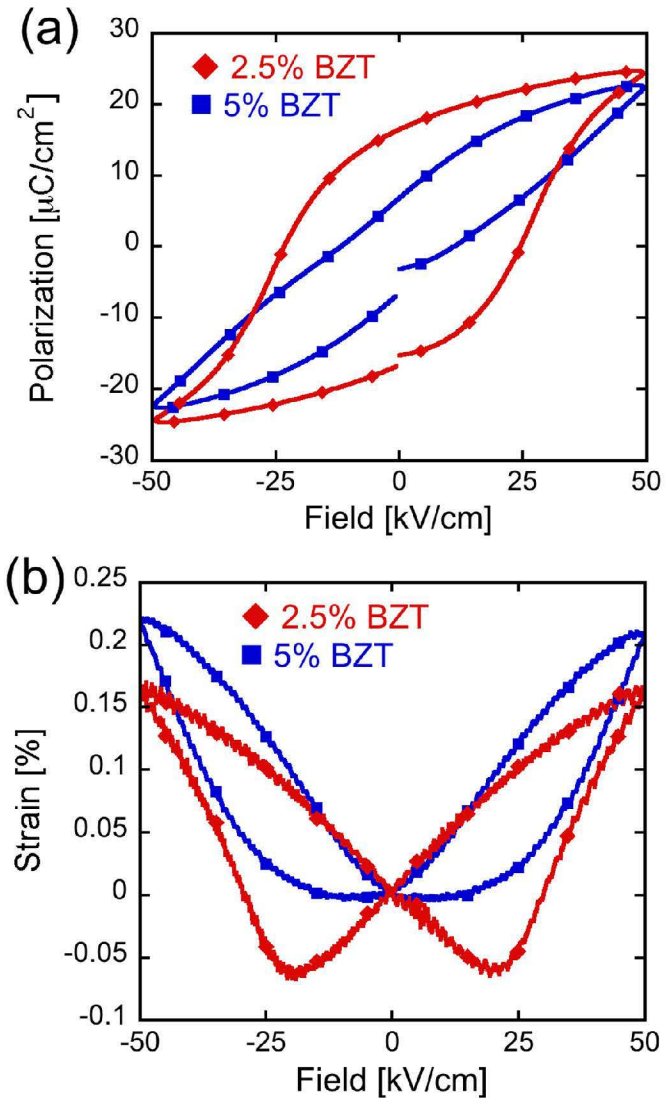

Fig. 8.1 *(a) Polarization and (b) strain behaviors of 2.5%BZT and 5%BZT showing typical ferroelectric loops that transition to a pinched, high electromechanical strain behavior with increased BZT content*

8.4 Results and Discussion

8.4.1 $2E_C$ Fatigue of 2.5%BZT (50 kV/cm)

Changes in the polarization and electromechanical strain behavior of a 2.5% BZT composition before and after 10^6 bipolar cycles at 50 kV/cm is shown in Fig. 8.2. Following the completion of one million cycles of fatigue at 50kV/cm, clear trends can be observed in the polarization hysteresis data. The coercive field was seen to decrease from approximately 25 to 20 kV/cm, a decrease of approximately 20%. Following an initial decrease in maximum polarization likely tied to stabilization of the domain structure, only a small increase in polarization of ~0.3 $\mu C/cm^2$ was measured over an initial value of 24.3 $\mu C/cm^2$. This amounts to a small 0.9% increase from the initial cycle to the 10^6 cycle. In the case of the remanent polarization (P_r), the opposite effect was observed with a slightly larger decrease of 4.6% in the average sample. The electromechanical strain data showed relatively small, but consistent decreases of approximately 10% in the maximum strain for both positive and negative applied fields. A similar loss in the negative strain was also observed. The symmetry of the strain hysteresis was maintained upon completion of the fatigue cycling.

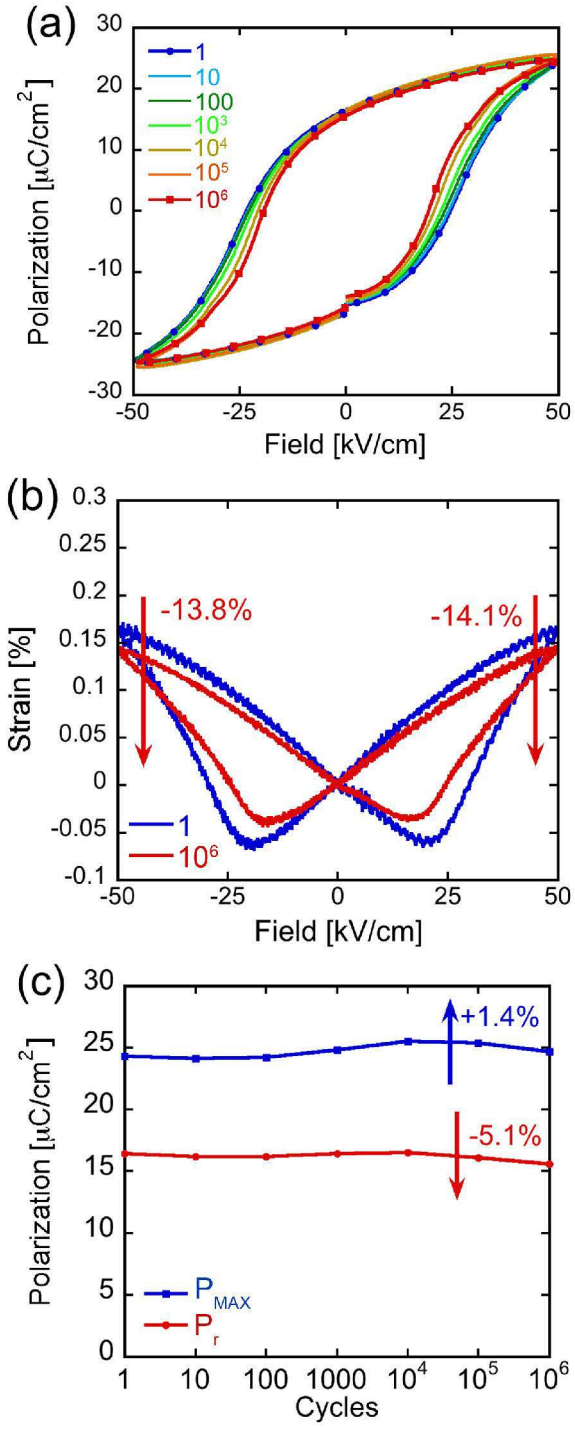

Fig. 8.2 *Fatigue results for a typical 2.5%BZT sample tested at 50kV/cm and 10Hz for (a) polarization hysteresis, (b) strain hysteresis, and (c) change in polarization values with increasing number of cycles completed*

8.4.2 5E_C Fatigue of 5%BZT (50 kV/cm)

In Fig. 8.3, the change in the polarization and electromechanical strain behavior of a 5% BZT composition before and after 10^6 bipolar cycles was obtained at 50 kV/cm is shown. In the data taken at a field of 50 kV/cm, similar to the 2.5% BZT composition, the E_C values steadily decreased by 20%. This was accompanied by an increase in the maximum polarization of approximately 5.7%. The remanent polarization in these samples decreased by an average of 8.5%. These changes in the polarization, while larger in both cases were not reflected by a correspondingly larger change in strain behavior. These results deviated sharply in comparison to that of the normal ferroelectric strain behavior observed for 2.5%BZT samples, with a minor increase in the maximum electromechanical strain of approximately 4%. It is also important to note that the strain loops maintained a high degree of symmetry after 10^6 cycles. No change in the amount of negative strain was observed for these samples.

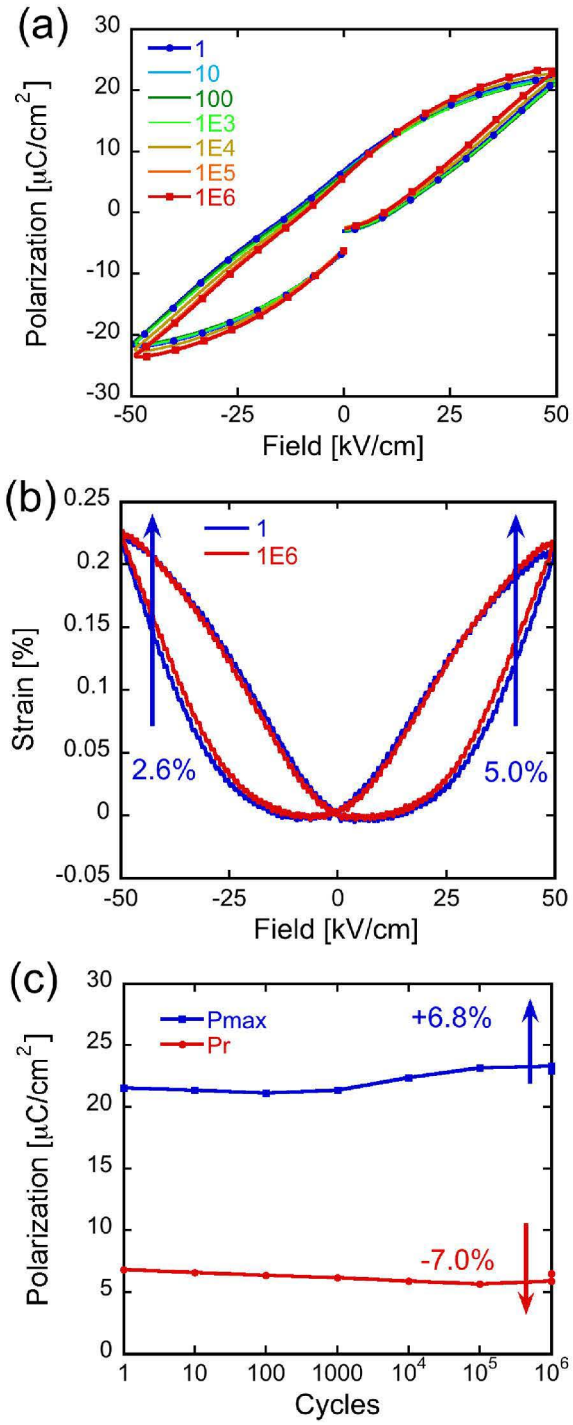

Fig. 8.3 *Fatigue results for a typical 5%BZT tested at 50kV/cm and 10Hz for (a) polarization hysteresis, (b) strain hysteresis, and (c) change in polarization values with increasing number of cycles completed*

8.4.3 $2E_C$ Fatigue of 5%BZT (20 kV/cm)

For 5% BZT samples tested at the lower field of 20 kV/cm similar, trends were for the most part observed. The value of E_C decreased by approximately 20% after 10^6 cycles. However, P_{MAX} increased by a slightly larger amount (~14%). The largest change in behavior was seen for any of the conditions tested in the case of remanent polarization. The P_r values of the samples were found to actually increase by ~20% rather than show the minor decreases seen in the other tests for both 2.5% and 5% BZT. The strain hysteresis was measured at both 20 kV/cm and 60 kV/cm before and after the 10^6 cycle fatigue test. Since the strain at 20 kV/cm resulted in strain levels that were insufficiently high compared to error limits of the probe utilized, the strain measurements at 60 kV/cm were needed to make a valid comparison. The data showed similar strain behavior to the data taken at 50 kV/cm with a minor increase in the maximum strain of 6% compared to the initial value. The general symmetry of the strain loop was also maintained in these samples. Overall, the electromechanical strain behavior of the 5%BZT samples were shown to be essentially free of fatigue out to 10^6 cycles independent of the cycling voltage used.

In fatigue tests of PZT-based materials, commonly an offset field is developed and increases drastically due to segregation of point defects[23, 27]. In the data in this study, only a small offset in coercive field was observed. Offsets on the order of ~0.50 kV/cm were recorded for the 5%BZT composition and an offset of 1.3 kV/cm for the 2.5%BZT composition when tested at 50 kV/cm. The offset in E_C of both positive and negative

applied fields remained similar throughout the fatigue testing, which decreased to nearly zero after 10^6 cycles for samples tested at 50kV/cm.

The performance of these materials represents a significant improvement on the fatigue data on PZT. The 5% BZT compositions showed no loss in electromechanical strain and the 2.5% showed a small decrease in the maximum strain values of approximately 10%. This decrease, however, is quite minimal when compared to the reduced strain and significant hysteresis asymmetry seen in previously published work on PZT. Two different mechanisms describe the loss in polarization of up to ~50% of the initial value when cycled at $2E_C$ (~20kV/cm) [21, 27]. In electrostrictive PZT compositions, discolored regions appear after $3x10^5$ cycles due to microcracking damage in the ceramic localized near the electrodes, which act to screen the rest of the bulk of the sample [21]. Importantly, no such discoloration was observed in either the 2.5% BZT or 5%BZT compositions in this study. The other fatigue mechanism is tied to the formation of defect agglomerates which is responsible for a ~50% reduction in polarization after $3x10^6$ cycles[27]. For PZT[27] and in BNT-BT[29], the coercive field increases as the fatigue mechanism progresses, which is the opposite of the behavior observed in the BZT-BKT-BNT system in this work. Although the fatigue in the 2.5%BZT case is much reduced compared to PZT, it may be possible to further enhance the stability with small CuO additions, as was recently demonstrated for the BNT-BT system[29, 30].

The explanation for the excellent fatigue characteristics in these BZT solid solutions is likely attributable to a lower concentration of intrinsic defects. In PZT-based materials, sintering temperatures in the range of 1200 to 1350°C are known to introduce

numerous point defects such as oxygen vacancies and Pb vacancies. The BZT-based materials in this study have significantly lower sintering temperatures between 1050 and 1100°C which would likely result in a significantly lower defect density. A set of experiments linking the fatigue characteristics to defect concentrations is currently underway.

This study has demonstrated that ceramics based on the solid solution of BZT-BNT-BKT exhibited essentially fatigue-free behavior compared to PZT-based materials. Compositions with 2.5% BZT show well saturated hysteresis loops similar to conventional ferroelectric materials, and after 10^6 bipolar cycles at 50 kV/cm the material experienced only a 10% loss in electromechanical strain. The P_{MAX} was increased by 0.9%, while P_r decreased by 4.6%. Compositions with 5% BZT exhibited large, hysteretic field-induced strains, and after 10^6 bipolar cycles at 50 kV/cm the electromechanical strain actually increased 4%. The P_{MAX} and P_r showed similar trends to the 2.5% BZT case, but changed by slightly larger amounts of +5.7% and -8.5%, respectively. In all of the samples tested at both 20 and 50kV/cm, the coercive field decreased by 20%. Based on these results, these Pb-free materials have great potential for use in piezoelectric applications requiring a large number of bipolar cycles such as MEMS devices and piezotransformers.

8.5 References

1. Y. Hiruma, Aoyagi, R., Nagata, H. and Takenaka, T., "Ferroelectric and Piezoelectric Properties of (Bi1/2K1/2)TiO3 Ceramics," *Jpn. J. Appl. Phys.,* 44[7A] 5040-44 (2005).

2. M. Nemoto, Nagata, H., Hiruma, Y., and Takenaka, T., "Fabrication and Piezoelectric Properties of Grain Oriented (Bi1/2K1/2)TiO3-BaTiO3 Ceramics," *Jpn. J. Appl. Phys.,* 47[5] 3829-32 (2008).

3. R. Ranjan, Dviwedi, A. , "Structure and dielectric properties of (Na0.50Bi0.50)1-xBaxTiO3: 0x0.10," *Sol. State Commun. ,* 135[6] 394-99 (2005).

4. S. Zhao, Li, G., Ding, A., Wang, T., Yin, Q., "Ferroelectric and piezoelectric properties of (Na,K)0.5Bi0.5TiO3 lead free ceramics. ," *J. Phys. D: Appl. Phys.,* 39[10] 2277-81 (2006).

5. S. Zhang, Shrout, T.R., Nagata, H., Hiruma, Y., Takenaka, T. , "Piezoelectric properties in (K0.5Bi0.5)TiO3-(Na0.5Bi0.5)TiO3-BaTiO3 lead-free ceramics," *IEEE Trans. Ultrason. Ferroelectr. Freq. Control,* 54[5] 910-17 (2007).

6. V. A. Isupov, "Ferroelectric Na0.5Bi0.5TiO3 and K0.5Bi0.5TiO3 Perovskites and Their Solid Solutions," *Ferroelect. Review,* 315 123-47 (2005).

7. H. Nagata, Yoshida, M., Makiuchi, Y. and Takenaka, T., "Large Piezoelectric Constant and High Curie Temperature of Lead-Free Piezoelectric Ceramic Ternary System Based on Bismuth Sodium Titanate-Bismuth Potassium Titanate-Barium Titanate near the Morphotropic Phase Boundary," *Jpn. J. Appl. Phys.,* 42[Part 1, No. 12] 7401-03 (2003).

8. T. Takenaka, Nagata, H., Hiruma, Y. , "Current Developments and Prospective of Lead-Free Piezoelectric Ceramics," *Jpn. J. Appl. Phys.,* 47[5] 3787-801 (2008).

9. T. R. Shrout and S. J. Zhang, "Lead-free piezoelectric ceramics: Alternatives for PZT?," *J. Electroceram,* 19 111-24 (2007).

10. T. Takenaka, Nagata, H., and Hiruma, Y., "Phase Transition Temperatures and Piezoelectric Properties of (Bi1/2Na1/2)TiO3-(Bi1/2K1/2)TiO3-Based Bismuth Perovskite Lead-Free Ferroelectric Ceramics," *IEEE Trans. Ultrason. Ferroelectr. Freq. Control* 56[8] 1595-612 (2009).

11. Y. Hiruma, Watanabe, T., Nagata, H. and Takenaka, T., "Piezelectric Properties of (Bi1/2Na1/2)TiO3-Based Solid Solutions," *Jpn. J. Appl. Phys.,* 47[9] 7659-63 (2008).

12. Y. Hiruma, Yoshii, K., Nagata, H., Takenaka, T., "Phase transition temperature and electrical properties of (Bi1/2Na1/2)TiO3-(Bi1/2A1/2)TiO3 (A=Li and K) lead-free ferroelectric ceramics.," *J. Appl. Phys.,* 103[8] 084121: 1-7 (2008).

13. W. Jo, J. E. Daniels, J. L. Jones, X. Tan, P. A. Thomas, D. Damjanovic, andJ. Rodel, "Evolving morphotropic phase boundary in lead-free (Bi[1/2]Na[1/2])TiO[3]--BaTiO[3] piezoceramics," *Journal of Applied Physics,* 109[1] 014110 (2011).

14. W. Jo, S. Schaab, E. Sapper, L. A. Schmitt, H.-J. Kleebe, A. J. Bell, andJ. Rodel, "On the phase identity and its thermal evolution of lead free (Bi[1/2]Na[1/2])TiO[3]-6 mol% BaTiO[3]," *Journal of Applied Physics,* 110[7] 074106 (2011).

15. W. Jo, Granzow, T., Aulbach, E., Rodel, J., and Damjanovic, D. , "Origin of the large strain response in (K0.5Na0.5)NbO3-modified (Bi0.5Na0.5)TiO3-BaTiO3 lead - free piezoceramics," *J. Appl. Phys.,* 105 094102 (2009).

16. J. E. Daniels, W. Jo, J. Rodel, V. Honkimaki, andJ. L. Jones, "Electric-field-induced phase-change behavior in (Bi0.5Na0.5)TiO3-BaTiO3-(K0.5Na0.5)NbO3: A combinatorial investigation," *Acta Materialia,* 58[6] 2103-11 (2010).

17. S.-T. Zhang, A. B. Kounga, E. Aulbach, H. Ehrenberg, andJ. Rodel, "Giant strain in lead-free piezoceramics Bi0.5Na0.5TiO3-BaTiO3-K0.5Na0.5NbO3 system," *Appl. Phys. Lett.,* 91[11] 112906 (2007).

18. P. Jarupoom, E. Patterson, B. Gibbons, G. Rujijanagul, R. Yimnirun, andD. Cann, "Lead-free ternary perovskite compounds with large electromechanical strains," *Applied Physics Letters,* 99[15] (2011).

19. R. Dittmer, W. Jo, J. Daniels, S. Schaab, andJ. Rödel, "Relaxor Characteristics of Morphotropic Phase Boundary (Bi1/2Na1/2)TiO3–(Bi1/2K1/2)TiO3 Modified with Bi(Zn1/2Ti1/2)O3," *Journal of the American Ceramic Society,* 94[12] 4283-90 (2011).

20. E. A. Patterson, D. P. Cann, J. Pokorny, andI. M. Reaney, "Electromechanical strain in Bi(Zn[1/2]Ti[1/2])O[sub 3]--(Bi[1/2]Na[s1/2])TiO[3]--(Bi[1/2]K[1/2])TiO[3] solid solutions," *Journal of Applied Physics,* 111[9] 094105-5 (2012).

21. N. Balke, Kungl, H., Granzow, T., Lupascu, D.C., Hoffman, M.J., and Rodel, J., "Bipolar Fatigue Caused by Field Screening in Pb(Zr,Ti)O3 Ceramics," *J. Am. Ceram. Soc.,* 90[12] 3869-74 (2007).

22. N. Balke, Lupascu, D.C., Granzow, T., and Rodel, J., "Fatigue of Lead Zirconate Titanate Ceramics I: Unipolar and DC Loading," *J. Am. Ceram. Soc.,* 90[4] 1081-87 (2007).

23. D. C. Lupascu, "Fatigue in Ferroelectric Ceramics and Related Issues," Vol. 61. Springer: Berlin, (2004).

24. W. Pan, Yue, C.F., and Tosyali, O., "Fatigue of Ferroelectric Polarization and the Electric Field Induced Strain in Lead Lanthanum Zirconate Titanate Ceramics," *J. Am. Ceram. Soc.,* 75[6] 1534-40 (1992).

25. C. Verdier, Lupascu, D.C., and Rodel, J., "Stability of defects in lead-zirconate-titanate after unipolar fatigue," *Appl. Phys. Lett.,* 81[14] 2596-98 (2002).

26. C. Verdier, Lupascu, D.C., and Rodel, J., "Unipolar fatigue of ferroelectric lead zirconate titanate," *J. Eur. Ceram. Soc.* , 23 7 (2003).

27. J. L. Nuffer, D.C., and Rodel, J., "Damage evolution in ferroelectric PZT induced by bipolar electric cycling.," *Acta. Mater.,* 48 3783-94 (2000).

28. Z. Luo, T. Granzow, J. Glaum, W. Jo, J. Rödel, andM. Hoffman, "Effect of Ferroelectric Long-Range Order on the Unipolar and Bipolar Electric Fatigue in Bi1/2Na1/2TiO3-Based Lead-Free Piezoceramics," *Journal of the American Ceramic Society,* 94[11] 3927-33 (2011).

29. M. Ehmke, J. Glaum, W. Jo, T. Granzow, andJ. Rödel, "Stabilization of the Fatigue-Resistant Phase by CuO Addition in (Bi1/2Na1/2)TiO3–BaTiO3," *Journal of the American Ceramic Society,* 94[8] 2473-78 (2011).

30. Z. Luo, J. Glaum, T. Granzow, W. Jo, R. Dittmer, M. Hoffman, andJ. Rödel, "Bipolar and Unipolar Fatigue of Ferroelectric BNT-Based Lead-Free Piezoceramics," *Journal of the American Ceramic Society,* 94[2] 529-35 (2011).

9 Summary and Future Work

In this chapter, the dielectric and piezoelectric properties of the KNN-based perovskites, the Bi-based perovskites, and finally the fatigue properties of both of these systems are summarized based on the results outlined in the previous chapters.

9.1 (K,Na)NbO_3 Based Systems:

Single phase perovskite ceramics were synthesized for three variations of the Li, Ta, and Sb modified (K,Na)NbO_3-based "LF4" piezoelectric system. Analysis of their dielectric properties revealed strong ferroelectric behavior with T_C values ranging from 245°C to 315°C, similar to those previously published in each case. It was found that the material's curie point, T_C, was lowered and the diffuseness of the transition increased with a decrease in the ratio of Nb/Sb content. For $(K_{0.44}Na_{0.52}Li_{0.04})(Nb_{0.86}Ta_{0.10}Sb_{0.04})O_3$, or LF4-2, dielectric loss values were below 0.05 for frequencies up to 100 kHz at room temperature.

Ferroelectric hysteresis measurements showed remanent polarizations of 16 and 20 μC/cm^2 and maximum polarization values of 21 and 25 μC/cm^2 for LF4-2 plus CuO and LF4-2, respectively. The addition of a relatively small amount of 0.2 wt% CuO had the dramatic effect of decreasing E_C from 18-20 to approximately 8-10 kV/cm. These results match the mixed A and B site doping proposed in the work of Li, *et al.* The substitution of Cu into the A site acts to reduce oxygen vacancies and lower the coercive field, but the B site replacement makes the samples more "hard" with increased Q_m and decreased k_p values. Values of low field d_{33}, were found to range from 167-182 pC/N for samples poled under dc bias of 40 kV/cm at 100°C for 30 minutes. While these are smaller than the previously reported value of 416 pC/N for LF4-1 ceramics under unique

texturing processing methods, they are still high compared to other known lead-free systems. In general, the high field d_{33}^* (500-600 pm/V) and S_{Max} (~0.23%) values for these samples are still promising for potential use in actuator devices.

9.2 Bi-based Systems

Single phase ceramics were fabricated in the BZT–BKT–BNT ternary system for a wide variety of compositional space, including up to a solubility limit of 20 mol% BZT. Based on the MPB 10BZT-90BKT composition, this ternary system was optimized for maximum strain at 10BZT-40BKT-50BNT, well to the BKT-side of the MPB in the BNT-BKT binary system. High temperature dielectric spectroscopy showed the T_{max} of the dielectric spectrum steadily decreased with a corresponding broadening of the transition as the BZT concentration increased (keeping either 40BKT or 50BNT constant) from 322°C at 2.5%BZT to 284°C at 20%BZT. At 2.5 BZT–40 BKT–57.5 BNT, a secondary transition commonly observed for MPB BNT–BKT was observed and is likely a weak non-symmetry breaking relaxation not uncommon in oxides with such complex crystal chemistry.

The polarization hysteresis data showed ferroelectric behavior at 2.5% BZT with a high remanent polarization of 20.8 μC/cm^2. At 20% BZT, the hysteresis loops become severely pinched, with a negligible P_r (2.3 μC/cm^2). In the case of the 2.5%BZT composition, the remanent polarization was also observed to decrease drastically as the temperature increased to 175°C, dropping to a similarly low value of 2.1 μC/cm^2. The onset of this transition corresponds to the lower temperature frequency dispersion

observed in the dielectric spectrum. In both of these cases there is also a large reduction to the coercive field.

The strain hysteresis also changed shape as the BZT concentration increased with the typical ferroelectric butterfly loop gradually shifting away from negative strain and widening to a parabolic shape. For compositions with 2.5% BZT, the strain data exhibited a classic "butterfly" shape with approximately –0.8% negative strain, typical of domain switching for a ferroelectric. The maximum strain value of S_{MAX} = 0.22-0.25% corresponded to a high-field effective d_{33}* of 408 pm/V. Maximum strain values of 0.33% were observed at the composition 5–40–55 which was accompanied by a large d_{33}^* = 547 pm/V. These results indicate excellent promise for future piezoelectric actuator devices.

The dielectric and ferroelectric properties of the binary BNT-BZT system was also investigated. Diffraction data on all of the specimens showed no significant secondary phases up to approximately 8 mol% BZT and clear peak splitting of the (001), (011), and (111) reflections. The temperature at which the relative permittivity is maximum (T_{max}) is largely independent of composition varying over the narrow range of 333 to 345°C. Below the dielectric maximum, all compositions exhibit a dielectric dispersion that is less pronounced above T_{max}. At low concentrations of BZT, the material behaves very much like a conventional ferroelectric, with well-saturated loops with high remanent polarization ($P_r \sim 35$ μC/cm^2). As the BZT content increased, the remanent polarization and coercive field decreased. Immediately after the polarization hysteresis measurements these samples exhibited low-field d_{33} values of between 40 to 80 pC/N,

which confirms the presence of domain alignment without prior application of a dc bias. The hysteresis data was characterized by features consistent with relaxor behavior. Temperature dependent hysteresis measurements showed that, on heating, the remanent polarization decreased significantly and the data showed double-loop characteristics. This finding, along with the observation of thermal hysteresis in the dielectric maximum (T_{max} shifts to lower temperatures on cooling (ΔT_{max} = 12-14°C) and the decrease in permittivity below T_{max} is less sharp), indicates the presence of a relaxor to ferroelectric transition in this material. These results include many common characteristics with similar perovskite systems that exhibit a relaxor to ferroelectric transition.

9.3 Fatigue

Unipolar or Bipolar piezoelectric fatigue measurements were explored for the most promising compositions for both the KKN-based and Bi-based lead-free systems described previously. Unipolar studies were performed for LF4-2 with and without CuO doping for a wide range of conditions. More aggressive bipolar fatigue conditions were studied for the higher strain BZT-BKT-BNT ternary system specifically for the 2.5% and 5%BZT compositions.

First, single phase perovskite ceramics were synthesized for two variations of the Pb-free LF4-2 piezoelectric material, as described in section 9.1. The unipolar fatigue behavior for this system was shown to be clearly dependent on applied field during testing and the initial poling conditions. For undoped LF4-2, after minor initial decreases

the polarization stabilized after 10 cycles for testing of 100,000 cycles duration with an overall increase of piezoelectric coefficient. For the 0.2 wt% CuO doped samples, in comparing poled and unpoled specimens, if the data for the first 10-100 cycles of the unpoled sample are ignored, the scale of the overall drop in P_{MAX} between the two are very similar. This is not observed in the highly poled commercial PZT samples tested in previous studies, further confirming the importance of the poling on the overall fatigue of the sample. For poled samples, increasing the testing field to $3E_C$ resulted in twice the decrease in P_{MAX} (-32%) compared to the $2E_C$ tests at 10^6 cycles (-17%). When testing at a field level of $2E_C$ for CuO doping, the polarization decreases continually through 10^7 cycles with the decreases in P_{MAX} and d_{33} both reaching a maximum (-22% and -30% respectively) after 10^7 cycles. In summary, while additions of 0.2 wt% CuO enhanced the initial piezoelectric properties, they simultaneously appeared to worsen the fatigue properties in this system.

Another comparison can be made between the bipolar polarization and strain hysteresis measurements taken before and after the unipolar fatigue was complete. From the change in strain hysteresis, it is clear that the decrease in strain is not uniform for positive and negative applied fields. At both the testing and saturation field levels, the positive applied field side of the strain curve clearly decreased to a greater extent. In the unipolar fatigue of PZT, there was not a true degradation of strain but rather an imprint from an offset polarization, causing the positive maximum strain value to be increased and the negative maximum strain value to decrease. In the 0.2 wt% CuO doped LF4-2 system, while a slight increase in symmetry is observed, it is the result of an overall

decrease in maximum strain for both positive and negative bias, thus showing a true degradation of strain more similar to the type observed in bipolar fatigue of PZT.

This study demonstrated that ceramics based on the solid solution of BZT-BNT-BKT exhibited essentially fatigue-free behavior compared to PZT-based materials. Compositions with 2.5% BZT show well saturated hysteresis loops similar to conventional ferroelectric materials, and after 10^6 bipolar cycles at 50 kV/cm the material experienced only a 10% loss in electromechanical strain. The coercive field was seen to decrease from approximately 25 to 20 kV/cm, a decrease of approximately 20%. The P_{MAX} was increased by 0.9%, while P_r decreased by only 4.6%. Compositions with 5% BZT exhibited large, hysteretic field-induced strains, and after 10^6 bipolar cycles at 50 kV/cm the electromechanical strain actually increased 4%. The P_{MAX} and P_r showed similar trends to the 2.5% BZT case, but changed by slightly larger amounts of +5.7% and -8.5%, respectively. In all of the samples tested at both 20 and 50kV/cm, the coercive field decreased by 20%. Overall, the electromechanical strain behavior of the 5%BZT samples were shown to be essentially free of fatigue out to 10^6 cycles independent of the cycling voltage used. The performance of these materials represents a significant improvement on the decreases in strain and severe hysteresis asymmetry that developed in previously published work typical of PZT. The explanation for the excellent fatigue characteristics in these BZT solid solutions is likely attributable to a lower concentration of intrinsic defects. Based on these results, these Pb-free compositions have the greatest potential for use in piezoelectric applications requiring a large number of bipolar cycles such as MEMS devices and piezotransformers.

10 Future Work

In order to further characterize the nature of the fatigue behavior of this lead free system, three separate fatigue studies are proposed for three Bi-based solid solutions. The systems chosen all rely on BNT being the majority component and were chosen to examine how varying from a binary to more complex ternary system will affect the fatigue characteristics, especially in comparison to the previously mentioned BNT-BKT-BZT system. For binary systems, the MPB composition of 80BNT-20BKT and the 96BNT-4BZT are of particular interest and should further clarify the benefits of adding BZT. In addition, a third ternary system between BNT-BKT-BMgT is suggested to determine if additions of Mg (or Ni) act similarly to stabilize the fatigue results. The testing needed in each case can be divided into three parts. First, bipolar fatigue of unpoled samples of three compositions will be tested immediately following the approach outlined by recent work at Darmstadt. The Bi-based ternary systems, generally, have shown complex poling behavior and it has been difficult to achieve repeatable low-field, piezoelectric coefficients (d_{33}). Therefore, poling of BNT-BZT and BNKT-BMgT, and BNT-BKT will be optimized based on depoling temperatures measured through a variety of methods as described in recent work by Darmstadt (Leist, *et al*). After optimizing the poling conditions for these compositions, unipolar fatigue tests will be performed on the poled samples. Fatigue measurements will be performed to match experiments done previously with a triangular waveform of 10Hz and amplitude of 50 kV/cm for 10^6 cycles on all sample sets. This will represent $2E_C$ or $5E_C$ for the binary or ternary compositions, respectively. The results of these experiments will help provide valuable information on

the suitability of these new Pb-free materials for high performance applications such as piezoelectric MEMS devices.

11 Bibliography

1. R. E. Newnham, "Properties of Materials: Anisotropy, Symmetry, Structure," Oxford, (2005).
2. K. C. Kao, "Dielectric Phenomena in Solids." Elsevier, (2004).
3. V. A. Isupov, "Ferroelectric Na0.5Bi0.5TiO3 and K0.5Bi0.5TiO3 Perovskites and Their Solid Solutions," *Ferroelect. Review,* **315** 123-47 (2005).
4. T. R. Shrout and S. J. Zhang, "Lead-free piezoelectric ceramics: Alternatives for PZT?," *J. Electroceram,* **19** 111-24 (2007).
5. P. Curie, Curie, J, "Development by Pressure of Polar Electricity in Hemihedral Crystals with Inclined Faces," *Bulletin de la Societe Mineralique de France,* **3** 90 (1880).
6. S. O. Kasap, "Electronic materials and Devices." McGraw-Hill: New York, (2002).
7. A. Hussain, C. W. Ahn, J. S. Lee, A. Ullah, andI. W. Kim, "Large electric-field-induced strain in Zr-modified lead-free Bi0.5(Na0.78K0.22)0.5TiO3 piezoelectricceramics," *Sens. Actuators, A,* **158** 84-89 (2010).
8. B. Jaffe, Cook, W.R., and Jaffe, H., "Piezoelectric Ceramics." Academic Press: New York, (1971).
9. J. Valasek, "Piezo-Electric and Allied Phenomena in Rochelle Salt," *Physical Review,* **17**[4] 475 (1921).
10. V. K. Pecharsky, Zavalij, P.Y. , "Fundamentals of Powder Diffraction and Structure Characterization of Materials." Kluwer Academic: Boston, (2003).
11. A. J. Moulson and J. M. Herbert, "Electroceramics: Materials, Properties, Applications." John Wiley & Sons, Ltd.: Hoboken, NJ, (2005).
12. M. Ozgul, Trolier-Mckinstry, S., and Randall, C.A., "Fatigue induced effects on bipolar strain loops in PZN-PT piezoelectric single crystals," *J. Electroceram,* **20** 133-38 (2008).
13. H. Sahota, "Simulation of butterfly loops in ferroelectric materials," *Coninuum Mech. Thermodyn.,* **16** 163-75 (2004).
14. A. S. Bhalla, Guo, R., Roy, R., "The perovskite structure - a review of its role in ceramic science and technology.," *Material Research Innovatioins,* **4**[1] 3-26 (2000).
15. R. E. Cohen, "Origin of ferroelectricity in perovskite oxides," *Nature,* **358**[6382] 136-38 (1992).
16. B.-q. Qin, C. Yi, Y. Jiang, Y. Jiang, X. Yue, D. Xiao, andJ. Zhu, "Preparation and Characterization of (1-x) BiInO3-xPbTiO3 ceramics," pp. 616-17 in Applications of Ferroelectrics, 2007. ISAF 2007. Sixteenth IEEE International Symposium on.

17. A. A. Belik, S. Y. Stefanovich, B. I. Lazoryak, andE. Takayama-Muromachi, "BiInO3: A Polar Oxide with GdFeO3-Type Perovskite Structure," *Chemistry of Materials,* **18**[7] 1964-68 (2006).

18. R. Guo, L. E. Cross, S. E. Park, B. Noheda, D. E. Cox, andG. Shirane, "Origin of the High Piezoelectric Response in PbZr1-xTixO3," *Physical Review Letters,* **84**[23] 5423 (2000).

19. V. M. Goldschmidt, *Naturwissenschaften* **14** 477 (1926).

20. R. E. Eitel, Randall, C.A., Shrout, T.R., Rehrig, P.W., Hackenberger, W., and Park, S.E., "New High Temperature Morphotropic Phase Boundary Piezoelectrics Based on Bi(Me)O3-PbTiO3 Ceramics," *Jpn. J. Appl. Phys.,* **40**[Part 1. No. 10] 5999-6002 (2001).

21. A. Halliyal, T. R. Gururaja, U. Kumar, andA. Safari, "Stability of Perovskite Phase in Pb(Zn1/3Nb2/3)O3and Other A(b'b'')O3Perovskites," pp. 437-41 in Applications of Ferroelectrics. 1986 Sixth IEEE International Symposium on.

22. N. Wakiya, N. Ishizawa, K. Shinozaki, andN. Mizutani, "Thermal stability of Pb(Zn1/3Nb2/3)O3 (PZN) and consideration of stabilization conditions of perovskite type compounds," *Materials Research Bulletin,* **30**[9] 1121-31 (1995).

23. O. Muller, Roy, R., "The Major Ternary Structural Families, ." Springer-Verlag: New York, (1974).

24. T. R. G. A. Halliyal, U. Umar and A. Safari, *IEEE 6th International Symposium on Application of Ferroelectrics,* **437** (1986).

25. D. C. Lupascu, "Fatigue in Ferroelectric Ceramics and Related Issues," **Vol. 61**. Springer: Berlin, (2004).

26. W. L. Warren, Dimos, D., Tuttle,, B.A., Pike, G.E., Schwartz, R.W., Clews, P.J. an dMcINtyre, D.C., "Polarizatin suppression in Pb(Zr,Ti)O3 thin films," *J. Appl. Phys.,* **77** 6695-701 (1995).

27. J. L. Nuffer, D.C., and Rodel, J., "Damage evolution in ferroelectric PZT induced by bipolar electric cycling.," *Acta. Mater.,* **48** 3783-94 (2000).

28. E. L. Colla, Tagantsev, A.K., Taylor, D.V., an dKholkin, A.L., "Fatigued state ofPt-{PZT}-PT system. ," *Integrated Ferroelectrics,* **29** 145-48 (1995).

29. E. L. Colla, Taylor, D.V., Tagantsev, A.K., and Setter, N. , "Discrimination between bulk and interface scenarios for the suppression of the switchable polarization (fatigue) in Pb(Zr,Ti)O3 thin fims capacitors with Pt electrodes.," *Appl. Phys. Lett.,* **72** 2478-80 (1998).

30. C. Verdier, Lupascu, D.C., and Rodel, J., "Stability of defects in lead-zirconate-titanate after unipolar fatigue," *Appl. Phys. Lett.,* **81**[14] 2596-98 (2002).

31. W. Pan, Yue, C.F., and Tosyali, O., "Fatigue of Ferroelectric Polarization and the Electric Field Induced Strain in Lead Lanthanum Zirconate Titanate Ceramics," *J. Am. Ceram. Soc.,* **75**[6] 1534-40 (1992).

32. W. Pan, Yue, C.F., and Tuttle, B.A., "Ferroelectric Fatigue in modified bulk lead zirconate titanate ceramics and thin films," *Ceramic Transactions, Ferroelectric Films,* **25** 358-97 (1992).

33. V. Y. Shur, Rumyantsev, E.L., Nikolaeva, E.V., Shishkin, E.I. and Baturin, I.S. , "Kinetic Approach to fatigue phenomena in ferroelectrics," *J. Appl. Phys.,* **90** 6312-15 (2001).

34. V. Y. Shur, Rumyantsev, E.L., Nikolaeva, E.V., Shishkin, E.I., Baturin, I.S., Ozgul, M., and Randall, C.A. , "Kinetics of fatigue effect," *Integrated Ferroelectrics,* **33** 117-32 (2001).

35. J. F. Scott, "Fatigue as a phase transition.," *Integrated Ferroelectrics,* **38** 125-33 (2001).

36. D. C. Lupascu, Rabe, U., "Cyclic cluster growth in ferroelectric perovskites," *Phys. Rev. Lett.,* **89** 187601 (2002).

37. N. Balke, Lupascu, D.C., Granzow, T., and Rodel, J., "Fatigue of Lead Zirconate Titanate Ceramics I: Unipolar and DC Loading," *J. Am. Ceram. Soc.,* **90**[4] 1081-87 (2007).

38. N. Balke, Lupascu, D.C., Granzow, T., and Rodel, J., "Fatigue of Lead Zirconate Titanate Ceramics II: Sesquipolar Loading," *J. Am. Ceram. Soc.,* **90**[4] 1088-93 (2007).

39. Y. Saito, H. Takao, T. Tani, T. Nonoyama, K. Takatori, T. Homma, T. Nagaya, andM. Nakamura, "Lead-free piezoceramics," *Nature,* **432** 84-87 (2004).

40. Y. Saito, H. Takao, T. Tani, T. Nonoyama, K. Takatori, T. Homma, T. Nagaya, andM. Nakamura, "High Performance Lead-free Piezoelectric Material," *R&D Review of Toyota CRDL,* **41**[2] 22-28 (2004).

41. S. Zhang, R. Xia, T. R. Shrout, G. Zan, andJ. Wang, "Piezoelectric properties in perovskite 0.948(K0.5Na0.5)NbO3-0.052LiSbO3 lead-free ceramics," *J. Appl. Phys.,* **100** 104108-1-6 (2006).

42. Y. Wang, J. Wu, D. Xiao, J. Zhu, Y. Jin, J. Zhu, P. Yu, L. Wu, andX. Li, "Microstructure, dielectric, and piezoelectric properties of (Li, Ag, Ta) modified (K0.50Na0.50)NbO3 lead-free ceramics with high Curie Temperature," *J. Appl. Phys.,* **102** 054101-1-5 (2007).

43. J. Wu, D. Xiao, Y. Wang, W. Wu, B. Zhang, J. Zhu, Z. Pu, andQ. Li, "Microstructure and electrical properties of (Li, Ag, Ta, Sb)-modified (K0.50Na0.50)NbO3 lead-free ceramics with good temperature stability," *J. Phys. D: Appl. Phys.* , **41** 125405-1-6 (2008).

44. E. Li, H. Kakemoto, S. Wada, andT. Tsurumi, "Influence of CuO on the Structure and Piezoelectric Properties of the Alkaline Niobate-Based Lead-Free Ceramics," *J. Am. Ceram. Soc.,* **90**[6] 1787-91 (2007).

45. J. Wu, D. Xiao, Y. Wang, J. Zhu, L. Wu, andY. Jiang, "Effects of K/Na ratio on the phase structure and electrical properties of (KxNa0.96-

xLi0.004)(Nb0.91Ta0.05Sb0.04)O3 lead-free ceramics," *Appl. Phys. Lett.,* **91** 252907-1-3 (2007).

46. R. Zuo, Z. Xu, andL. Li, "Dielectric and piezoelectric properties of Fe2O3-doped (Na0.5K0.5)0.96Li0.04Nb0.86Ta0.1Sb0.04O3 lead-free ceramics," *Journal of Physics and Chemistry of Solids,* **69**[7] 1728-32 (2008).

47. Y. Ding, Liu, J.S., Qin, H.X., Zhu, J.S., and Wang, Y.N., "Why lanthanum-substituted bismuth titanate becomes fatigue free ferroelectric capacitor with platinum electrodes," *Appl. Phys. Lett.,* **78**[26] 4175-77 (2001).

48. S. Zhang, H. Hao, H. Liu, andT. R. Shrout, "Mitigation of thermal and fatigue behvior in K0.5Na0.5NbO3-based lead free piezoceramics," *Appl. Phys. Lett.,* **92** 152904-1-3 (2008).

49. P. S. Baettig, C.F., LeSar, R., Waghmare, U.V., and Spaldin, N.A., "Theoretical Prediction of New High-Performance lead-Free Piezoelectrics," *Chem. Mater.,* **17** 1376-80 (2005).

50. M. R. Suchomel, A. M. Fogg, M. Allix, H. J. Niu, J. B. Claridge, andM. J. Rosseinsky, "Bi2ZnTiO6: A lead-free closed-shell polar perovskite with a calculated ionic polarization of 150 mu C cm(-2)," *Chemistry of Materials,* **18**[21] 4987-89 (2006).

51. Y. Hiruma, Aoyagi, R., Nagata, H. and Takenaka, T., "Ferroelectric and Piezoelectric Properties of (Bi1/2K1/2)TiO3 Ceramics," *Jpn. J. Appl. Phys.,* **44**[7A] 5040-44 (2005).

52. M. Nemoto, Nagata, H., Hiruma, Y., and Takenaka, T., "Fabrication and Piezoelectric Properties of Grain Oriented (Bi1/2K1/2)TiO3-BaTiO3 Ceramics," *Jpn. J. Appl. Phys.,* **47**[5] 3829-32 (2008).

53. R. Ranjan, Dviwedi, A. , "Structure and dielectric properties of (Na0.50Bi0.50)1-xBaxTiO3: 0x0.10," *Sol. State Commun. ,* **135**[6] 394-99 (2005).

54. S. Zhao, Li, G., Ding, A., Wang, T., Yin, Q., "Ferroelectric and piezoelectric properties of (Na,K)0.5Bi0.5TiO3 lead free ceramics. ," *J. Phys. D: Appl. Phys.,* **39**[10] 2277-81 (2006).

55. S. Zhang, Shrout, T.R., Nagata, H., Hiruma, Y., Takenaka, T. , "Piezoelectric properties in (K0.5Bi0.5)TiO3-(Na0.5Bi0.5)TiO3-BaTiO3 lead-free ceramics," *IEEE Trans. Ultrason. Ferroelectr. Freq. Control,* **54**[5] 910-17 (2007).

56. H. Nagata, Yoshida, M., Makiuchi, Y. and Takenaka, T., "Large Piezoelectric Constant and High Curie Temperature of Lead-Free Piezoelectric Ceramic Ternary System Based on Bismuth Sodium Titanate-Bismuth Potassium Titanate-Barium Titanate near the Morphotropic Phase Boundary," *Jpn. J. Appl. Phys.,* **42**[Part 1, No. 12] 7401-03 (2003).

57. T. Takenaka, Nagata, H., Hiruma, Y. , "Current Developments and Prospective of Lead-Free Piezoelectric Ceramics," *Jpn. J. Appl. Phys.,* **47**[5] 3787-801 (2008).

58. T. Takenaka, Nagata, H., and Hiruma, Y., "Phase Transition Temperatures and Piezoelectric Properties of (Bi1/2Na1/2)TiO3-(Bi1/2K1/2)TiO3-Based Bismuth

Perovskite Lead-Free Ferroelectric Ceramics," *IEEE Trans. Ultrason. Ferroelectr. Freq. Control* **56**[8] 1595-612 (2009).

59. Y. Hiruma, Watanabe, T., Nagata, H. and Takenaka, T., "Piezelectric Properties of (Bi1/2Na1/2)TiO3-Based Solid Solutions," *Jpn. J. Appl. Phys.,* **47**[9] 7659-63 (2008).

60. Y. Hiruma, Yoshii, K., Nagata, H., Takenaka, T., "Phase transition temperature and electrical properties of (Bi1/2Na1/2)TiO3-(Bi1/2A1/2)TiO3 (A=Li and K) lead-free ferroelectric ceramics.," *J. Appl. Phys.,* **103**[8] 084121: 1-7 (2008).

61. C. C. Huang, Naratip, V, Cann, D.P. , "Structure and ferroelectric properties of Bi(Zn(1/2)Ti(1/2))O3-(Bi(1/2)K(1/2))TiO3 perovskite solid solutions," *IEEE Trans. Ultrason. Ferroelectr. Freq. Control,* **56**[7] 1304-08 (2009).

62. K. Yoshii, Hiruma, Y, Nagata, H., Takenaka, T., "Electrical properties and depolarization temperature of (Bi1/2Na1/2)TiO3-(Bi1/2K1/2)TiO3 lead-free piezoelectric ceramics.," *Jap. J. Appl. Phys. Part 1,* **45**[5B] 4493-96 (2006).

63. T. Qi, I. Grinberg, andA. M. Rappe, "First-principles investigation of the highly tetragonal ferroelectric material Bi(Zn_{1/2}Ti_{1/2})O_{3}," *Physical Review B,* **79**[9] 094114 (2009).

64. K.-I. Kakimoto, I. Masuda, andH. Ohsato, "Solid-Solution Structure and Piezoelectric Property of KNbO3 Ceramics Doped with Small Amounts of Elements," *Jap. J. Appl. Phys.,* **43**[9B] 6706-10 (2004).

65. E. Aksel, J. S. Forrester, J. L. Jones, P. A. Thomas, K. Page, andM. R. Suchomel, "Monoclinic crystal structure of polycrystalline Na(0.5)Bi(0.5)TiO(3)," *Applied Physics Letters,* **98**[15] (2011).

66. A. Sasaki, T. Chiba, Y. Mamiya, andE. Otsuki, "Dielectric and Piezoelectric Properties of (Bi0.5Na0.5)TiO3-Bi0.5K0.5TiO3 Systems," *Japanese Journal of Applied Physics,* **38**[Copyright (C) 1999 Publication Board, Japanese Journal of Applied Physics] 5564-67 (1999).

67. J. Kling, X. Tan, W. Jo, H.-J. Kleebe, H. Fuess, andJ. Rödel, "In Situ Transmission Electron Microscopy of Electric Field-Triggered Reversible Domain Formation in Bi-Based Lead-Free Piezoceramics," *Journal of the American Ceramic Society,* **93**[9] 2452-55 (2010).

68. S.-T. Zhang, A. B. Kounga, E. Aulbach, H. Ehrenberg, andJ. Rodel, "Giant strain in lead-free piezoceramics Bi0.5Na0.5TiO3-BaTiO3-K0.5Na0.5NbO3 system," *Appl. Phys. Lett.,* **91**[11] 112906 (2007).

69. G. A. Smolenskii, V. A. Isupov, A. I. Agranovskaya, andN. N. Krainik, "New Ferroelectrics of Complex Composition IV. ," *Sov. Phys. Solid State,* **2** 2651 (1961).

70. C. S. Tu, I. G. Siny, andV. H. Schmidt, "Sequence of dielectric anomalies and high-temperature relaxation behavior in Na(1/2)Bi(1/2)TiO(3)," *Physical Review B,* **49**[17] 11550-59 (1994).

71. J. Suchanicz, A. Jeżowski, andR. Poprawski, "Low-Temperature Thermal and Dielectric Properties of Na0.5Bi0.5TiO3," *physica status solidi (a),* **169**[2] 209-15 (1998).

72. K. Roleder, I. Franke, A. M. Glazer, P. A. Thomas, S. Miga, andJ. Suchanicz, "The piezoelectric effect in Na(0.5)Bi(0.5)TiO3 ceramics," *Journal of Physics: Condensed Matter,* **14**[21] 5399 (2002).

73. Y. Hiruma, Nagata, H. and Takenaka, T., "Thermal depoling process and piezoelectric properties of bismuth sodium titanate ceramics " *J. Appl. Phys.,* **105** 084112 (2009).

74. J. Suchanicz and J. Kwapulinski, "X-ray diffraction study of the phase transitions in Na0.5Bi0.5TiO3," *Ferroelectrics,* **165**[1] 249-53 (1995).

75. G. O. Jones and P. A. Thomas, "Investigation of the structure and phase transitions in the novel A-site substituted distorted perovskite compound Na0.5Bi0.5TiO3," *Acta Crystallographica Section B,* **58**[2] 168-78 (2002).

76. E. Aksel, J. S. Forrester, B. Kowalski, J. L. Jones, andP. A. Thomas, "Phase transition sequence in sodium bismuth titanate observed using high-resolution x-ray diffraction," *Applied Physics Letters,* **99**[22] 222901 (2011).

77. Y.-R. Zhang, J.-F. Li, B.-P. Zhang, andC.-E. Peng, "Piezoelectric and ferroelectric properties of Bi-compensated (Bi[1/2]Na[1/2])TiO[3]-(Bi[1/2]K[1/2])TiO[3] lead-free piezoelectric ceramics," *Journal of Applied Physics,* **103**[7] 074109 (2008).

78. A. Sasaki, T. Chiba, Y. Mamiya, andE. Otsuki, "Dielectric and Piezoelectric Properties of (Bi0.5Na0.5)TiO3–(Bi0.5K0.5)TiO3 Systems," *Japanese Journal of Applied Physics,* **38** 5564 (1999).

79. T. Takenaka, Maruyama, K, and Sakata, K., "(Bi1/2Na1/2)TiO3-BaTiO3 System for Lead-Free Piezoelectric Ceramics," *Jpn. J. Appl. Phys.,* **30**[9B] 2236-39 (1991).

80. Z. Luo, T. Granzow, J. Glaum, W. Jo, J. Rödel, andM. Hoffman, "Effect of Ferroelectric Long-Range Order on the Unipolar and Bipolar Electric Fatigue in Bi1/2Na1/2TiO3-Based Lead-Free Piezoceramics," *Journal of the American Ceramic Society,* **94**[11] 3927-33 (2011).

81. Z. Luo, J. Glaum, T. Granzow, W. Jo, R. Dittmer, M. Hoffman, andJ. Rödel, "Bipolar and Unipolar Fatigue of Ferroelectric BNT-Based Lead-Free Piezoceramics," *Journal of the American Ceramic Society,* **94**[2] 529-35 (2011).

82. M. Ehmke, J. Glaum, W. Jo, T. Granzow, andJ. Rödel, "Stabilization of the Fatigue-Resistant Phase by CuO Addition in (Bi1/2Na1/2)TiO3–BaTiO3," *Journal of the American Ceramic Society,* **94**[8] 2473-78 (2011).

83. A. B. Kounga, S.-T. Zhang, W. Jo, T. Granzow, andJ. Rodel, "Morphotropic phase boundary in (1-x)Bi0.5Na0.5TiO3 - (x)K0.5Na0.5NbO3 lead-free piezoceramics," *Applied Physics Letters,* **92**[22] 222902-02-3 (2008).

84. H. Ishii, H. Nagata, andT. Takenaka, "Morphotropic Phase Boundary and Electrical Properties of Bisumuth Sodium Titanate-Potassium Niobate Solid-Solution Ceramics," *Jpn. J. Appl. Phys.,* **40** 3 (2001).

85. C. Zhou, and Liu, X., "Dielectric and piezoelectric properties of bismuth-containing complex perovkite solid solution of Bi1/2Na1/2TiO3-Bi(Mg2/3Nb1/3)O3," *J. Mater. Sci,* **43** 1016-19 (2008).

86. Y. Hiruma, H. Nagata, andT. Takenaka, "Phase diagrams and electrical properties of (Bi1/2Na1/2)TiO3-based solid solutions," *Journal of Applied Physics,* **104**[12] 124106 (2008).

87. K. Sakata and Y. Masuda, "Ferroelectric and antiferroelectric properties of (Na 0.5Bi 0.5)TiO3-SrTiO3 solid solution ceramics," *Ferroelectrics,* **7** 347-49 (1974).

88. X. X. Wang, X. G. Tang, andH. L. W. Chan, "Electromechanical and ferroelectric properties of (Bi[1/2]Na[1/2])TiO[3]--(Bi[1/2]K[1/2])TiO[3]-BaTiO[3] lead-free piezoelectric ceramics," *Applied Physics Letters,* **85**[1] 91-93 (2004).

89. J. Shieh, K. C. Wu, andC. S. Chen, "Switching characteristics of MPB compositions of (Bi0.5Na0.5)TiO3-BaTiO3-(Bi0.5K0.5)TiO3 lead-free ferroelectric ceramics," *Acta Materialia,* **55**[9] 3081-87 (2007).

90. J. Yoo, D. Oh, Y. Jeong, J. Hong, andM. Jung, "Dielectric and piezoelectric characteristics of lead-free Bi0.5(Na0.84K0.16)0.5TiO3 ceramics substituted with Sr," *Materials Letters,* **58**[29] 3831-35 (2004).

91. X. Y. Wang, C. L. Wang, M. L. Zhao, J. F. Wang, K. Yang, andJ. C. Li, "Ferroelectric properties of lithia-doped (Bi0.95Na0.75K0.20)0.5Ba0.05TiO3 ceramics," *Materials Letters,* **61**[18] 3847-50 (2007).

92. S.-T. Zhang, L. Wang, Y.-F. Chen, andA. B. Kounga, "Phase Characteristics and Piezoelectric Properties in the Bi0.5Na0.5TiO3–BaTiO3–K0.5Na0.5NbO3 System," *Journal of the American Ceramic Society,* **93**[6] 1561-64 (2010).

93. J. E. Daniels, W. Jo, J. Rodel, V. Honkimaki, andJ. L. Jones, "Electric-field-induced phase-change behavior in (Bi0.5Na0.5)TiO3-BaTiO3-(K0.5Na0.5)NbO3: A combinatorial investigation," *Acta Materialia,* **58**[6] 2103-11 (2010).

94. Y. J. Dai, S. Zhang, T. R. Shrout, andZ. W. Zhang, "Piezoelectric and Ferroelectric Properties of Li-Doped (Bi0.5Na0.5)TiO3-(Bi0.5K0.5)TiO3-BaTiO3 Lead-Free Piezoelectric Ceramics," *J. Am. Ceram. Soc.,* **93**[4] 1108-13 (2010).

95. P. Jarupoom, E. Patterson, B. Gibbons, G. Rujijanagul, R. Yimnirun, andD. Cann, "Lead-free ternary perovskite compounds with large electromechanical strains," *Applied Physics Letters,* **99**[15] (2011).

96. C.-C. Huang and D. P. Cann, "Phase transitions and dielectric properties in Bi(Zn[1/2]Ti[1/2])O[3] - BaTiO[3] perovskite solid solutions," *Journal of Applied Physics,* **104**[2] 024117 (2008).

97. M. R. Suchomel and P. K. Davies, "Enhanced tetragonality in (x)PbTiO3-(1-x)Bi(Zn1/2Ti1/2)O3 and related solid solution systems," *Applied Physics Letters,* **86**[26] 262905 (2005).

98. M. I. Morozov and D. Damjanovic, "Hardening-softening transition in Fe-doped Pb(Zr,Ti)O3 ceramics and evolution of the third harmonic of the polarization response," *Journal of Applied Physics,* **104**[3] 034107-07-8 (2008).

99. G. Robert, D. Damjanovic, andN. Setter, "Preisach modeling of ferroelectric pinched loops," *Applied Physics Letters,* **77**[26] 4413-15 (2000).

100. V. Y. Shur, B. L. Rumyantsev, G. G. Lomakin, O. V. Yakutova, D. V. Pelegov, A. Sternberg, andM. Kosec, "AC Switching of Relaxor PLZT Ceramics," *Ferroelectrics,* **314**[1] 245-53 (2005).

101. S. Schaab and T. Granzow, "Temperature dependent switching mechanism of (Pb[0.92]La[0.08])(Zr[0.65]Ti[0.35])O[3] investigated by small and large signal measurements," *Applied Physics Letters,* **97**[13] 132902 (2010).

102. Z. Yu, C. Ang, R. Guo, andA. S. Bhalla, "Piezoelectric and strain properties of Ba(Ti[1 - x]Zr[x])O3 ceramics," *Journal of Applied Physics,* **92**[3] 1489-93 (2002).

103. Z. Yu, C. Ang, R. Guo, andA. S. Bhalla, "Ferroelectric-relaxor behavior of Ba(Ti[0.7]Zr[0.3])O[3] ceramics," *Journal of Applied Physics,* **92**[5] 2655-57 (2002).

104. W. Jo, S. Schaab, E. Sapper, L. A. Schmitt, H.-J. Kleebe, A. J. Bell, andJ. Rodel, "On the phase identity and its thermal evolution of lead free (Bi[1/2]Na[1/2])TiO[3]-6 mol% BaTiO[3]," *Journal of Applied Physics,* **110**[7] 074106 (2011).

105. K. T. P. Seifert, Jo, W., and Rodel, J., "Temperature-Insensitive Large Strain of (Bi1/2Na1/2)TiO3-(Bi1/2K1/2)TiO3-(K1/2Na1/2)NbO3 Lead-Free Piezoceramics," *J. Am. Ceram. Soc.,* **93**[5] 1392-96 (2010).

106. R. Dittmer, W. Jo, J. Daniels, S. Schaab, andJ. Rödel, "Relaxor Characteristics of Morphotropic Phase Boundary (Bi1/2Na1/2)TiO3–(Bi1/2K1/2)TiO3 Modified with Bi(Zn1/2Ti1/2)O3," *Journal of the American Ceramic Society,* **94**[12] 4283-90 (2011).

107. W. Jo, J. E. Daniels, J. L. Jones, X. Tan, P. A. Thomas, D. Damjanovic, andJ. Rodel, "Evolving morphotropic phase boundary in lead-free (Bi[1/2]Na[1/2])TiO[3]--BaTiO[3] piezoceramics," *Journal of Applied Physics,* **109**[1] 014110 (2011).

108. W. Jo, Granzow, T., Aulbach, E., Rodel, J., and Damjanovic, D. , "Origin of the large strain response in (K0.5Na0.5)NbO3-modified (Bi0.5Na0.5)TiO3-BaTiO3 lead - free piezoceramics," *J. Appl. Phys.,* **105** 094102 (2009).

109. E. A. Patterson, D. P. Cann, J. Pokorny, andI. M. Reaney, "Electromechanical strain in Bi(Zn[1/2]Ti[1/2])O[3]--(Bi[1/2]Na[1/2])TiO[3]--(Bi[1/2]K[1/2])TiO[3] solid solutions," *Journal of Applied Physics,* **111**[9] 094105-5 (2012).

110. N. Balke, Kungl, H., Granzow, T., Lupascu, D.C., Hoffman, M.J., and Rodel, J., "Bipolar Fatigue Caused by Field Screening in Pb(Zr,Ti)O3 Ceramics," *J. Am. Ceram. Soc.,* **90**[12] 3869-74 (2007).

111. C. Verdier, Lupascu, D.C., and Rodel, J., "Unipolar fatigue of ferroelectric lead zirconate titanate," *J. Eur. Ceram. Soc. ,* **23** 7 (2003).